IJOCTA
An International Journal of Optimization and Control: Theories & Applications
2010

ISSN:2146-0957
eISSN:2146-5703

Volume:12 Number:1
January 2022

An International Journal of Optimization and Control:

Theories & Applications

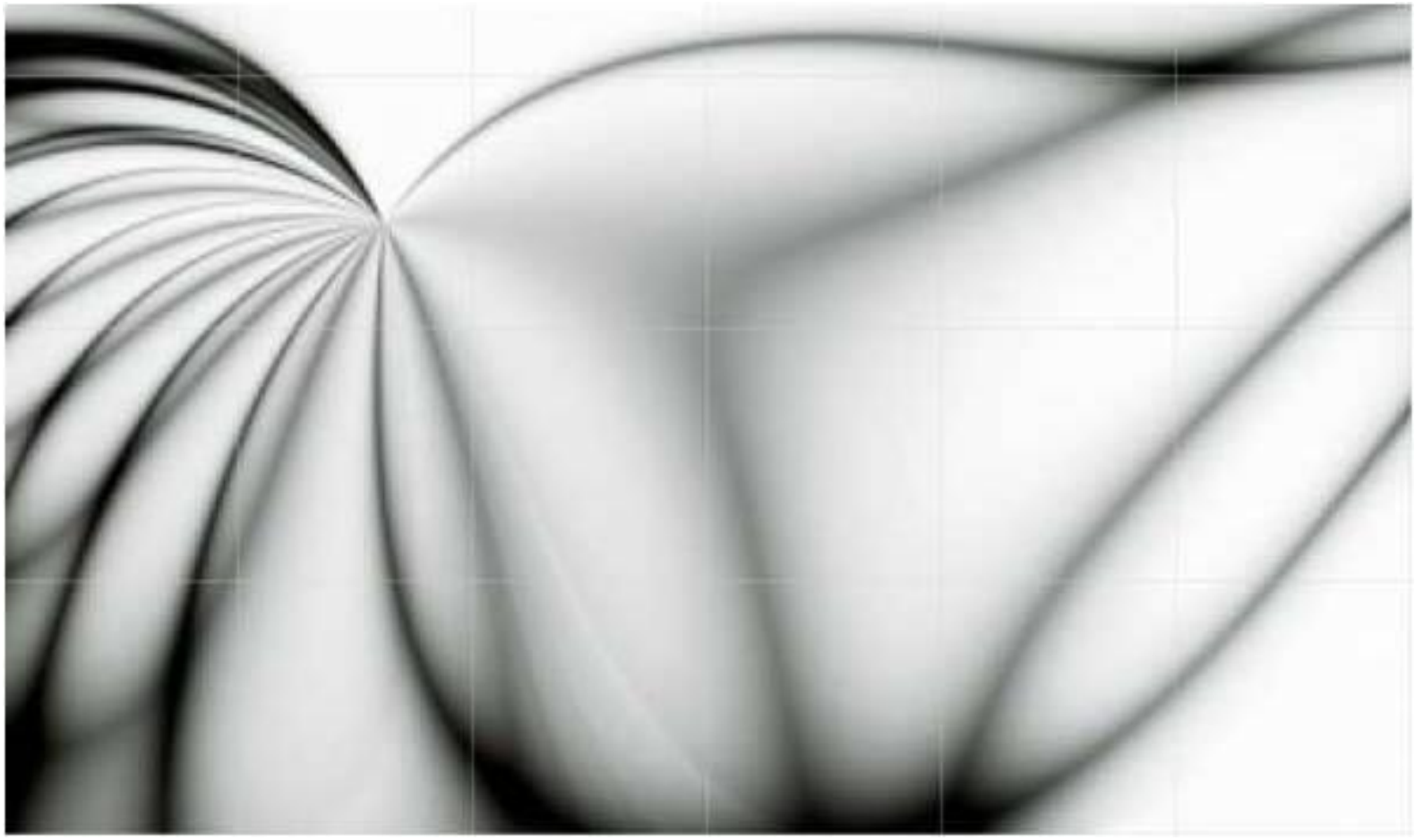

www.ijocta.org

IJOCTA
An International Journal of Optimization and Control: Theories & Applications
2010

http://www.ijocta.org
editor@ijocta.org

An International Journal of Optimization and Control: Theories & Applications

Volume: 12, Number: 1

January 2022

Publisher & Owner *(Yayımcı & Sahibi)*:
Prof. Dr. Ramazan YAMAN
Atlas Vadi Campus 2020, Anadolu St. No. 40, Istanbul, Turkey
Atlas Vadi Kampüsü 2020, Anadolu Cad. No. 40, Avcılar, İstanbul, Türkiye

ISSN: 2146-0957
eISSN: 2146-5703

Press *(Basımevi)*:
Bizim Dijital Matbaa (SAGE Publishing), Kazım Karabekir Street, Kültür Market, No:7 / 101-102, İskitler, Ankara, Turkey
Bizim Dijital Matbaa (SAGE Yayıncılık), Kazım Karabekir Caddesi, Kültür Çarşısı, No:7 / 101-102, İskitler, Ankara, Türkiye

Date Printed *(Basım Tarihi)*:
January 2022
Ocak 2022

Responsible Director (Sorumlu Müdür):
Prof. Dr. Ramazan YAMAN

IJOCTA is an international, bi-annual, and peer-reviewed journal indexed/ abstracted by *(IJOCTA, yılda iki kez yayımlanan ve aşağıdaki indekslerce taranan/dizinlenen uluslararası hakemli bir dergidir)*:

- Scopus - Applied Mathematics
- Scopus - Control and Optimization
- Zentralblatt MATH
- ProQuest - Electronics & Communications Abstracts
- Proquest - Computer & Information Systems Abstracts
- Proquest - Mechanical & Transportation Eng. Abstracts
- EBSCOHost
- MathSciNet
- TR Dizin - Ulakbim (Science Database)
- Directory of Open Access Journals (DOAJ)

crossref

We Use Plagiarism Detection iThenticate Learn More »

iThenticate plagiarism check service is granted by Balikesir University.

An International Journal of Optimization and Control:
Theories & Applications
Volume: 12 Number: 1
January 2022

CONTENTS

RESEARCH ARTICLES

An International Journal of Optimization and Control: Theories & Applications
ISSN:2146-0957 eISSN:2146-5703
Vol.12, No.1, pp.1-7 (2022)
http://doi.org/10.11121/ijocta.01.2022.001070

RESEARCH ARTICLE

On a special case of non-symmetric resource extraction games with unbounded payoffs

Illia Sylenko*

National University of Kyiv-Mohyla Academy, Ukraine
i.sylenko@ukma.edu.ua

ARTICLE INFO

Article History:
Received 31 December 2020
Accepted 16 June 2021
Available 14 September 2021

Keywords:
Stochastic games
Resource extraction
Markov perfect equilibrium
Isoelastic utility
Geometric random walk

AMS Classification 2010:
91A06; 91A15; 91A50;
91B51; 91B62

ABSTRACT

The game of resource extraction/capital accumulation is a stochastic infinite-horizon game, which models a joint utilization of a productive asset over time. The paper complements the available results on pure Markov perfect equilibrium existence in the non-symmetric game setting with an arbitrary number of agents. Moreover, we allow that the players have unbounded utilities and relax the assumption that the stochastic kernels of the transition probability must depend only on the amount of resource before consumption. This class of the game has not been examined beforehand. However, we could prove the Markov perfect equilibrium existence only in the specific case of interest. Namely, when the players have constant relative risk aversion (CRRA) power utilities and the transition law follows a geometric random walk in relation to the joint investment. The setup with the chosen characteristics is motivated by economic considerations, which makes it relevant to a certain range of real-word problems.

1. Introduction

The game of resource extraction (also known as the capital accumulation game) belongs to a class of nonzero-sum stochastic infinite-horizon games. It is also an extension of the famous discrete-time one-sector optimal growth model (see [1, 2]) to a strategic interaction of competing agents. The seminal study on the topic is by Levhari and Mirman [3], in which the authors considered a two-agent deterministic version of the game with the identical logarithmic one-period utilities of the players and the Cobb-Douglas production function regulating the resource quantity. The existence of a non-randomized stationary Nash equilibrium in a deterministic game setting was later established by Sundaram [4]. It is worth mentioning that some extensions to the game in its deterministic formulation are also being studied nowadays (e.g., a recent paper [5] on fishery extraction with more than one species). The result of Sundaram relied on the assumptions that the preferences of the players are identical and bounded in the state space, i.e., the space of all possible resource stocks. Both of these assumptions were also helpful in reporting the existence of a stationary Nash equilibrium in different stochastic frameworks of the game. The condition that the players have the same preferences makes a game *symmetric*. For the results on a stationary Nash equilibrium existence in the symmetric setup of resource extraction games the reader is referred to [6–10]. Studies [11, 12] tackled the problem in the non-symmetric case while assuming that the preferences of the players are bounded. Such condition was also important for studying non-symmetric stochastic games in a general context [13]. Moreover, the existing literature on non-symmetric *supermodular* stochastic games relies on the assumptions of either a bounded state space [14, 15] or bounded utilities [16].

*Corresponding Author

Finally, some partial results of the Nash equilibrium existence in non-symmetric resource extraction games with unbounded payoffs were obtained in [17, 18]. These extensions were achieved at the cost of additional structural assumptions. In the paper of Amir [17] the model does not only require that the spaces of player's actions are bounded by some constants, but also includes a very restrictive convexity assumption on the transition probability. A discussion on the relevance of such transition was covered in [18], concluding that it only makes sense in the case of a bounded state space. The approach in [18] by Jaśkiewicz and Nowak is more general. Authors set the transition probability to be a convex combination of stochastic kernels which depend on the state variable, or, in other words, the resource stock before consumption. Coefficients of the combination, as in the case of [17], are allowed to depend on a joint investment of players. However, the idea that a joint investment, which is the amount of the resource left after consumption, can influence only the coefficients was still limiting.

In this study we extend our view to the unexamined class of non-symmetric resource extraction games. In which, not only the players' utilities are unbounded, but the transition probability is a Markov kernel dependent on a *joint investment*. Moreover, the number of players in the game may be larger than two. At the same time, we restrict our attention to a specific form of the preferences and a concrete stochastic production function, the choices of which are motivated by economic considerations. Such settings, on which we elaborate below, enable us to prove the existence of a non-randomized stationary Markov perfect equilibrium in the game.

Our first assumption is that the utilities of the players are concave power functions. This type of preferences belongs to the Constant Relative Risk Aversion (CRRA) family. CRRA is a typical example of an established unbounded utility, and it is commonly used in economics. The arguments favouring exploiting CRRA utility functions are often supported by the existing empirical studies on investors' behaviour (see [19–21]).

The second assumption is that the transition law is determined by the state equation $s' = p \cdot \xi$, where p is a joint investment of players and ξ is a random shock, which adds a stochastic nature to the process. The model with multiplicative random shocks is known in economic literature as a geometric random walk. It is widely used in forecasting, especially for stock market data, where it is the default model. In order to avoid dealing with infinite values of players' expected discounted rewards within the structure, an additional natural constraint is imposed on the random variable ξ, restricting the growth rate of the stock.

The main result is presented as a theorem, the proof of which is based on the optimality principle of discounted dynamic programming. The preceding lemmata is aimed at finding the value functions which solve the corresponding Bellman equation for every player.

2. The model

A nonzero-sum m-person stochastic resource extraction game is described by the properties:

(i) The game is played in discrete moments $t = 1, 2, 3, \ldots$.

(ii) $S := [0; +\infty)$ is the state space, i.e., the space of all possible resource stocks.

(iii) $A(s) := [0; s]$ is the space of actions available to each player in state $s \in S$.
$D(s) := \left\{(x_1, \ldots, x_m) \in [0, s]^m : \sum_{i=1}^m x_i \leq s\right\}$
denotes the space of feasible action profiles in state $s \in S$. Define also
$D := \left\{(s, x_1, \ldots, x_m) \in S^{m+1} : \sum_{i=1}^m x_i \leq s\right\}$.

(iv) $u_i : S \to [0; +\infty)$ is player i's continuous utility function.

(v) The stochastic law of motion among states is described by the state equation $s' = M(s, x_1, \ldots, x_m, \xi)$,
where s is the previous state of the game, $(x_1, \ldots, x_m) \in D(s)$ are players' feasible decisions, ξ is a random disturbance, and M is a continuous function with the property $M(0, (0, \ldots, 0), \cdot) = 0$, meaning that $s = 0$ is an absorbing state.

(vi) $\beta_i \in (0, 1)$ is player i's discount factor.

The game is interpreted as follows. Several agents (numbered 1 to m) jointly own a productive asset, the evolution of which is represented by the state variable. At each of infinitely many stages of the game, players observe the state $s \in S$ and simultaneously choose their actions $(x_1, \ldots, x_m) \in A(s)^m$, expressing which part of the available stock each of them wishes to utilize for consumption. Provided that the actions are feasible, i.e., $(x_1, \ldots, x_m) \in D(s)$, players receive their appropriate utilities $u_1(x_1), \ldots, u_m(x_m)$, and the game moves to the next stage, where the new state is obtained from a stochastic technology $M(s, x_1, \ldots, x_m, \xi)$, the output of which depends on the realization of the random variable ξ on a probability space, drawn independently at every stage of the game. If the actions $(x_1, \ldots, x_m)$

happen to be infeasible, then players must revise their decisions. Therefore, we will restrict our attention only to strategies which generate feasible actions.

Let $I := \{1, 2, \dots, m\}$.

Our further assumptions to the model are:

A1: $u_i(x) = c_i \cdot x^{\alpha_i}$, where $c_i \in (0; +\infty)$ and $\alpha_i \in (0; 1)$ for every $i \in I$.

A2: $M(s, x_1, \dots, x_m, \xi) = (s - \sum_{i=1}^{m} x_i) \cdot \xi$, where the random variable ξ takes values in $[0; +\infty)$ with a probability distribution that is known to the players, and whose expectation is $\mathbb{E}$.

A3: $l_i := \beta_i \cdot \mathbb{E}\,(\xi^{\alpha_i}) \in (0; 1)$ for every $i \in I$.

Player's general *strategy* is a Borel mapping from the space of all possible histories of the game to the space of available actions. The set of all strategies for player $i \in I$ is denoted by Π_i.

A strategy profile $\pi = (\pi_1, \dots, \pi_m) \in \Pi_1 \times \ldots \times \Pi_m$ is called *feasible* if for any state $s \in S$ and every possible sequence of preceding states and actions h, the vector $\big(\pi_1(h, s), \dots, \pi_m(h, s)\big) \in D(s)$.

Let F be the set of all Borel measurable functions $f : S \to S$ such that $f(s) \in A(s)$ for every $s \in S$.

A *stationary Markov strategy* for player i is a constant sequence $(\pi_{it})_{t \in \mathbb{N}}$, where $\pi_{it} = f_i \in F$ for all $t \in \mathbb{N}$. Thus, a stationary Markov strategy for a player can be identified with a mapping $f \in F$. We will say that a stationary Markov strategy profile $(f_1, \dots, f_m)$ is feasible if and only if it belongs to the space

$$\Phi := \Big\{(f_1, \dots, f_m) \in F^m : \sum_{i=1}^{m} f_i(s) \le s \ \forall s \in S\Big\}.$$

Let $H := D \times D \times D \times \dots$ be the space of all infinite histories of the game. For every initial state $s_1 = s \in S$ and any feasible strategy profile $\pi = (\pi_1, \dots, \pi_m)$ we can define a probability measure P_s^{π} and a stochastic process $\{S_t, X_t\}$ on H in a canonical way (see Chapter 7 in [22]), where S_t and X_t are random variables describing respectively the state and the action profile at time t. Then, for each initial state $s \in S$ and a feasible strategy profile π, player i's *expected discounted reward* is

$$\gamma_i(\pi)(s) = \mathbb{E}_s^{\pi}\left[\sum_{t=1}^{\infty} \beta_i^{t-1}\, u_i(X_{ti})\right],$$

where X_{ti} is the i-th coordinate of the random vector X_t and $\mathbb{E}_s^{\pi}$ is the expectation operator with respect to the probability measure P_s^{π}.

Notation: Let $\bar{y} = (y_1, \dots, y_m)$ be a vector with coordinates belonging to some set Y. If $z_i \in Y$, then $(z_i, \bar{y}_{-i})$ signifies the vector $\bar{y}$ with coordinate y_i replaced by z_i.

A feasible strategy profile $\pi^* = (\pi_1^*, \dots, \pi_m^*) \in \Pi_1 \times \ldots \times \Pi_m$ is called a *Nash equilibrium* if for each $s \in S$, every player $i \in I$ and any $\pi_i \in \Pi_i$ such that (π_i, π_{-i}^*) is feasible,

$$\gamma_i(\pi^*)(s) \ge \gamma_i(\pi_i, \pi_{-i}^*)(s).$$

A Stationary Markov Perfect Equilibrium (SMPE) is a Nash equilibrium which belongs to the class of strategy profiles Φ.

3. Results

Let V be the space of all nonnegative Borel measurable functions $v : S \to \mathbb{R}$ such that $v(0) = 0$. For every $\bar{f} = (f_1, \dots, f_m) \in \Phi$ and $v \in V$ define m distinct backward induction dynamic programming operators associated with the game:

$$T_i(\bar{f}, v)(s) := u_i\big(f_i(s)\big) + \beta_i\, \mathbb{E}\left[v\big(M(s, \bar{f}(s), \xi)\big)\right], \quad i = \overline{1, m}.$$

We start with a preliminary problem. For a fixed set $(v_1, \dots, v_m) \in V^m$ consider a system of equations:

$$\begin{cases} f_1 = \arg\max_{y_1 \in F} T_1\big((y_1, \bar{f}_{-1}), v_1\big)(s) \\ \dots \\ f_m = \arg\max_{y_m \in F} T_m\big((y_m, \bar{f}_{-m}), v_m\big)(s). \end{cases} \tag{1}$$

Note that it is not immediately clear whether there exists a profile $\bar{f} = (f_1, \dots, f_m) \in \Phi$ which would satisfy system (1) for all $s \in S$. However, an affirmative answer can be obtained if the functions $v_1, \dots, v_m$ are additionally specified.

Define spaces $V_1, \dots, V_m$, where

$$V_i := \big\{v : S \to \mathbb{R} \mid v(s) = k \cdot s^{\alpha_i}, \ \ k \in (0; +\infty)\big\}.$$

Lemma 1. *For every set $(v_1, \dots, v_m) \in V_1 \times \ldots \times V_m$ there exists a unique profile $\bar{\phi} = (\phi_1, \dots, \phi_m) \in \Phi$ which solves the corresponding system (1) for all $s \in S$. Moreover, $T_i(\bar{\phi}, v_i)(s) \in V_i$ for each $i \in I$.*

Proof. For all $i \in I$ let $v_i(s) = k_i\, s^{\alpha_i}$, where $k_i \in (0; +\infty)$.

Define $w_i : D \to \mathbb{R}$ for every $i \in I$, such that

$$w_i(s, x_1, \dots, x_m) := c_i\,(x_i)^{\alpha_i} + k_i\, l_i \left(s - \sum_{j=1}^{m} x_j\right)^{\alpha_i}.$$

The motivation behind introducing functions w_i in the above formulation is explained by the following equalities:

$$T_i(\bar f, v_i)(s) = u_i\big(f_i(s)\big)+$$
$$+\beta_i\ \mathbb{E}\left[v_i\big(M(s, f_1(s),\dots,f_m(s),\xi)\big)\right] =$$
$$= c_i\left(f_i(s)\right)^{\alpha_i} + \beta_i\ \mathbb{E}\left[k_i\Big(s-\sum_{j\in I} f_j(s)\Big)^{\alpha_i}\xi^{\alpha_i}\right] =$$
$$= c_i\left(f_i(s)\right)^{\alpha_i} + k_i\, l_i\Big(s-\sum_{j\in I} f_j(s)\Big)^{\alpha_i} =$$
$$= w_i\big(s, f_1(s),\dots,f_m(s)\big)$$

for every $i\in I,\ s\in S$ and $\bar f=(f_1,\dots,f_m)\in\Phi$.

Notation: $I(i):=\{j\in\mathbb{N}$ such that $1\le j\le m$ and $j\ne i\}$.

Arbitrarily choose $i\in I$ and a set of functions $(f_j)_{j\in I(i)}$ such that $(0,\bar f_{-i})\in\Phi$. Fix $s\in S$ and consider a maximization problem

$$\max w_i\Big(s,\big(x_i,\bar f_{-i}(s)\big)\Big)\quad\text{subject to}\qquad(2)$$
$$x_i\in\Big[0; s-\sum_{j\in I(i)} f_j(s)\Big].$$

The problem (2) has a trivial solution $x_i=0$ in the case when $\sum_{j\in I(i)} f_j(s)=s$.

Suppose that $s\in(0;+\infty)$ and $\sum_{j\in I(i)} f_j(s)\in[0;s)$.

Then, for every $x_i\in\big(0; s-\sum_{j\in I(i)} f_j(s)\big)$ we have that

$$\frac{\partial^2}{\partial x_i^2}\ w_i\Big(s,\big(x_i,\bar f_{-i}(s)\big)\Big) = c_i\,\alpha_i\,(\alpha_i-1)\,x_i^{\alpha_i-2}+$$
$$+k_i\,l_i\,\alpha_i\,(\alpha_i-1)\Big(s-\sum_{j\in I(i)} f_j(s)-x_i\Big)^{\alpha_i-2}<0.$$

Thus, $w_i\big(s,(x_i,\bar f_{-i}(s))\big)$ is a concave function with respect to x_i by being concave in the interior of the domain and continuous.

Notice that there exists a point $\tilde x_i\in\big(0; s-$ $-\sum_{j\in I(i)} f_j(s)\big)$ which turns $\frac{\partial}{\partial x_i} w_i\big(s,(x_i,\bar f_{-i}(s))\big)$ into zero, namely

$$\tilde x_i=\left(1+\left(\frac{k_i\,l_i}{c_i}\right)^{\frac{1}{1-\alpha_i}}\right)^{-1}\Big(s-\sum_{j\in I(i)} f_j(s)\Big).$$

By the sufficient extremum condition, the point $\tilde x_i$ is a local maximum of $w_i\big(s,(x_i,\bar f_{-i}(s))\big)$. Furthermore, $\tilde x_i$ is a global maximum of $w_i\big(s,(x_i,\bar f_{-i}(s))\big)$ due to concavity of the objective function with respect to x_i.

We have that

$$\underset{x_i\in[0;s-\sum_{j\in I(i)} f_j(s)]}{\arg\max}\ w_i\Big(s,\big(x_i,\bar f_{-i}(s)\big)\Big) =$$
$$=\begin{cases}0, & \text{for } s\in S \text{ such that } \sum_{j\in I(i)} f_j(s)=s;\\ \left(1+\left(\frac{k_i\,l_i}{c_i}\right)^{\frac{1}{1-\alpha_i}}\right)^{-1}\Big(s-\sum_{j\in I(i)} f_j(s)\Big), & \\ \text{for } s\in(0;+\infty) \text{ s.t. } \sum_{j\in I(i)} f_j(s)\in[0;s).\end{cases}$$

Therefore, a function

$$\tilde y_i(s):=\left(1+\left(\frac{k_i\,l_i}{c_i}\right)^{\frac{1}{1-\alpha_i}}\right)^{-1}\Big(s-\sum_{j\in I(i)} f_j(s)\Big),$$

defined for all $s\in S$, maximizes the operator $T_i\big((y_i,\bar f_{-i}),v_i\big)(s)$ for any $s\in S$ and any set of functions $(f_j)_{j\in I(i)}$ such that $(0,\bar f_{-i})\in\Phi$.

Consequently, system (1) can be rewritten as

$$\begin{cases} f_1=\dfrac{1}{1+\left(\frac{k_1\,l_1}{c_1}\right)^{\frac{1}{1-\alpha_1}}}\Big(s-\sum_{j\in I(1)} f_j(s)\Big)\\ \dots\\ f_m=\dfrac{1}{1+\left(\frac{k_m\,l_m}{c_m}\right)^{\frac{1}{1-\alpha_m}}}\Big(s-\sum_{j\in I(m)} f_j(s)\Big)\\ (f_1,\dots,f_m)\in\Phi.\end{cases}\qquad(3)$$

Let $q_i:=\left(\frac{c_i}{k_i\,l_i}\right)^{\frac{1}{1-\alpha_i}}$. Clearly, $q_i\in(0;+\infty)$ for all $i\in I$.

In accordance with this notation, the first m equations of system (3) are equivalent to

$$\begin{cases}\frac{1}{q_1}\,f_1(s)=s-\sum_{j=1}^m f_j(s)\\ \dots\\ \frac{1}{q_m}\,f_m(s)=s-\sum_{j=1}^m f_j(s),\end{cases}$$

which is a system of linear equations with a unique solution $\bar\phi=(\phi_1,\dots,\phi_m)$, where

$$\phi_i(s):=\frac{q_i\ s}{1+\sum_{j=1}^m q_j}.$$

The fact that for every $s\in S$

$$\sum_{i=1}^m\phi_i(s)=\frac{\sum_{j=1}^m q_j}{1+\sum_{j=1}^m q_j}\,s<s$$

implies that $\bar\phi\in\Phi$. Therefore, $\bar\phi$ is a unique solution of system (1) for all $s\in S$.

It remains to calculate $T_i(\bar\phi,v_i)(s)$ for every $i\in I$.

$$T_i(\bar{\phi}, v_i)(s) = c_i \left(\phi_i(s)\right)^{\alpha_i} + k_i\, l_i \cdot$$
$$\cdot \left(s - \sum_{j=1}^{m} \phi_j(s)\right)^{\alpha_i} = \frac{c_i\ q_i^{\alpha_i}\ s^{\alpha_i}}{\left(1 + \sum_{j=1}^{m} q_j\right)^{\alpha_i}} + k_i\, l_i \cdot$$
$$\cdot \left(s - \frac{\sum_{j=1}^{m} q_j}{1 + \sum_{j=1}^{m} q_j}\, s\right)^{\alpha_i} = \frac{k_i\, l_i\ s^{\alpha_i}}{\left(1 + \sum_{j=1}^{m} q_j\right)^{\alpha_i}} \cdot$$
$$\cdot \left(\frac{c_i\ q_i^{\alpha_i}}{k_i\, l_i} + 1\right) = \frac{(q_i + 1)\ k_i\, l_i\ s^{\alpha_i}}{\left(1 + \sum_{j=1}^{m} q_j\right)^{\alpha_i}}. \qquad (4)$$

Hence, $T_i(\bar{\phi}, v_i)(s) \in V_i$ for every $i \in I$. □

For all $i \in I$ define functions $R_i : (0; +\infty)^m \to (0; +\infty)$ with the formula representing the coefficient in (4):

$$R_i(k_1, \ldots, k_m) := \frac{\left(1 + \left(\frac{c_i}{k_i\, l_i}\right)^{\frac{1}{1-\alpha_i}}\right) k_i\, l_i}{\left(1 + \sum_{j=1}^{m} \left(\frac{c_j}{k_j\, l_j}\right)^{\frac{1}{1-\alpha_j}}\right)^{\alpha_i}}.$$

Lemma 2. *There exist values $k_1^*, \ldots, k_m^* \in (0; +\infty)$ that satisfy a system of equations*

$$\begin{cases} k_1^* = R_1(k_1^*, \ldots, k_m^*) \\ \ldots \\ k_m^* = R_m(k_1^*, \ldots, k_m^*). \end{cases} \qquad (5)$$

Proof. Let $g : [1; +\infty) \to \mathbb{R}$ be the following function:

$$g(z) := \frac{1}{z} \left(\sum_{i=1}^{m} \frac{z^{\alpha_i}}{l_i} - m + 1\right).$$

Notice that

(a) $g(z)$ is continuous in $[1; +\infty)$;
(b) $g(1) > 1$;
(c) $\lim_{z \to +\infty} g(z) = 0$.

Property (b) follows directly from **A3**, while (c) from the choice of α_i ($i \in I$) in **A1**.

Together, (a)–(c) infer that there exists a point $z^* \in (1; +\infty)$ where $g(z^*) = 1$.

Thus,

$$z^* = \sum_{i=1}^{m} \frac{(z^*)^{\alpha_i}}{l_i} - m + 1.$$

For $i \in I$ define values q_i^* as expressions of z^*:

$$q_i^* := \frac{(z^*)^{\alpha_i}}{l_i} - 1. \qquad (6)$$

Since $z^* \in (1; +\infty)$, then each value q_i^* belongs to $(0; +\infty)$ for $i \in I$.

Note that

$$1 + \sum_{i=1}^{m} q_i^* = \sum_{i=1}^{m} \frac{(z^*)^{\alpha_i}}{l_i} - m + 1 = z^*. \qquad (7)$$

We can use equality (7) to rewrite equations (6) and obtain that values $q_1^*, \ldots, q_m^*$ satisfy the following properties for every $i \in I$:

$$q_i^* = \frac{\left(1 + \sum_{j=1}^{m} q_j^*\right)^{\alpha_i}}{l_i} - 1,$$

which is equivalent to

$$\frac{(q_i^* + 1)\ l_i}{\left(1 + \sum_{j=1}^{m} q_j^*\right)^{\alpha_i}} = 1. \qquad (8)$$

For each $i \in I$ introduce values $k_i^* \in (0; +\infty)$ as

$$k_i^* := \frac{c_i}{l_i\, (q_i^*)^{1-\alpha_i}}.$$

Rewriting (8) in terms of k_i^* and multiplying both sides of the equation by k_i^* provides the result which was needed to prove:

$$k_i^* = \frac{\left(\left(\frac{c_i}{k_i^* l_i}\right)^{\frac{1}{1-\alpha_i}} + 1\right) k_i^* l_i}{\left(1 + \sum_{j=1}^{m} \left(\frac{c_j}{k_j^* l_j}\right)^{\frac{1}{1-\alpha_j}}\right)^{\alpha_i}} = R_i(k_1^*, \ldots, k_m^*)$$

for all $i \in I$. □

We are now ready to formulate the main result.

Theorem 1. *Every resource extraction game defined by* (i)–(vi) *and* **A1**–**A3** *has a non-randomized SMPE.*

Proof. For every $i \in I$ put

$$v_i^*(s) := k_i^*\, s^{\alpha_i}$$

and

$$f_i^*(s) := \frac{\left(\frac{c_i}{k_i^* l_i}\right)^{\frac{1}{1-\alpha_i}}\ s}{1 + \sum_{j=1}^{m} \left(\frac{c_j}{k_j^* l_j}\right)^{\frac{1}{1-\alpha_j}}}.$$

By Lemmas 1 and 2, we have that for every $i \in I$ and any $s \in S$

$$v_i^*(s) = T_i(\bar{f}^*, v_i^*)(s) = \max_{y \in F} T_i\big((y, \bar{f}_{-i}^*), v_i^*\big)(s), \qquad (9)$$

where $\bar{f}^* = (f_1^*, \ldots, f_m^*)$.

In order to appropriately apply dynamic programming theorems, it remains to check whether $\lim_{t \to \infty} \mathbb{E}_s^{\pi} \left[\beta_i^{t-1}\, v_i^*(S_t)\right]$ equals to zero for every $i \in I$, every initial state $s_1 = s \in S$ and every strategy $\pi_i \in \Pi_i$ such that $\pi = (\pi_i, \bar{f}_{-i}^*)$ is feasible.

Observe that for any initial state of the game $s \in S$ and any feasible strategy profile $\pi \in$

$\Pi_1 \times \ldots \times \Pi_m$, the corresponding stochastic process $\{S_t, X_t\}$ has the following property:

$$S_{t+1} = M(S_t, X_t, \xi_t) = \left(S_t - \sum_{i=1}^{m} X_{ti}\right) \xi_t \leq S_t\, \xi_t,$$

where ξ_t is a random realization of the random variable ξ at stage t.

Then, for every $i \in I$, every $s \in S$ and every strategy $\pi_i \in \Pi_i$ such that $\pi = (\pi_i, \bar{f}^*_{-i})$ is feasible,

$$\begin{aligned}
&\lim_{t\to\infty} \mathbb{E}^{\pi}_s \left[\beta_i^{t-1} v_i^*(S_t)\right] = \lim_{t\to\infty} \mathbb{E}^{\pi}_s \left[\beta_i^{t-1} k_i^* \left(S_t\right)^{\alpha_i}\right] \leq \\
&\leq \lim_{t\to\infty} \mathbb{E}^{\pi}_s \left[\beta_i^{t-1}\, k_i^* (S_1\, \xi_1 \cdot \ldots \cdot \xi_{t-1})^{\alpha_i}\right] = \\
&= \lim_{t\to\infty} \mathbb{E} \left[\beta_i^{t-1}\, k_i^* (s\, \xi_1 \cdot \ldots \cdot \xi_{t-1})^{\alpha_i}\right] = \\
&= k_i^*\, s^{\alpha_i} \lim_{t\to\infty} \beta_i^{t-1}\, \mathbb{E} \left[\xi_1^{\alpha_i} \cdot \ldots \cdot \xi_{t-1}^{\alpha_i}\right] = \\
&= k_i^*\, s^{\alpha_i} \lim_{t\to\infty} \left(\beta_i\, \mathbb{E}\left[\xi^{\alpha_i}\right]\right)^{t-1} = 0. \qquad (10)
\end{aligned}$$

The last equality is due to Assumption **A3**.

Equation (9) together with property (10) imply by discounted dynamic programming arguments (see [1]) that

$$v_i^*(s) = \gamma_i(\bar{f}^*)(s) = \sup_{\pi_i \in \Pi_i} \gamma_i(\pi_i, \bar{f}^*_{-i})(s)$$

for every $i \in I$ and every $s \in S$. Hence, $\bar{f}^*$ is a SMPE. □

4. Concluding remarks

Remark 1. *As a consequence of Lemma 1, there also exists a unique Markov Perfect equilibrium in the similarly defined finite-horizon game, where at the final stage players split the available resource in the pre-determined relations.*

Indeed, if player i's utility at the horizon time T is equal to $k_i\, s_T^{\alpha_i}$, where $k_i \in (0; +\infty)$ and s_T is the observed state, then Lemma 1 ensures that there is a unique equilibrium solution to every appropriate one-shot subproblem obtained sequentially via the backward induction. Together they constitute, by the optimality principle, a unique (backwardly constructed) Markov Perfect Equilibrium of the game.

Remark 2. *A numerical calculation of the SMPE from Theorem 1 and the corresponding rewards is straightforward. By their construction, it suffices to simply find a point z^*, which turns the function $g(z)$ into 1. Since $g(z)$ is continuous, the task can be easily executed with standard numerical methods.*

References

[1] Stokey, N.L., Lucas, R.E., & Prescott, E.C. (1989). *Recursive Methods in Economic Dynamics*. Harvard University Press.

[2] Ulus, A.Y. (2017). On discrete time infinite horizon optimal growth problem. *An International Journal of Optimization and Control: Theories & Applications (IJOCTA)*, 8(1), 102–116.

[3] Levhari, D., & Mirman, L.J. (1980). The great fish war: An example using a dynamic Cournot-Nash solution. *The Bell Journal of Economics*, 11(1), 322–334.

[4] Sundaram, R.K. (1989). Perfect equilibrium in non-randomized strategies in a class of symmetric dynamic games. *Journal of Economic Theory*, 47(1), 153–177.

[5] Górniewicz, O., & Wiszniewska-Matyszkiel, A. (2018). Verification and refinement of a two species fish wars model. *Fisheries Research*, 203, 22–34.

[6] Majumdar, M., & Sundaram, R. (1991). Symmetric stochastic games of resource extraction: The existence of non-randomized stationary equilibrium. *In: Theory and Decision Library*, Springer Netherlands, 175–190.

[7] Dutta, P.K., & Sundaram, R. (1992). Markovian equilibrium in a class of stochastic games: existence theorems for discounted and undiscounted models. *Economic Theory*, 2(2), 197–214.

[8] Balbus, Ł., & Nowak, A.S. (2004). Construction of Nash equilibria in symmetric stochastic games of capital accumulation. *Mathematical Methods of Operational Research*, 60(2), 267–277.

[9] Jaśkiewicz, A., & Nowak, A.S. (2018). On symmetric stochastic games of resource extraction with weakly continuous transitions. *TOP*, 26(2), 239–256.

[10] Asienkiewicz, H., & Balbus, Ł. (2019). Existence of Nash equilibria in stochastic games of resource extraction with risk-sensitive players. *TOP*, 27(3), 502–518.

[11] Szajowski, P. (2006). Constructions of Nash equilibria in stochastic games of resource extraction with additive transition structure. *Mathematical Methods of Operations Research*, 63(2), 239–260.

[12] Balbus, Ł., & Nowak, A.S. (2008). Existence of perfect equilibria in a class of multigenerational stochastic games of capital accumulation. *Automatica*, 44(6), 1471–1479.

[13] He, W., & Sun, Y. (2017). Stationary markov perfect equilibria in discounted stochastic

games. *Journal of Economic Theory*, 169, 35–61.

[14] Curtat, L.O. (1996). Markov equilibria of stochastic games with complementarities. *Games and Economic Behavior*, 17(2), 177–199.

[15] Balbus, Ł., Reffett, K., & Woźny, Ł. (2014). A constructive study of markov equilibria in stochastic games with strategic complementarities. *Journal of Economic Theory*, 150, 815–840.

[16] Nowak, A.S. (2007). On stochastic games in economics. *Mathematical Methods of Operations Research*, 66(3), 513–530.

[17] Amir, R. (1996). Continuous stochastic games of capital accumulation with convex transitions. *Games and Economic Behavior*, 15(2), 111–131.

[18] Jaśkiewicz, A., & Nowak, A.S. (2015). Stochastic games of resource extraction. *Automatica*, 54, 310–316.

[19] Friend, I., & Blume, M.E. (1975). The demand for risky assets. *The American Economic Review*, 65(5), 900–922.

[20] Szpiro, G.G. (1986). Relative risk aversion around the world. *Economics Letters*, 20(1), 19–21.

[21] Chiappori, P.A., & Paiella, M. (2011). Relative risk aversion is constant: Evidence from panel data. *Journal of the European Economic Association*, 9(6), 1021–1052.

[22] Bertsekas, D.P., & Shreve, S.E. (1978). *Stochastic optimal control : the discrete time case*. Academic Press New York.

Illia Sylenko *is a PhD student at the National University of Kyiv-Mohyla Academy, Ukraine. Previously obtained a Bachelor degree in Applied Mathematics (National University of Kyiv-Mohyla Academy), a Master's degree in Scientific Computing (Université Lille 1) and a Master's degree in Optimization (Université Paris-Sud).*

https://orcid.org/0000-0002-5366-8763

An International Journal of Optimization and Control: Theories & Applications
ISSN: 2146-0957 eISSN: 2146-5703
Vol.12, No.1, pp.8-19 (2021)
https://doi.org/10.11121/ijocta.2021.1034

RESEARCH ARTICLE

Analysis of make-to-stock queues with general processing times and start-up and lost sales costs

Sinem Özkan*, Önder Bulut

Department of Industrial Engineering, Yaşar University, Turkey
sinem.ozkan@stu.yasar.edu.tr, onder.bulut@yasar.edu.tr

ARTICLE INFO

Article history:
Received: 19 October 2020
Accepted: 7 October 2021
Available Online: 23 October 2021

Keywords:
Production
Make-to-stock
Production and inventory control
Queueing theory
Renewal theory

AMS Classification 2010:
90B30, 90B05, 60K25, 60K05

ABSTRACT

We consider a make-to-stock environment with a single production unit that corresponds to a single machine or a line. Production and hence inventory are controlled by the *two-critical-number policy*. Production times are independent and identically distributed general random variables and demands are generated according to a stationary Poisson process. We model this production-inventory system as an M/G/1 make-to-stock queue. The main contribution of the study is to extend the control of make-to-stock literature by considering general production times, lost sales and fixed production costs at the same time. We characterize the long-run behaviour of the system and also propose a simple but very effective approximation to calculate the control parameters of the *two-critical-number policy*. An extensive numerical study exhibits the effects of the production time distribution and the system parameters on the policy control levels and average system cost.

1. Introduction

Most real-life production-inventory systems experience non-deterministic production and inter-demand-arrival times. In order to minimize the production and inventory related costs, performance evaluation and effective control of such systems are vital. This study addresses the production-inventory control problem of an environment with production start-up costs and general production times. Demands are generated according to a stationary Poisson process and the unsatisfied ones are immediately lost. The underlying system is controlled by the *two-critical-number policy* and modelled as an M/G/1 make-to-stock (MTS) queue. We develop a method to calculate the long-run average system cost. Furthermore, we determine the steady-state distribution of the inventory level and the production status (on or off) when production start-up cost is negligible.

The *two-critical-number policy* is known to be optimal for single-resource systems with backorders. Here, single-resource corresponds to a single machine or a single production line, which is the 'single-server' in queueing theory terminology. According to the *two-critical-number policy*, the production line is activated whenever inventory drops to the lower control level and production continues until the inventory reaches to the upper control level again.

To explain the practical significance of the problem, we can first scrutinize powder coating (powdered paint) production consisting of pre-mixing, extrusion and particle size reduction stages. Pre-mixing is the fastest stage of powder coating lines (can be further accelerated using additional caldrons) and therefore it can be assumed that extruder never starves. Although this process is a multi-stage one, in most real-life applications, it progresses in a continuous manner once the homogeneous mixture is obtained. After pre-mixing, without any interruption and intermediate buffers, particles are guided by air flow throughout the extrusion and size reduction stages. Thus, these two stages can be considered as a single operation while developing production policies. Furthermore, just before the start of a new production cycle the entire line is cleaned to get rid of dried paint chemicals and particle residues, which incur a start-up cost. In this paper, we aim to control production for single machine systems with ample supply and production start-up cost such as described above. Moreover, motivated from the powder coating example, it is also possible to generalize the practical use of our study to any lost sales make-to-stock system where the final station rarely

*Corresponding author

starves and production can be restarted with a fixed cost. Systems that are already single-station or have negligible start-up cost are special cases of this general perspective.

Our study extends the related literature by considering general production times, production start-up costs and lost-sales at the same time. Our contribution can be highlighted as: *i.* Majority of the earlier studies are for backordering environment. On the other hand, the studies with lost-sales either assume specific processing times (deterministic or Markovian) or zero start-up cost. We relax these restrictive assumptions and allow generally distributed processing times and non-zero start-up cost for the lost-sales case. *ii.* The first technical contribution is to develop an analogy between MTS queues and the capacitated M/G/1 queues. Using this analogy, the steady-state distribution of the considered MTS system is obtained when the production start-up cost is negligible. *iii.* For the systems with production start-up costs, we calculate the long-run expected average cost benefiting from renewal and queueing theories. We calculate the cycle cost with a first passage analysis and also show that the length of a production period can be written as the convolution of the lengths of capacitated M/G/1 busy periods. *iv.* We propose a well-performing approximation for the difference between the control levels of the *two-critical-number policy*.

The earlier studies consider single-server and single-demand-class systems with start-up and/or shut-down costs. The analyses are mostly based on queueing and inventory theory techniques. Gavish and Graves [1] is one of the initial milestone studies. They consider a single-demand-class backordering setting with production start-up cost. Production times are assumed to be constant and demands are generated according to a compound Poisson process with fixed sizes. For the two-critical-number policy, they calculate the average system cost and propose a search procedure to find the optimal values of the policy parameters. Gavish and Graves [2], and Lee and Srinivasan [3] extend [1] to general processing times. Both of these studies assume unit demand sizes. Graves and Keilson [4] and Srinivasan and Lee [5] consider compound demand extensions of [3]. Altıok [6] restricts production times to phase-type but studies both backordering and lost sales cases. Tijms [7] considers a system with general production times and finds the optimal control levels by a denumerable state Semi-Markov decision process. All the above-mentioned studies are actually MTS extensions of Heyman [8] and Sobel [9] who characterize the *two-critical-number policy* for the classical M/G/1 and G/G/1 queuing systems.

There are also related studies considering the systems where production occurs at a constant rate. De Kok et al. [10] analyses such a backordering production–inventory system where demands for a single product arrive according to a compound Poisson process and the production rate can be dynamically switched between two alternatives. Under some service level requirements, they derive approximations for the control parameters of the two-critical-number policy. De Kok [11] and De Kok and Tijms [12] study approximations for the lost-sales case. De Kok [13] provides an approximation for the time average of inventory holding and switching costs subject to a service level constraint. The recent work of Lin [14] considers a similar setting but the variation in the inventory level is modelled with a Brownian motion.

In more recent studies, the production-inventory problem is also considered as a control problem and Markov Decision Process (MDP) models are developed. The recent studies mostly assume negligible start-up costs. Ha [15] considers a setting with an exponential server, no start-up cost, several demand classes generating independent Poisson demands and lost-sales. He proves that the optimal production and rationing policies are of base-stock and static threshold level type, respectively. Bulut and Fadıloğlu [16] extends [15] and consider multiple production channels. They provide partial characterizations of the optimal policies and an extensive numerical study. Özkan and Bulut [17] considers the same environment with production start-up costs and proposes near optimal production and rationing policies.

Ha [18] considers the backordering version of [15] and characterizes the optimal policy by monotone switching curves for the two demand classes. For the same setting but with several demand classes, De Véricourt et al. [19] provides an algorithm to compute optimal rationing levels. Erlangian service times are considered by Ha [20] and Gayon et al. [21] for single-server lost-sales and backordering systems, respectively. They both show that threshold type policies based on work storage level are optimal. Pang et al. [22] allows batch demand and phase-type processing time distributions. Yücel and Bulut [23] assumes Coxian production times with non-zero production start-up cost. They propose an easy-to-apply, near optimal production policy.

In addition to the literature cited above, different system characteristics studied/assumed in the classical inventory control literature such as deteriorating items, more general demand structures, and environmental performance measures can also be adapted to production-inventory control literature. The following are example studies from the classical inventory and supply chain control literature that consider such characteristics: Pervin et al. [24], Tirkolaee et al. [25], Lofti et al. [26], and Paksoy et al. [27].

Our study is mostly related to [2] and [3]. We extend these studies to the lost-sales environment. The only existing study considering non-Exponential production times and lost sales is [6]. However, [6] is restricted to phase-type production times and thus Markovian analysis is still possible.

The rest of this paper is organized as follows: In Section 2, M/G/1 Make-to-Stock Queue with no production start-up cost is analysed and limiting probabilities and

expected average system cost are calculated. In Section 3, we present a renewal approach to calculate the expected average system cost for the systems with production start-up costs. We also propose a near-optimal alternative for the difference of policy control levels. Section 4 is devoted to numerical experiments. Finally, Section 5 summarizes the study along with a discussion on future research directions.

2. Steady state analysis of M/G/1 make-to-stock queue with no start-up cost

We consider a make-to-stock (MTS) facility producing a single-item on a single production unit (e.g. a machine or a line). Demands are generated according to a stationary Poisson process with rate λ and production times are independent and identically distributed general random variables with rate μ. Unsatisfied demands are immediately lost and a cost of c is incurred per unit lost. Inventory holding cost rate is h.

In most of the production systems, inventory is replenished one-by-one at production completion instants. Hence, these systems are closely related to the classical queueing systems and are referred to as MTS queues. Our system is a lost-sales M/G/1 MTS queue that is controlled by the *two-critical-number policy*, in short (s,S) policy. S is the maximum inventory level at which production is stopped. The time period starting from S until reaching s is the non-production period. Whenever the inventory level drops to s, production is triggered with a start-up cost of K. The production-period continues until the inventory level reaches S again.

This section assumes negligible production start-up costs, i.e. $K = 0$. For such settings, Base-stock policy is optimal, i.e. $(s,S) = (S-1,S)$. We conduct the steady-state analysis of the lost-sales M/G/1 MTS queue under $(S-1,S)$ policy using the dynamics of the (typical) M/G/1/S queue. The analogy between two queues is given in Table 1. If there are $i \in \{0,1 \dots, S\}$ units of stock in the production-inventory system, then there are $(S-i)$ many "customers", which are the outstanding production orders, in the corresponding M/G/1/S queue.

Table 1. The analogy between 'M/G/1 MTS queue controlled by $(S-1,S)$' and 'M/G/1/S queue'

	M/G/1 MTS Queue	M/G/1/S Queue
Customers	Demands	Outstanding production orders
System State	On-hand inventory	Outstanding production orders
Steady-state Probabilities $i = 0,1, \dots, S$	π_i^{MTSQ}	π_i^{Q}
	$\pi_i^{MTSQ} = \pi_{S-i}^{Q}$	

In order to calculate the long-run probabilities of the M/G/1/S queue, we follow the method proposed by Bose [28]. First, the steady-state distribution of the embedded Markov chain that tracks the system at the customer arrival instants is calculated. This distribution is equivalent to the steady state distribution of the considered M/G/1/S queue by PASTA (Poisson Arrivals See Time Averages) property. To obtain the steady state distribution of the embedded chain when the system is observed at the arrival instants, we benefit from the steady state distribution of another embedded chain that tracks the system at the departure instants.

The number of customers left behind in the M/G/1/S system at any customer departure instant in the long run follows a Markov Chain. The chain is described in (1). The state variable n_j is the number of customers left behind in the system at the time of j^{th} customer departure. The evolution of n_j depends on the number of new arrivals that occur during the service time of the j^{th} customer, which is denoted by a_j in (1), and the queue capacity $(S-1)$.

$$n_{j+1} = \begin{cases} min\{a_{j+1}, S-1\}, & n_j = 0, \\ min\{n_j - 1 + a_{j+1}, S-1\}, & 1 \le n_j \le (S-1) \end{cases}. \quad (1)$$

The steady-state probabilities of the chain described in (1) are denoted by p_i^d where $i \in \{0,1 \dots, S-1\}$ is the number of customers left behind in the system at the time of any customer departure in the long run. That is,

$$p_i^d = \lim_{j \to \infty} P\{n_j = i\}. \quad (2)$$

These limiting probabilities can be easily calculated by using the transition probability matrix induced by (1). Once we characterize the steady state solution for the embedded Markov chain of M/G/1/S queue that tracks the system at the departure epochs, the next is to characterize the embedded chain that tracks the system at the arrival epochs. Due to Kleinrock's Result,

$$p_i^{ac} = p_i^d \quad (3)$$

where p_i^{ac}, $i \in \{0,1 \dots, S-1\}$, is the probability that an arrival (a new customer) finds i customers in the system in the long run. It should be noted that (3) holds only when the arrivals that find the system not full are accounted (Bose [28]). Therefore, the upper bound of i is $S-1$.

The unconditional state probabilities at the arrival instants (regardless of whether the customer enters the system or leaves without joining the queue) are defined by $p_i^a, i \in \{0,1 \dots, S\}$. For all $i \in \{0,1 \dots, S-1\}$, the relation between the unconditional and conditional state probabilities (between p_i^a and p_i^{ac}) at the arrival instants is given in (4). Equation (4) also states that the steady state probability of the original system (π_i^Q) equals to the steady state probability when the system is observed at the arrival instants (p_i^a). This holds due to the PASTA property.

$$\pi_i^Q = p_i^a = \left(1 - \pi_S^Q\right) p_i^{ac} \tag{4}$$

In (4), $\left(1 - \pi_S^Q\right)$ is the probability that the system is not full in the long run and hence an arriving customer enters the system. In Equation (5), π_0^Q, which is the idleness rate of the system, is written in terms of π_S^Q.

$$\pi_0^Q = 1 - \rho = 1 - \frac{\lambda\left(1-\pi_S^Q\right)}{\mu} \tag{5}$$

In (5), ρ and $\lambda\left(1 - \pi_S^Q\right)$ denote the utilization and effective arrival rate of the system, respectively. Once the system of equations defined by (3), (4), and (5) is solved, the steady-state distribution of the M/G/1/S queue is obtained. Using the analogy given in Table 1, the steady state distribution of the M/G/1 MTS queue controlled by $(S-1, S)$ policy is found. Using the steady state distribution, the expected average system cost is calculated in (6).

$$\begin{aligned} AC(S-1,S) &= \lambda c \pi_S^Q + h \sum_{i=1}^{S} i \pi_{S-i}^Q \\ &= \lambda c \pi_0^{MTSQ} + h \sum_{i=1}^{S} i \pi_i^{MTSQ} \end{aligned} \tag{6}$$

The above analysis covers the cases where $s = (S-1)$. However, if a fixed start-up cost (K) is incurred to activate a line, then $s < (S-1)$ for most of the practical settings. For such instances of *the two-critical-number policy*, the adaptation of the described method is not direct. The main reason of the complication is the increase in the length of the non-production period, which can be measured by $\Delta = (S - s)$. If $\Delta > 1$, for any inventory level i such that $s < i < S$, it is not possible to certainly identify whether the server is on or off. Such states are visited both in the production and non-production periods. We overcome this extra level of complexity with a new method that directly calculates the long-run average cost without finding the steady-state distribution.

3. Expected long-run average cost of M/G/1 make-to-stock queue with start-up cost

In this section we consider the case where the production start-up cost K is positive. As [3] and [5] do for the backordering environment, we develop a renewal approach to calculate the average system cost.

We define the regeneration point of renewal cycles as the maximum inventory level S and decompose cycles into production and non-production periods (sub-cycles). When the inventory level reaches S, production is stopped and a new renewal cycle starts with its non-production period in which inventory is depleted by the demands. Upon hitting the lower control level s, non-production period ends and production period of the cycle starts. During this period, inventory level follows a realization increasing with production completions and decreasing with demand arrivals. Production period and the current renewal cycle is completed when the inventory level reaches S again. The basic notation used in the remaining part of the section is provided in Table 2.

Table 2. Basic notation of the renewal analysis

X	the random variable denoting the production time with cdf $G_X(x)$ and rate μ
$N(t)$	Poisson demand process with rate λ,
X_d	the random variable denoting the production time given that $N(X) = d$,
$E[X_d]$	$E[X \mid N(X) = d]$,
$C_N(s,S)$	expected cost of a non-production period,
$C_P(s,S)$	expected cost of a production period,
$L_N(s,S)$	expected length of a non-production period,
$L_P(s,S)$	expected length of a production period,
$AC(s,S)$	expected average cost.

By the Renewal Reward Theorem, the long-run expected average system cost can be written as follows:

$$AC(s,S) = \frac{C_N(s,S) + C_P(s,S) + K}{L_N(s,S) + L_P(s,S)} \tag{7}$$

Expected cost of a non-production period is relatively easy to calculate because the only relevant component is the holding cost and the average time spent at each inventory level $i \in \{s+1 \dots, S\}$ is $1/\lambda$. Then,

$$C_N(s,S) = \sum_{i=s+1}^{S} \frac{hi}{\lambda} \tag{8}$$

On the other hand, calculating the expected cost of a production period is more cumbersome. For $i, j \in \{0, \dots, S\}$ and $j \geq i$, if we let $E\left[\mathcal{F}_{i,j}\right] = f_{i,j}$ denote the expectation of the accumulated cost starting from the time instant when the process enters i until the inventory level is raised to j for the first time, then

$C_P(s,S)$ can be written as

$$C_P(s,S) = f_{s,S} = \sum_{i=s}^{S-1} f_{i,(i+1)} \quad (9)$$

In order to apply the stepwise approach defined by (9) we condition on the number of demand arrivals during the production time of an item.

$$f_{i,(i+1)} = E\left[\mathcal{F}_{i,(i+1)}\right] = E\left[E\left[\mathcal{F}_{i,(i+1)}|N(X)\right]\right] \quad (10)$$

The inner expectation of (10) can be calculated in two parts. In the first part, for each inventory level i and number of demand arrivals d, the cost accumulated throughout a production time period is calculated and denoted by P_{id}. The second part is to calculate the first passage cost of the new state, which is determined by the current state i and the number of demand arrivals d. Mathematically speaking, the inner expectation of (10) can be written as (11). In (11), given i and d, the new state is calculated as $(max(i-d,0)+1)$. The calculation is based on the lost sales assumption and the additional unit of inventory due to the production completion. For the sake of completeness, $f_{i,i}$ is set to zero for all inventory levels i.

$$E\left[\mathcal{F}_{i,(i+1)}|N(X)=d\right] = P_{id} + f_{(max(i-d,0)+1),(i+1)} \quad (11)$$

We calculate P_{id} in (12). The first part corresponds to the expected holding cost of all the items in the inventory. For each item $n \in \{1,\dots,i\}$, given that d demand arrivals occur during the production time, we let τ_{nd} be the length of the time that the n^{th} item spends in the inventory (holding time of the n^{th} item). In the second part, expected lost sales cost calculated where $(E[X_d]-\tau_{id})$ is the conditional expected length of the shortage period within the production time.

$$P_{id} = \sum_{n=1}^{i} h\tau_{nd} + c\,\lambda(E[X_d]-\tau_{id}) \quad (12)$$

To calculate τ_{nd} we make use of the following observation: holding time of the nth item is the arrival time of the nth demand. Since $N(t)$ is a Poisson process, the joint distribution of the conditional arrival times has the same distribution as the order statistics of independent Uniform random variables defined on the interval $[0, X_d]$ where X_d is the length of the production time given d demand arrivals, i.e., $N(X)=d$. Based on this fact, when $d > n$, the expected holding of the nth item is proportional to n divided by the total number of stochastically identical time intervals, which is $(d+1)$. When $d \le n$, on the other hand, nth item is held in the inventory during the whole production time. That is,

$$\tau_{nd} = \begin{cases} \frac{nE[X_d]}{d+1}, & d > n \\ E[X_d], & d \le n \end{cases} \quad (13)$$

Furthermore, using Bayes` Theorem and the shorthand notation $\alpha_d = P(N(X)=d)$, conditional expected production time $E[X_d]$ can be calculated as follows:

$$E[X_d] = E[X|N(X)=d] = \frac{1}{\alpha_d}\int_u u\frac{e^{-\lambda u}(\lambda u)^d}{d!}\partial G(u) \quad (14)$$

where

$$\alpha_d = \int_u P(N(u)=d \mid U=u)\,\partial G(u) = \int_u \frac{e^{-\lambda u}(\lambda u)^d}{d!}\partial G(u) \quad (15)$$

After obtaining the inner expectation, the outer expectation of (10), which is over the realizations of $N(X)$, can be written as,

$$f_{i,(i+1)} = E\left[P_{id} + f_{(\max(i-d,0)+1),(i+1)}\right] = \sum_d \alpha_d\left(P_{id} + f_{(\max(i-d,0)+1),(i+1)}\right) \quad (16)$$

In order to find the values of the unknown $f_{i,j}$`s the system of linear equations defined by (16) can be solved recursively. The starting point is the calculation of $f_{0,1}$: $f_{0,1} = \sum_d \alpha_d\left(P_{id} + f_{1,1}\right) = \sum_d \alpha_d P_{id}$. Once the first passage costs are calculated, the expected cost of a production period can be compiled using (9).

After $C_N(s,S)$ and $C_P(s,S)$, the next step is to calculate the period lengths. Expected length of a non-production period can be directly written as

$$L_N(s,S) = \frac{S-s}{\lambda} \quad (17)$$

Although calculating production period length requires more effort, we succeed to develop a quick method that benefits from the analysis of capacitated M/G/1 queue. As it is discussed in Section 2, M/G/1 MTS queues are closely related with the capacitated M/G/1 queues. Our method to calculate $L_P(s,S)$ is based on the following observations:

(i) Production period starts when the inventory level drops to *s* from (*s*+1). This is equivalent to start a busy period of an M/G/1/(*s*+1) queue where the customers are the outstanding production orders. The capacity of the queue is (*s*+1) due to the lost sales assumption: there can be at most s more orders in addition to the one that triggers the busy period.

(ii) Within the busy period, each arrival event of the M/G/1/(*s*+1) queue decreases the inventory level of the original MTS system but each departure event on the other hand increases it. Furthermore, departure events are realized after the corresponding arrival events. Because of this zero-net flow, inventory level of the original MTS system at the end of the busy period would be (*s*+1), which is the inventory position when the busy period starts.

(iii) Similar to the above, once the inventory level hits (s+1), a busy period of M/G/1/(s+2) queue starts; and inductively this scheme repeats until the level reaches S.

If we let B_i denote the expected busy period length of an M/G/1/i queue, $i \in \{s+1 \dots, S\}$, then

$$L_P(s,S) = \sum_{i=s+1}^{S} B_i = \sum_{i=s+1}^{S} \left(\frac{1-\pi_0^{Qi}}{\lambda \pi_0^{Qi}}\right) \quad (18)$$

where π_0^{Qi} is the steady state probability of having zero customer in an M/G/1/i queue.

For given s and S values, all the components of (7), which are required to calculate the expected average system cost, are obtained. From the optimization perspective, on the other hand, we suggest the following EOQ-type formula for $\Delta = (S - s)$ instead of a two-dimensional enumerative search for the control parameters:

$$\Delta_{EOQ} = \left[\sqrt{\frac{2K\lambda}{h}}\right] \quad (19)$$

where [.] returns the nearest integer.

Δ_{EOQ} is a near-optimal alternative for Δ^*, which is the optimal difference between the control parameters. Using Δ_{EOQ} we only search for s and then obtain S as $s + \Delta_{EOQ}$. In Section 4, it is shown that the proposed near-optimal solution performs very well.

4. Numerical study

In this section, we present the results of the numerical study and mainly show that how the optimal and near-optimal control levels and average cost react to changes in system parameters and processing time distributions. The discussion is enriched with managerial insights.

Study 1: We first show how changes in control levels s and S affect the average cost. For this study, the processing time is assumed to follow an Erlang-r distribution with parameters $\mu = 2$ and $r = 2$ where r is the number of processing stages (phases) and μ is the system processing rate (the rate of each stage is 4). That is, we consider an M/E_2/1 make-to-stock queue. Erlang distribution, which is a member of phase-type distribution family, enables to model production time distributions with different variance. While keeping μ constant, as r increases, variance of the production time decreases.

For the base case of the numerical study section, we let $(K, h, c, \lambda, \mu, r) = (10, 2, 40, 2, 2, 2)$. For the base case, Figure 1 exhibits that how the average cost changes with respect to s and S. The optimal control levels are $(s^*, S^*) = (5, 9)$ and the optimal average cost is 15.66, which are found by enumerative search. Furthermore, for the base case, the approximation for the difference between control levels is calculated as $\Delta_{EOQ} = 4$ that equals to the optimal difference $\Delta^* = (S^* - s^*) = 4$.

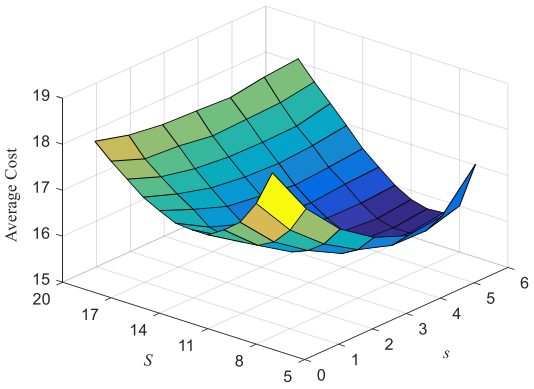

Figure 1. The average cost with respect to s and S

Study 2: In the second study, we aim to examine the impact of λ and $\Delta = (S - s)$ on the average cost. We present the study for $\lambda \in \{0.5, 1.0, 1.5, 2.0, 2.5\}$ and $\Delta \in \{1, 2, \dots, 15\}$. Given λ and Δ, we search for the optimal value of s and then calculate the optimal produce-up-to level as $S = \Delta + s$. We conduct the study for the base case introduced in Study 1 but this time traffic intensity of the system varies as λ changes.

In Figure 2, one can observe that when the traffic intensity $\rho = \frac{\lambda}{\mu}$ is lower, the average cost first decreases and then increases as Δ increases. On the other hand, as ρ increases, the flatness of the average cost function increases. That is, change in Δ does not affect the average cost significantly when the arrivals are more frequent. For such cases, due to heavy traffic, average inventory level would be low and shortage cost would be the dominant cost component.

In this study, we also would like to point out the use of constant Δ for the practitioners. When Δ is fixed, it is easy to calculate the expected length of a non-production period, which is Δ/λ. Such a fixation can be useful to solve the capacity allocation problem of multi-product systems. During the non-production period of an item, the available production capacity can be used for the others. Such a heuristic solution would simplify multi-product make-to-stock problems for the practitioners.

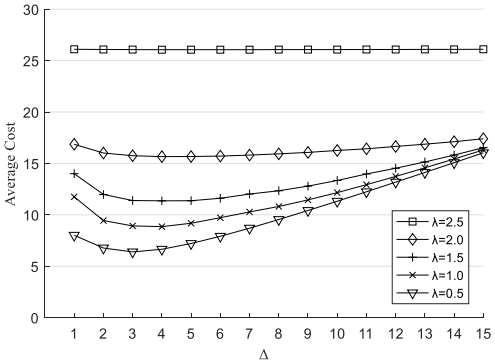

Figure 2. The impact of $\Delta = (S - s)$ on the average cost with different demand rates

Study 3: We now concentrate on the impact of various processing time distributions with the same mean ($E[X] = 0.50$) and variance ($\sigma^2(X) = 0.125$), and hence the same coefficient of variation ($c_X = \frac{\sigma(X)}{E[X]} = 0.71$). For this study, Log-normal, Erlang-r and Coxian-r distributions are considered. The first reason to select these distributions is that they have at least two parameters that enable us to work with the same mean and variance. Besides, the selected distributions are from different families; Conditional Normal and Phase-type. It is clear from Table 3 that as long as the first two moments of the processing time distributions are the same, the impact of different distributions on the average cost values and the optimality gaps is not remarkable. The optimality gap between $AC_{\Delta_{EOQ}}$ and AC^*, which are the costs of near-optimal and optimal solutions, are almost zero for all the cases. It can be concluded that our near optimal solution performs well under different processing time distributions having the same first two moments.

Study 4: We now focus on the impact of different $E[X]$ and $\sigma^2(X)$ values. For this purpose, we use the following parameters of the base case: $(K, h, c, \lambda) = (10, 2, 40, 2)$. The other parameters are displayed in Table 4 where $E[X]$ and $\sigma^2(X)$ are different for the considered distributions but c_X is the same for all.

In Table 4, distributions are placed from left to right in the descending order of means and variances. As one can expect that the average cost decreases as the first two moments of the processing time decrease. More interestingly, for all the considered cases, the optimality gap is almost zero. We can again conclude that EOQ-type formulation performs well under different processing time distributions and different distribution parameters.

Table 3. The impact of processing time distributions with same $E[X]$, $\sigma^2(X)$ and c_X

	Lognormal (0.50,0.354)	Erlang-2	Coxian-2 (3.92,3.92,0.96)
$E[X]$	0.50	0.50	0.50
$\sigma^2(X)$	0.125	0.125	0.125
c_X	0.71	0.71	0.71
AC^*	15.62	15.66	16.03
$AC_{\Delta_{EOQ}}$	15.62	15.66	16.05
Optimality Gap: $AC_{\Delta_{EOQ}}$ vs AC^*	0.00%	0.00%	0.12%

Table 4. The impact of processing time distributions with different $E[X]$ and $\sigma^2(X)$ but same c_X

	Lognormal (0.75,0.53)	Erlang-2	Coxian-2 (8,8,0.98)
$E[X]$	0.75	0.50	0.25
$\sigma^2(X)$	0.280	0.125	0.031
c_X	0.71	0.71	0.71
AC^*	29.70	15.66	11.54
$AC_{\Delta_{EOQ}}$	29.73	15.66	11.54
Optimality Gap: $AC_{\Delta_{EOQ}}$ vs AC^*	0.10%	0.00%	0.00%

Table 5. Processing time distributions with the corresponding parameter values

	Erlang-1	Erlang-2	Erlang-3	Erlang-5	Erlang-10	Erlang-500
$E[X]$	0.50	0.50	0.50	0.50	0.50	0.50
$\sigma^2(X)$	0.250	0.125	0.083	0.050	0.025	0.001
c_X	1.00	0.71	0.58	0.45	0.32	0.05

Table 6. The impact of processing time distributions

	Δ^*	s^*	AC^*	Δ_{EOQ}	$s_{\Delta_{EOQ}}$	$AC_{\Delta_{EOQ}}$	Optimality Gap: $AC_{\Delta_{EOQ}}$ vs AC^*
Erlang-1	5	5	17.41	4	6	17.43	0.11%
Erlang-2	4	5	15.66	4	5	15.66	0.00%
Erlang-3	4	5	14.96	4	5	14.96	0.00%
Erlang-5	4	5	14.32	4	5	14.32	0.00%
Erlang-10	4	4	13.84	4	4	13.84	0.00%
Erlang-500	4	4	13.31	4	4	13.31	0.00%

Study 5: This time we only fix the expected value of the processing time but let different variances. In order to assess the impact of such cases, we consider the base case of Study 1 and Erlang processing time distribution with different r (number of stages) values. While keeping the expected value constant, as r increases, the variance decreases and converges to zero in the limit (deterministic case).

Table 5 presents the considered processing time distributions with their means, variances and coefficient of variations. For the cases considered in Table 5, we provide optimal and near-optimal solutions, and optimality gaps in Table 6 where the distributions are ordered from high to low variances. While the variance decreases, Δ^*, s^*, and AC^* are non-increasing. As the processing time variance, s^* and Δ^* decrease, the lengths of both non-production and production periods also decrease. Therefore, the amount of cyclic safety stock and AC^* become less.

As it is seen in Table 6, Erlang-1, i.e. Exponential, distribution has the highest variance and therefore relatively higher optimality gap. On the other hand, optimality gaps are less than 0.12% for all the cases. Hence, it can be concluded that our EOQ-type formulation performs very well and is robust to changes in distribution and variance.

Study 6: Using the base case, in Figure 3, we investigate the joint effect of changes in production start-up cost K and Δ. When $\Delta > 10$, the cost function increases almost linearly and the effect of start-up cost on the average cost is limited. As Δ increases, the system pays less fixed cost and hence the portion of the start-up cost within the average cost decreases. As Δ increases, in the limit, the average cost would be same for all K values because the holding cost would dominate the other cost components. On the other hand, for smaller values of Δ, the effect of K is prominent: Lower start-up cost, lower the average cost.

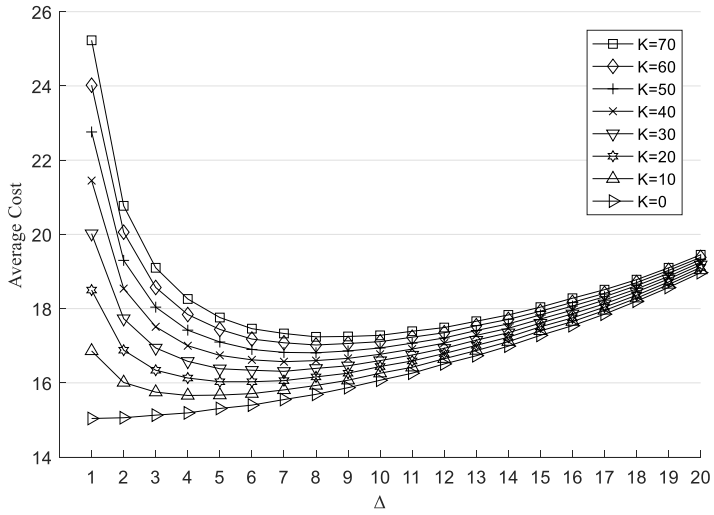

Figure 3. The average cost vs. $\Delta = (S - s)$ for each value of the fixed cost for Erlang-2

Study 7: We lastly examine the effects of changes in start-up cost K, lost-sales cost c, and holding cost h on optimal and near-optimal control levels, average costs, and optimality gaps. We conduct an extensive experimental study capturing different combinations of $K \in \{0,10,20\}$, $h \in \{1,2,3\}$, and $c \in \{h, 10h, 20h\}$. Tables 7 and 8 show the results for Erlang-2 and Uniform processing time distributions, respectively. For both of the distributions, expected processing time is 0.5.

As can be seen in Table 7, whatever h and c are, if the fixed cost to activate the line is negligible ($K = 0$), the optimal policy is a Base-Stock-type, i.e. $\Delta^* = (S^* - s^*) = 1$. For any given h and c values, as K increases, Δ^* increases to continue production for a longer time once it is triggered. On the other hand, s^* is non-increasing in K. Due to these behaviours, $S^* = s^* + \Delta^*$ is non-decreasing in K.

For a given K value, as c decreases or h increases, production is demotivated as inventory level increases. This is because of the trade-off between holding and shortage costs. Hence, the optimal production trigger point s^* and the optimal produce-up-to level S^*, diminish as c decreases or h increases. At the opposite direction, it is better to keep the line active at higher inventory levels to minimize the risk of stock out, which is now costlier.

The optimal average cost AC^* is increasing in K, c, and h as expected. However, the effect of K on the average cost is not as prominent as the effects of c and h. As K increases, both non-production and production period prolong and frequency of incurring the fixed cost reduces.

All the above observations and comments are also valid

for the cases with Uniform processing time whose results are presented in Table 8.

To show the effectiveness of our heuristic approach, we compare the average cost calculated using Δ_{EOQ} with the optimized production trigger and produce-up-to levels, which are $s_{\Delta_{EOQ}}$ and $S_{\Delta_{EOQ}}$, respectively, with the optimal average cost. In Tables 7 and 8, the first one is represented as $AC_{\Delta_{EOQ}}$ and the second one as AC^*.

When $K = 0$, independent from the values of h and c are, the approximation finds the optimal solution. That is, for such cases the optimality gap is 0.00%. However, as K increases, optimality gap increases for small values of h and c. But, optimality gap is still around 0.00% for moderate and large values of h and c even for large K values. Considering all the cases, average optimality gaps are calculated as 0.38% and 0.55% for Erlang-r and Uniform distributions, respectively. In conclusion, we believe that our approach performs well at different levels of cost parameters under different distributions.

Table 7. Impact of system cost parameters for Erlang-2

K	h	c	Δ^*	s^*	S^*	AC^*	Δ_{EOQ}	$s_{\Delta_{EOQ}}$	$S_{\Delta_{EOQ}}$	$AC_{\Delta_{EOQ}}$	Optimality Gap: $AC_{\Delta_{EOQ}}$ vs AC^*
0	1	1	1	0	1	1.50	1	0	1	1.50	0.00%
0	1	10	1	4	5	5.25	1	4	5	5.25	0.00%
0	1	20	1	6	7	7.52	1	6	7	7.52	0.00%
0	2	2	1	0	1	3.00	1	0	1	3.00	0.00%
0	2	20	1	4	5	10.50	1	4	5	10.50	0.00%
0	2	40	1	6	7	15.04	1	6	7	15.04	0.00%
0	3	3	1	0	1	4.50	1	0	1	4.50	0.00%
0	3	30	1	4	5	15.75	1	4	5	15.75	0.00%
0	3	60	1	6	7	22.56	1	6	7	22.56	0.00%
10	1	1	5	0	5	3.08	6	0	6	3.12	1.18%
10	1	10	6	2	8	5.93	6	2	8	5.93	0.00%
10	1	20	5	5	10	8.01	6	4	10	8.01	0.00%
10	2	2	4	0	4	5.19	4	0	4	5.19	0.00%
10	2	20	4	3	7	11.37	4	3	7	11.37	0.00%
10	2	40	4	5	9	15.66	4	5	9	15.66	0.00%
10	3	3	4	0	4	7.15	4	0	4	7.15	0.00%
10	3	30	4	3	7	16.75	4	3	7	16.75	0.00%
10	3	60	4	5	9	23.25	4	5	9	23.25	0.00%
20	1	1	7	0	7	3.74	9	0	9	3.98	6.54%
20	1	10	7	2	9	6.29	9	1	10	6.35	0.88%
20	1	20	7	4	11	8.28	9	3	12	8.33	0.55%
20	2	2	5	0	5	6.17	6	0	6	6.24	1.18%
20	2	20	6	2	8	11.87	6	2	8	11.87	0.00%
20	2	40	5	5	10	16.03	6	4	10	16.03	0.02%
20	3	3	5	0	5	8.38	5	0	5	8.38	0.00%
20	3	30	5	3	8	17.35	5	3	8	17.35	0.00%
20	3	60	5	5	10	23.68	5	5	10	23.68	0.00%

Table 8. Impact of system cost parameters for Uniform (0.1,0.9)

K	h	c	Δ^*	s^*	S^*	AC^*	Δ_{EOQ}	$s_{\Delta_{EOQ}}$	$S_{\Delta_{EOQ}}$	$AC_{\Delta_{EOQ}}$	Optimality Gap: $AC_{\Delta_{EOQ}}$ vs AC^*
0	1	1	1	0	1	1.50	1	0	1	1.50	0.00%
0	1	10	1	4	5	4.86	1	4	5	4.86	0.00%
0	1	20	1	6	7	6.89	1	6	7	6.89	0.00%
0	2	2	1	0	1	3.00	1	0	1	3.00	0.00%
0	2	20	1	4	5	9.72	1	4	5	9.72	0.00%
0	2	40	1	6	7	13.78	1	6	7	13.78	0.00%
0	3	3	1	0	1	4.50	1	0	1	4.50	0.00%
0	3	30	1	4	5	14.58	1	4	5	14.58	0.00%
0	3	60	1	6	7	20.67	1	6	7	20.67	0.00%
10	1	1	5	0	5	2.96	6	0	6	3.02	1.88%
10	1	10	6	2	8	5.52	6	2	8	5.52	0.00%
10	1	20	6	4	10	7.37	6	4	10	7.37	0.00%
10	2	2	4	0	4	5.02	4	0	4	5.02	0.00%
10	2	20	4	3	7	10.55	4	3	7	10.55	0.00%
10	2	40	4	5	9	14.39	4	5	9	14.39	0.00%
10	3	3	4	0	4	6.95	4	0	4	6.95	0.00%
10	3	30	4	3	7	15.56	4	3	7	15.56	0.00%
10	3	60	4	5	9	21.38	4	5	9	21.38	0.00%
20	1	1	6	0	6	3.58	9	0	9	3.88	8.34%
20	1	10	7	2	9	5.86	9	1	10	5.95	1.54%
20	1	20	7	4	11	7.64	9	3	12	7.71	0.95%
20	2	2	5	0	5	5.93	6	0	6	6.04	1.88%
20	2	20	6	2	8	11.03	6	2	8	11.03	0.00%
20	2	40	6	4	10	14.74	6	4	10	14.74	0.00%
20	3	3	5	0	5	8.11	5	0	5	8.11	0.00%
20	3	30	4	3	7	16.10	5	2	7	16.13	0.17%
20	3	60	4	5	9	21.78	5	4	9	21.78	0.00%

5. Conclusion

We study a single-product make-to-stock system with a single production resource, production start-up cost, lost-sales, general production times and Poisson demand arrivals. Production and inventory are controlled by the *two-critical-number policy*.

As the production start-up cost is negligible, we find the steady-state distribution of the system with a method using the analogy between the considered MTS queue and the capacitated M/G/1 queue. In addition, for the systems with production start-up cost, we develop a method that directly calculates the long-run expected average cost. Our method benefits from renewal and queueing theories. We calculate the cycle cost with a first passage analysis. This analysis provides a system of equations, which is solved in a recursive manner. On the other hand, cycle length is calculated using busy period analysis of capacitated M/G/1 queues: We show that the length of a production period can be written as the convolution of the lengths of capacitated M/G/1 busy periods. Furthermore, we propose a well-performing approximation for the difference between the control levels of the *two-critical-number policy*. Finally, with an extensive numerical study, impacts of production time distributions, traffic intensity, and production start-up, lost-sales and holding costs are discussed.

As a possible extension of the study, multi-product or multi-demand class systems can be considered. A more compelling extension, on the other hand, would be examining multi-server systems.

References

[1] Gavish, B., Graves, S.C., (1980). A one-product production/inventory problem under continuous review policy. *Operations Research*, 28(5), 1228-1236.

[2] Gavish, B., Graves, S.C., (1981). Production/inventory systems with a stochastic production rate under a continuous review policy. *Computers & Operations Research*, 8(3), 169-183.

[3] Lee, H.S. Srinivasan, M.M., (1987). *The continuous review (s, S) policy for production/inventory systems*

with Poisson demands and arbitrary processing times. Technical Report, 87-33.

[4] Graves, S.C., Keilson, J., (1981). The compensation method applied to a one-product production/inventory problem. *Mathematics of Operations Research*, 6(2), 246-262.

[5] Srinivasan, M.M., Lee, H.S., (1991). Random review production/inventory systems with compound Poisson demands and arbitrary processing times. *Management Science*, 37(7), 813-833.

[6] Altiok, T., (1989). (R, r) production/inventory systems. *Operations Research*, 37(2), 266-276.

[7] Tijms, H.C., (1980). An algorithm for average costs denumerable state semi-Markov decision problems with application to controlled production and queueing system. In R. Hartley, L. C. Thomas, & D. J. White, Recent developments in Markov decision processes (pp. 143-179), Academic Press.

[8] Heyman, D. P., (1968). Optimal operating policies for M/G/1 queuing systems. *Operations Research*, 16(2), 362-382.

[9] Sobel, M.J., (1969). Optimal average-cost policy for a queue with start-up and shut-down costs. *Operations research*, 17(1), 145-162.

[10] De Kok, A.G., Tijms, H.C., Van der Duyn Schouten, F.A., (1984). Approximations for the single-product production-inventory problem with compound Poisson demand and service-level constraints. *Advances in Applied Probability*, 16(2), 378-401.

[11] De Kok, A.G., (1985). Approximations for a lost-sales production/inventory control model with service level constraints. *Management Science*, 31(6), 729-737.

[12] De Kok, A.G., Tijms, H.C., (1985). A stochastic production/inventory system with all-or-nothing demand and service measures. *Communications in Statistics. Stochastic Models*, 1(2), 171-190.

[13] De Kok, A.G., (1987). Approximations for operating characteristics in a production-inventory model with variable production rate. *European journal of operational research*, 29(3), 286-297.

[14] Lin, H.J., (2017). Two-critical-number control policy for a stochastic production inventory system with partial backlogging. *International Journal of Production Research*, 55(14), 4123-4135.

[15] Ha, A.Y., (1997a). Inventory rationing in a make-to-stock production system with several demand classes and lost sales. *Management Science*, 43(8), 1093-1103.

[16] Bulut, Ö., Fadiloğlu, M.M., (2011). Production control and stock rationing for a make-to-stock system with parallel production channels. *IIE Transactions*, 43(6), 432-450.

[17] Özkan, S., Bulut, Ö. (2020). Control of make-to-stock production systems with setup costs. *Journal of the Faculty of Engineering and Architecture of Gazi University*, 35(3), 1199-1212.

[18] Ha, A.Y., (1997b). Stock-rationing policy for a make-to-stock production system with two priority classes and backordering. *Naval Research Logistics (NRL)*, 44(5), 457-472.

[19] De Véricourt, F., Karaesmen, F., Dallery, Y., (2002). Optimal stock allocation for a capacitated supply system. *Management Science*, 48(11), 1486-1501.

[20] Ha, A.Y., (2000). Stock rationing in an M/Ek/1 make-to-stock queue. *Management Science*, 46(1), 77-87.

[21] Gayon, J.P., De Vericourt, F., Karaesmen, F., (2009). Stock rationing in an M/Er/1 multi-class make-to-stock queue with backorders. *IIE Transactions*, 41(12), 1096-1109.

[22] Pang, Z., Shen, H., Cheng, T.C.E., (2014). Inventory Rationing in a Make-to-Stock System with Batch Production and Lost Sales. *Production and Operations Management*, 23(7), 1243-1257.

[23] Yücel, Ö., Bulut, Ö., (2019). Control of M/Cox-2/s make-to-stock systems. *An International Journal of Optimization and Control: Theories & Applications (IJOCTA)*, 10(1), 26-36.

[24] Pervin, M., Roy, S.K., Weber, G.W. (2018). Analysis of inventory control model with shortage under time-dependent demand and time-varying holding cost including stochastic deterioration. *Annals of Operations Research*, 260(1), 437-460.

[25] Tirkolaee, E.B., Goli, A., Weber, G.W. (2019). Multi-objective aggregate production planning model considering overtime and outsourcing options under fuzzy seasonal demand. In *International Scientific-Technical Conference Manufacturing*, (pp. 81-96). Springer, Cham.

[26] Lotfi, R., Weber, G.W., Sajadifar, S.M., Mardani, N. (2020). Interdependent demand in the two-period newsvendor problem. *Journal of Industrial & Management Optimization*, 16(1), 117-140.

[27] Paksoy, T., Özceylan, E., Weber, G.W. (2010). A multi objective model for optimization of a green supply chain network. In *AIP conference proceedings* (Vol. 1239, No. 1, pp. 311-320). American Institute of Physics.

[28] Bose, S. K. (2002). Basic Queueing Theory. In *An Introduction to Queueing Systems* (pp. 9-54). Springer, Boston, MA.

Sinem Özkan *received her MSc degree from the Industrial Engineering Department of Yaşar University in 2016. She has been continuing her PhD studies in the same department since 2016. Her research interests include production/inventory systems and stochastic modeling.*

http://orcid.org/0000-0002-7181-5800

Önder Bulut *is Assistant Professor in the Department of Industrial Engineering at Yaşar University. He received his Ph.D. degree from the Industrial Engineering Department of Bilkent University. His research interests include stochastic modeling, production and inventory systems, simulation, dynamic programming and optimal control.*

http://orcid.org/0000-0003-1476-6333

An International Journal of Optimization and Control: Theories & Applications (http://ijocta.balikesir.edu.tr)

An International Journal of Optimization and Control: Theories & Applications
ISSN:2146-0957 eISSN:2146-5703
Vol.12, No.1, pp.20-38 (2022)
http://doi.org/10.11121/ijocta.2022.1108

RESEARCH ARTICLE

Theory and applications of new fractional-order chaotic system under Caputo operator

Ndolane Sene*

Département de Mathématiques de la Décision, Faculté des Sciences Economiques et Gestion, Université Cheikh Anta Diop de Dakar, Dakar Fann, Senegal
ndolanesene@yahoo.fr

ARTICLE INFO

Article History:
Received 6 May 2021
Accepted 16 August 2021
Available 27 October 2021

Keywords:
Phase portraits
Fractional-order chaotic system
Attractors
Lyapunov exponents
Chaotic behavior

AMS Classification 2010:
34C28; 37D45; 26A33

ABSTRACT

This paper introduces the properties of a fractional-order chaotic system described by the Caputo derivative. The impact of the fractional-order derivative has been focused on. The phase portraits in different orders are obtained with the aids of the proposed numerical discretization, including the discretization of the Riemann-Liouville fractional integral. The stability analysis has been used to help us to delimit the chaotic region. In other words, the region where the order of the Caputo derivative involves and where the presented system in this paper is chaotic. The nature of the chaos has been established using the Lyapunov exponents in the fractional context. The schematic circuit of the proposed fractional-order chaotic system has been presented and simulated in via Mutltisim. The results obtained via Multisim simulation of the chaotic circuit are in good agreement with the results with Matlab simulations. That provided the fractional operators can be applied in real- worlds applications as modeling electrical circuits. The presence of coexisting attractors for particular values of the parameters of the presented fractional-order chaotic model has been studied.

1. Introduction

The applications of fractional operators in modeling real-world problems continue to receive many impressions. In the literature, there exist many investigations, including fractional operators in mathematical physics [1–3], physics [4], science and engineering [4–6] and many other domains [7]. Modeling using fractional operators is nowadays preferred to modeling with integer-order derivative because it is mentioned in the literature that fractional operators consider memory effects and generalize the classical derivative. The Caputo derivative [1, 8] receive more much interest because the classical initial condition used in physics can also be used. The Riemann-Liouville derivative is not physical tools because the initial conditions of the model problem should be in integral form. It is the main inconvenience in physics to have an initial condition in integral form. In the last ten years, there exist some interest in modeling chaotic systems using fractional-order derivatives. Theory of chaos in fractional context begin to receive attractions [9–11]. The reasons are, with the variation of the order of the used derivative, we can conserve or lost chaotic behaviors of the systems. Many new attractors born also with the fractional operators, see in [12–15]. Another reason is the definitions used to characterize the nature of the chaos. For example, in a fractional context, there exist hyperchaotic systems with one positive Lyapunov exponent.

Before the motivations and the works described in this paper, we give a brief literature review concerning modeling chaotic systems with and without fractional-order derivative. Recently, Sene et al. introduce several fractional chaotic systems via Caputo derivative and study their phase

*Corresponding Author

portraits, bifurcations diagrams, Lyapunov exponents, sensitivity to the initial conditions, and influence of the fractional orders in obtaining new types of attractors, see in the following investigations [11, 14, 16–18]. In [13], In the fractional context, Pacheco et al. introduce and investigate fractional chaotic systems with hidden and self-excited attractors. Akgul in [12] study chaotic oscillations using fractional operator memcapacitor. In this paper [12], the auteur draws the circuit schematic associated with the proposed fractional chaotic system and simulates it and proved the experimental results are in good agreement with the result obtained with the numerical scheme. Akgul and al. have also introduced many other chaotic systems where they use fractional operators; the readers can read the following investigations by the same author [19, 20]. The fractional-order chaotic systems with non-singular kernels have been recently introduced in the following papers [10, 21]. In [22], Rajagopal et al. presented a multi-scroll chaotic system with sigmoid nonlinearity and have proposed the fractional context of their model; they notably investigate with Caputo fractional derivative and the predictor-corrector method of Adams-Bashforth-Moulton to obtain the phase portraits. For more investigations by Rajagopal in the fractional chaotic systems, look to [23]. For a fractional-order chaotic system with conformable derivative, the readers can refer to Perez works in the following paper [9]. In [24], Ruiz et al. have used the variable-order fractional derivative, which is a very novel operator to model fractional chaotic system. In [25], Danca stipulated the definition saying; we have hyperchaotic behaviors with two positive Lyapunov exponents; this definition seems not adequate in fractional context because there exist fractional hyperchaotic systems with one positive Lyapunov exponent. This conclusion addressed by Danca opens new problems in modeling a chaotic system with fractional operators. See more investigations in chaotic systems in [26].

In this paper, we propose modeling a chaotic system using the fractional operator. Motivated by the initial condition, we use the Caputo derivative in our modeling. In this paper, we will focus on the influence of the Caputo derivative in the dynamics of our considered chaotic system. The main question will be to determine the chaotic region and simulate the fractional chaotic system in Multisim using the circuit schematic of our proposed chaotic system. Note that the circuit schematic will include the capacitors and resistors, and other electrical tools. After modeling, we will study the influence generated by the variation of the model's parameters via the bifurcation diagrams on the dynamics of our chaotic system. We will confirm the chaotic region by calculating the Lyapunov exponents. It will be established our considered chaotic system is dissipative as well. The local stability of the equilibrium points of our system will be illustrated via the Matignon criterion.

2. On fractional operators in fractional calculus

We recall the fractional operators which we will utilize in this paper. There exist many types of fractional operators which can be classified into two families; the first family is the fractional operators with the singular kernels: Caputo derivative and Riemann-Liouville derivative, and the second family is composed of the fractional operators with nonsingular kernels: the fractional derivative with exponential kernel and the fractional derivative with Mittag-Leffer kernel. Many other operators exist in fractional calculus, but here we consider the operators with a great audience and englobing all the papers in the literature. Therefore the rest of the paper, we recall the Caputo derivative, the Riemann-Liouville derivative, the Riemann-Liouville integral, and the Laplace transform of the Caputo derivative.

We begin by defining the fractional integral known as the name Riemann-Liouville fractional integral, which will be used to establish the numerical scheme utilized in this paper.

Definition 1. *[1, 8] The Riemann-Liouville integral of a considered function* $m : [0, +\infty[\longrightarrow \mathbb{R}$ *is*

$$\left(I^{\alpha} m\right)(t) = \frac{1}{\Gamma(\alpha)} \int_0^t (t-s)^{\alpha-1} m(s) ds, \quad (1)$$

where we define the function $\Gamma(...)$ *as the Gamma Euler function and we set also the order* $\alpha > 0$.

The above derivative is generalized in the following definition established in the literature by Thabet and Fahd in [7].

Definition 2. *[7] The generalized Riemann-Liouville fractional integral of a given function* $m : [0, +\infty[\longrightarrow \mathbb{R}$ *is defined by*

$$I^{\alpha,\rho} m(t) = \frac{1}{\Gamma(\alpha)} \int_0^t \left(\frac{t^{\rho} - s^{\rho}}{\rho}\right)^{\alpha-1} m(s) \frac{ds}{s^{1-\rho}}, \quad (2)$$

with the orders defined as α, *and* ρ *satisfying in particular the condition* α, $\rho > 0$, *the Gamma function is denoted by* $\Gamma(...)$, *and for all* $t > 0$.

The classical Riemann-Liouville derivative is obtained when the orders of the generalized fractional derivative satisfy the condition $\alpha = \rho = 1$. We now define the Caputo derivative, which will be used in modeling the chaotic system studied in this paper. The choice is due to its initial condition, which is physic, and the memory effect generated by the Caputo derivative.

Definition 3. *[1,8] The Caputo fractional derivative of order α satisfying the condition $\alpha \in (0,1)$, for the function $m : [0,+\infty[\longrightarrow \mathbb{R}$ is defined by the function*

$$D_c^{\alpha} m(t) = \frac{1}{\Gamma(1-\alpha)} \int_0^t (t-s)^{-\alpha} m'(s) ds, \quad (3)$$

where the Gamma Euler function is represented the function $\Gamma(...)$.

The generalization of the Caputo derivative is also introduced in the literature by Thabet and Jarad, and the following definition defines it.

Definition 4. *[7] The generalized form of the Caputo derivative of order α satisfying the condition $\alpha \in (0,1)$, is described for the the function $m : [0,+\infty[\longrightarrow \mathbb{R}$ by the form*

$$D^{\alpha,\rho} m(t) = \frac{1}{\Gamma(1-\alpha)} \int_0^t \left(\frac{t^{\rho} - s^{\rho}}{\rho} \right)^{-\alpha} m'(s) ds, \quad (4)$$

with the orders α, and ρ satisfying the relations $\alpha \in (0.1)$, $\rho > 0$, the Gamma function denoted by $\Gamma(...)$., and for all $t > 0$.

The Caputo derivative also admits the Laplace transform and obeys many properties, which can be found in the literature of the fractional calculus. We advise the reader to take a look at the following investigations [1,8], in details.

3. Fractional-order attractor system

A new fractional chaotic system is addressed in this section. The fractional differential equations satisfied by this new chaotic system using the Caputo derivative is described as the following form

$$\begin{aligned} D_c^{\alpha} x &= dx - yz, & (5)\\ D_c^{\alpha} y &= e - ay + xz + cy, & (6)\\ D_c^{\alpha} z &= -bz + xy. & (7) \end{aligned}$$

The chaotic system is sensitive to the initial conditions. In the present work, the chaotic behaviors are obtained using the following initial conditions

$$x(0) = x_0 = 1, y(0) = y_0 = 1, z(0) = z_0 = 1. \quad (8)$$

Later the impact of the initial conditions in the dynamics will be focused. The strange attractor is obtained with the values of the parameters of the model described by the system (5)-(7) set as the forms $a = 9$, $b = 4$, $c = 1.5$, $d = 2.85$, and $e = 0.2$. The values of the parameters of the chaotic systems also play a significant role in the attractors. In other words, the variation of the model's parameters can generate the removal of the chaotic behaviors. There exist many fractional operators in fractional calculus, here we opted to use the Caputo derivative due to the fact, it takes into account the memory effect, and the derivative takes into account also the initial conditions in form (8), contrary to the Riemann-Liouville derivative where the initial conditions should be in an integral form which is irrealistic in real-world problems. Another main motivation for the use of fractional operators is, in general, in the chaotic system, they generate new types of attractors according to their variations in specific intervals. The interval where the fractional chaotic system has chaotic behaviors will be determined with the Matignon criterion in the present paper.

The next section will be the subject of the numerical approximation. The numerical algorithm will be used to depict the phase portraits of the present chaotic system. The last remark in this section is that when the order $\alpha = 1$, then we obtain the following chaotic system defined by the equations

$$\begin{aligned} x' &= dx - yz, & (9)\\ y' &= e - ay + xz + cy, & (10)\\ z' &= -bz + xy. & (11) \end{aligned}$$

The same initial conditions (8) are considered for the model (9)-(11) with integer-order derivative. Model (9)-(11) will not be considered in this section. Still, it is important to mention that all classical models with an integer-order derivative can be obtained when the fractional operators converge to 1..

4. Numerical procedure of the fractional chaotic system

In this section, we recall the numerical discretizations which we will use to depict the phase portraits of the present model. Numerical discretization exists in the literature; here, we describe the numerical discretization for our present model. We begin with the analytical solution of the model, which can be represented using the Riemann-Liouville integral; we have the following form

$$x(t) = x(0) + I^{\alpha}\varpi(t,v), \quad (12)$$
$$y(t) = y(0) + I^{\alpha}\kappa(t,v), \quad (13)$$
$$z(t) = z(0) + I^{\alpha}\omega(t,v). \quad (14)$$

Where $v = (x, y, z)$. The functions ϖ, κ and ω come from the primary model described in Eq. (5)-(7). Therefore, we have the following forms

$$\varpi(t,v) = dx - yz, \quad (15)$$
$$\kappa(t,v) = e - ay + xz + cy, \quad (16)$$
$$\omega(t,v) = -bz + xy. \quad (17)$$

Before beginning the discretization of the Riemann-Liouville integral at the point t_n, we evaluate Eqs. (12)-(14) at this point t_n, we have the following representations

$$x(t_n) = x(0) + I^{\alpha}\varpi(t_n,v), \quad (18)$$
$$y(t_n) = y(0) + I^{\alpha}\kappa(t_n,v), \quad (19)$$
$$z(t_n) = z(0) + I^{\alpha}\omega(t_n,v). \quad (20)$$

Let the step size h, and we define $t_n = nh$, the Riemann-Liouville integral can be written as the following equations for the functions ϖ,κ and ω

$$I^{\alpha}\varpi(t_n,v) = h^{\alpha}\sum_{j=1}^{n} d_{n-j}\varpi(t_j,v_j), \quad (21)$$
$$I^{\alpha}\kappa(t_n,v) = h^{\alpha}\sum_{j=1}^{n} d_{n-j}\kappa(t_j,v_j), \quad (22)$$
$$I^{\alpha}\omega(t_n,v) = h^{\alpha}\sum_{j=1}^{n} d_{n-j}\omega(t_j,v_j), \quad (23)$$

with the parameters given as the following forms

$$d_{n-j} = ((n-j+1)^{\alpha} - (n-j)^{\alpha})/\frac{1}{\Gamma(1+\alpha)}$$

and

$$d_n = ((n+1)^{\alpha} - (n)^{\alpha})/\frac{1}{\Gamma(1+\alpha)}.$$

We consider the first-order interpolant polynomial of the functions $\varpi(\tau)$, $\kappa(\tau)$ and $\omega(\tau)$ represented as the following relationships [27]

$$\varpi(\tau) = \varpi(t_{j+1}, v_{j+1}) + \frac{\tau - t_{j+1}}{h}\left[\varpi(t_{j+1}, v_{j+1}) - \varpi(t_j, v_j)\right], \quad (24)$$

$$\kappa(\tau) = \kappa(t_{j+1}, v_{j+1}) \frac{\tau - t_{j+1}}{h}\left[\kappa(t_{j+1}, v_{j+1}) - \kappa(t_j, v_j)\right], \quad (25)$$

$$\omega(\tau) = \omega(t_{j+1}, v_{j+1}) \frac{\tau - t_{j+1}}{h}\left[\omega(t_{j+1}, v_{j+1}) - \omega(t_j, v_j)\right]. \quad (26)$$

Plugin Eqs. (24)-(26) into the Eqs. (21)-(23), we obtain the following representations of the discretizations of the Riemann-Liouville integrals, we have that

$$I^{\alpha}\varpi(t_n,v) = h^{\alpha}\left[\bar{d}_n^{(\alpha)}\varpi(0) + \sum_{j=1}^{n} d_{n-j}^{(\alpha)}\varpi(t_j,v_j)\right], \quad (27)$$

$$I^{\alpha}\kappa(t_n,v) = h^{\alpha}\left[\bar{d}_n^{(\alpha)}\kappa(0) + \sum_{j=1}^{n} d_{n-j}^{(\alpha)}\kappa(t_j,v_j)\right], \quad (28)$$

$$I^{\alpha}\omega(t_n,v) = h^{\alpha}\left[\bar{d}_n^{(\alpha)}\omega(0) + \sum_{j=1}^{n} d_{n-j}^{(\alpha)}\omega(t_j,v_j)\right], \quad (29)$$

under the parameters set explicitly as the following representations

$$\bar{d}_n^{(\alpha)} = \frac{(n-1)^{\alpha} - n^{\alpha}(n-\alpha-1)}{\Gamma(2+\alpha)}, \quad (30)$$

and when $n = 1, 2, ...$, the parameters d of the discretization can be rewritten as the following equations

$$d_0^{(\alpha)} = \frac{1}{\Gamma(2+\alpha)} \text{ and}$$
$$d_n^{(\alpha)} = \frac{(n-1)^{\alpha+1} - 2n^{\alpha+1} + (n+1)^{\alpha+1}}{\Gamma(2+\alpha)}. \quad (31)$$

Finally, under the above representations, then the numerical scheme of the fractional differential equation (5)-(7) under consideration is represented by the following relationships

$$x(t_n) = x(0) + h^{\alpha}\left[\bar{d}_n^{(\alpha)}\varpi(0) + \sum_{j=1}^{n}\kappa_{n-j}^{(\alpha)}\varpi(t_j, v_j)\right], \tag{32}$$

$$y(t_n) = y(0) + h^{\alpha}\left[\bar{d}_n^{(\alpha)}\kappa(0) + \sum_{j=1}^{n}\kappa_{n-j}^{(\alpha)}\kappa(t_j, v_j)\right], \tag{33}$$

$$z(t_n) = z(0) + h^{\alpha}\left[\bar{d}_n^{(\alpha)}\omega(0) + \sum_{j=1}^{n}\kappa_{n-j}^{(\alpha)}\omega(t_j, v_j)\right]. \tag{34}$$

The numerical discretization of the functions ϖ, κ and ω are represented in the following equations

$$\varpi(t_j, v_j) = dx_j - y_j z_j, \tag{35}$$
$$\kappa(t_j, v_j) = e - ay_j + x_j z_j + cy_j, \tag{36}$$
$$\omega(t_j, v_j) = -bz_j + x_j y_j. \tag{37}$$

The convergence and the stability are not detailed in this section; see in for more pieces of information [27]; here, we give pieces of information related to these two properties. We assume that $x(t_n), y(t_n)$ and $z(t_n)$ are the approximate numerical solutions of the fractional system represented in Eq. (5)-(7) and x_n, y_n and z_n are the exact solutions, the residuals functions with Caputo derivative are given by the expressions

$$|x(t_n) - x_n| = \mathcal{O}\left(h^{\min\{\alpha+1,2\}}\right), \tag{38}$$
$$|y(t_n) - y_n| = \mathcal{O}\left(h^{\min\{\alpha+1,2\}}\right), \tag{39}$$
$$|z(t_n) - z_n| = \mathcal{O}\left(h^{\min\{\alpha+1,2\}}\right). \tag{40}$$

We can notice the convergence of the numerical discretization presented in this section is obtained when the step-size h converges 0 [27]. The stability of our numerical scheme is obtained from the Lipchitz criterion of the functions u, v, and w.

We finish this part by illustrating the numerical scheme described in this section. We consider for graphical representations the orders $\alpha = 0.86$, $\alpha = 0.94$ and $\alpha = 0.97$. We begin by the order $\alpha = 0.86$, we depict by the phase portraits in all planes $(x-y-z)$, $(x-y)$, $(x-z)$ and $(y-z)$. We have the following Figures 1a-1b,2a-2b.

Let the order of the Caputo derivative given by $\alpha = 0.94$, we draw by the phase portraits in all planes $(x-y-z)$, $(x-y)$, $(x-z)$ and $(y-z)$. We have the Figures 3a-3b, 4a-4b.

We continue with the order of the Caputo derivative defined by $\alpha = 0.97$, we depict the phase portraits in all planes $(x-y-z)$, $(x-y)$, $(x-z)$ and $(y-z)$. We have the following Figures 5a,5b,6a,6b.

5. Bifurcation maps for detecting chaotic regions

In this section, we address the chaotic regions according to the variations of the parameters of the model. For the rest of the paper, we consider the order of the fractional derivative fixed to $\alpha = 0.97$. We first consider the variation of the parameters a into the interval $(8, 12)$. We consider a small step-size $h = 0.0025$ to see the structure of the curve. The bifurcation map related to the parameter a is represented in the Figure 7.

The chaotic region can be observed into the interval $(8.8, 12)$. The system enters this region via period-doubling bifurcation. Into the interval $(8, 8.8)$, we notice the presence of limits cycles. The sectors of limit cycles are divided into two regions which are the region $(8, 8.4)$ and the region $(8.4, 8.8)$ as it can be observed in Figure7. For illustrations of the chaotic behaviors, we consider the parameter $a = 10.2$ and calculate the Lyapunov exponents associated with this parameter value.

In the second part, we consider the parameter b. We suppose it varies into the interval $(1, 4.5)$. The considered step-size for clarity is $h = 0.0025$. The bifurcation map associated to the small variation of the parameter b can be observed in Figure 10.

We notice the system ends the chaotic region in the interval $(4, 4.2)$ via period-doubling bifurcation. The region $(4.2, 4.5)$ corresponds to our present fractional model to the periodic region. The chaotic region is observed into the interval $(1, 4.2)$. For illustrations of the chaotic behaviors, we consider $b = 3.8$, and we calculate the Lyapunov exponents to confirm the chaotic behaviors when the parameter b takes this value.

We consider the variation of the parameter c in a small interval $(1, 2)$. The objective is to repeat the previous method to detect the chaotic region. The bifurcation map according to the variation of the parameter c is represented in Figure13.

In Figure 13 we observe the chaotic region is into the interval $(1, 1.7)$. After this region, we get periodic behaviors for our fractional model. For the Figure 13 the considered step-size is $h = 0.005$. We can also notice the chaotic behaviors of the system in the chaotic region is not uniform; in the interval $(1, 1.575)$ and $(1.575, 1.7)$, the behaviors of the system are different.

Let us consider the variation of the parameter d in a small interval $(2, 3.5)$. The bifurcation map

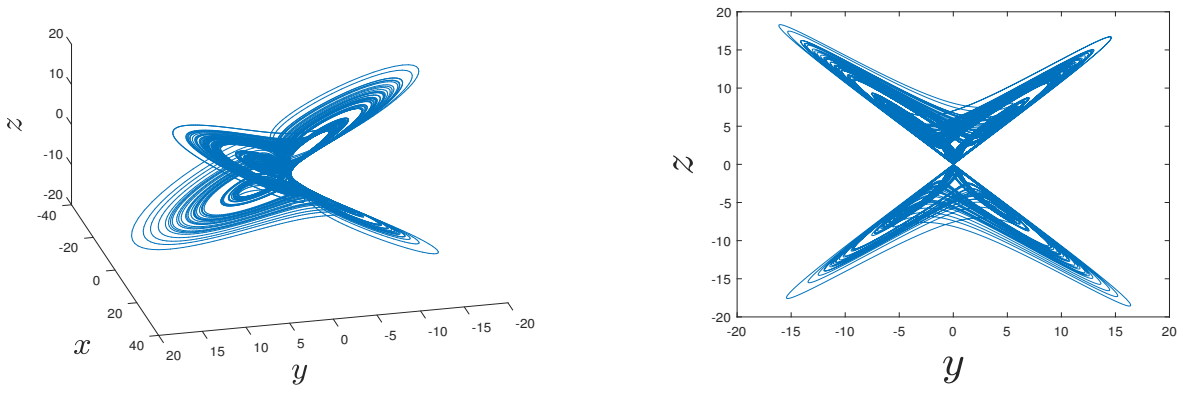

(a) **(b)**

Figure 1. $(x-y-z)$ and $(y-z)$ plane with the order $\alpha = 0.86$ for Eqs. (5)-(7).

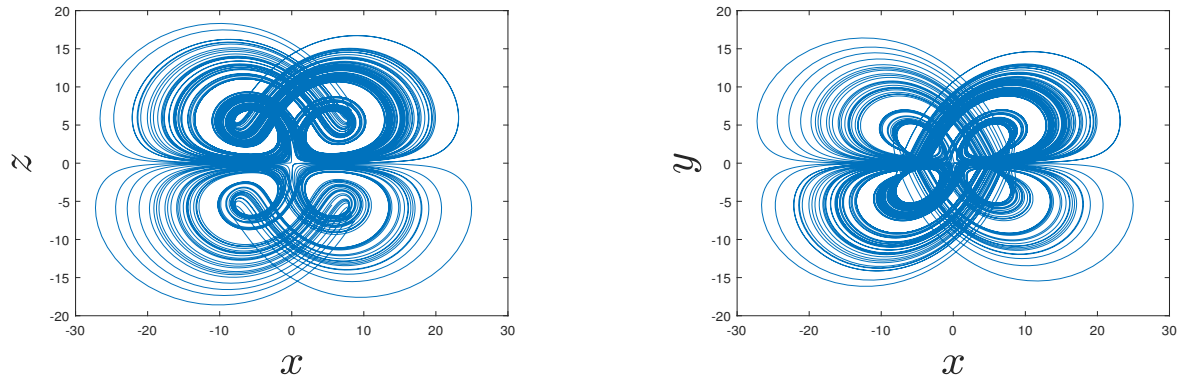

(a) **(b)**

Figure 2. $(x-y)$ and $(x-z)$ planes with the order $\alpha = 0.86$ for Eqs. (5)-(7).

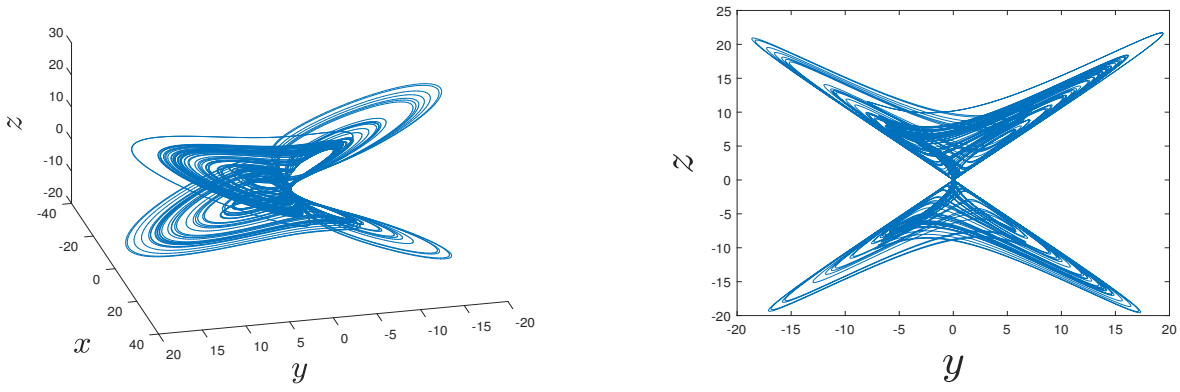

(a) **(b)**

Figure 3. $(x-y-z)$ and $(y-z)$ plane with the order $\alpha = 0.94$ for Eqs. (5)-(7).

versus the variation of the parameter d is represented in Figure 14.

The first remark is there exists a minor difference in the influence of parameter c and the parameter d. In our interval of variation, the chaotic region is observed into the interval $(2, 2.9)$. The periodic behaviors are observed in the rest of the interval. The main interest of this section is we can observe the chaotic region can be divided into two sections. The section $(2, 2.87)$ and $(2.87, 2.9)$ where the dynamics of the solutions are different as it can be observed in Figure 14. For illustrations of this difference we consider the phase portrait at $a = 2.65$ and $a = 2.875$.

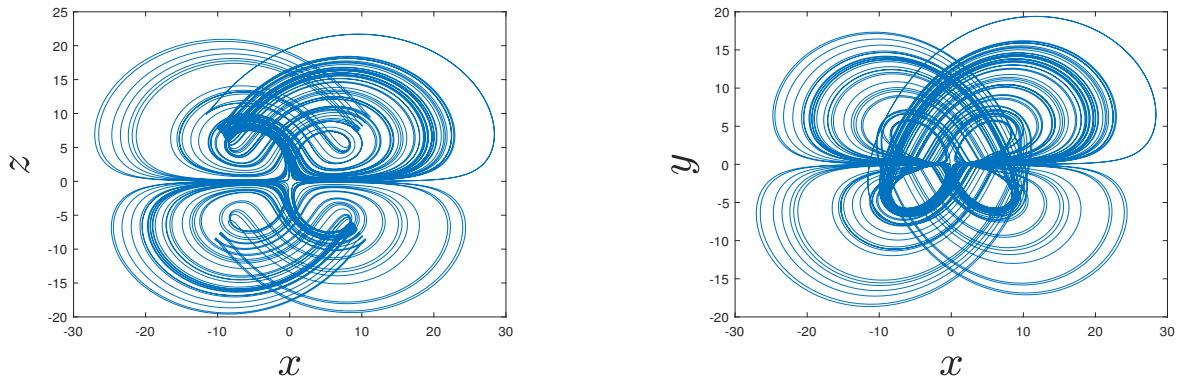

(a) (b)

Figure 4. $(x-y)$ and $(x-z)$ planes with the order $\alpha = 0.94$ for Eqs. (5)-(7).

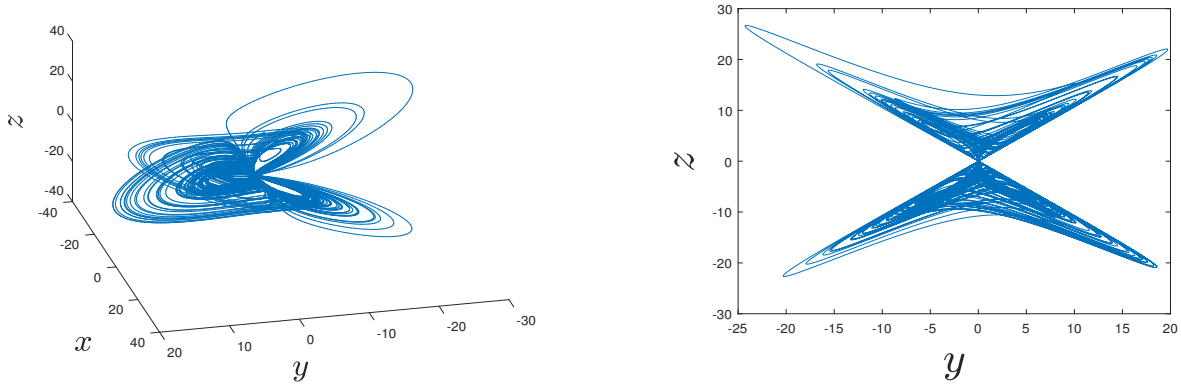

(a) (b)

Figure 5. $(x-y-z)$ and $(y-z)$ plane with the order $\alpha = 0.97$ for Eqs. (5)-(7).

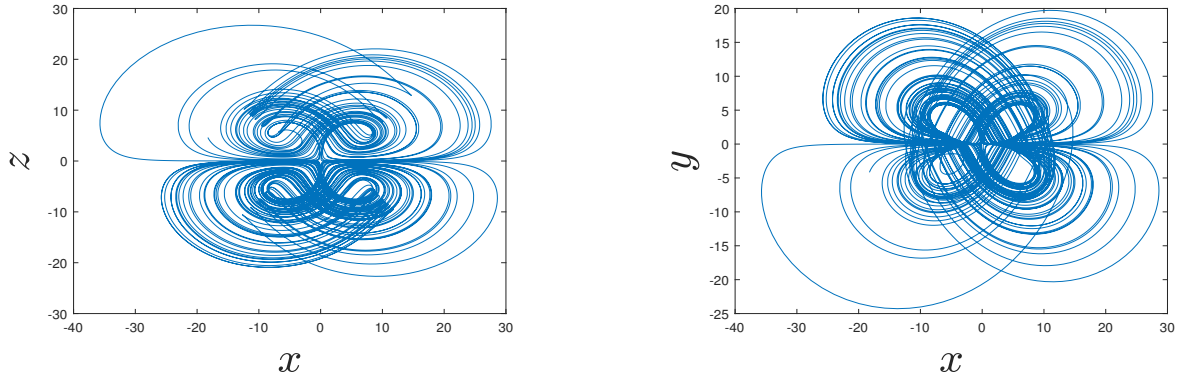

(a) (b)

Figure 6. $(x-y)$ and $(x-z)$ planes with the order $\alpha = 0.97$ for Eqs. (5)-(7).

6. Co-existing attractors for the fractional model

In this section, we illustrate the existence of a pair of attractors at two different initial conditions by considering the variation of the model's parameters (5)-(7). The considered initial conditions in this section are $(1,1,1)$ and $(-1,-1,-1)$. In the literature, the notion of coexisting attractors is present when at least two initial conditions are considered, and the parameters vary into a certain interval. According to the variation of the model's parameters, when the existence of a pair of attractors exists, it can also be observed via the bifurcation maps. Therefore this section will

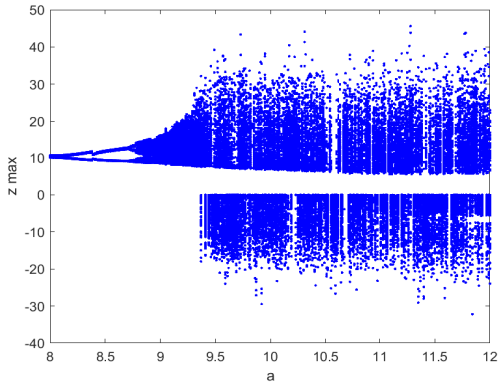

Figure 7. Bifurcation map according to the parameter a at order $\kappa = 0.97$.

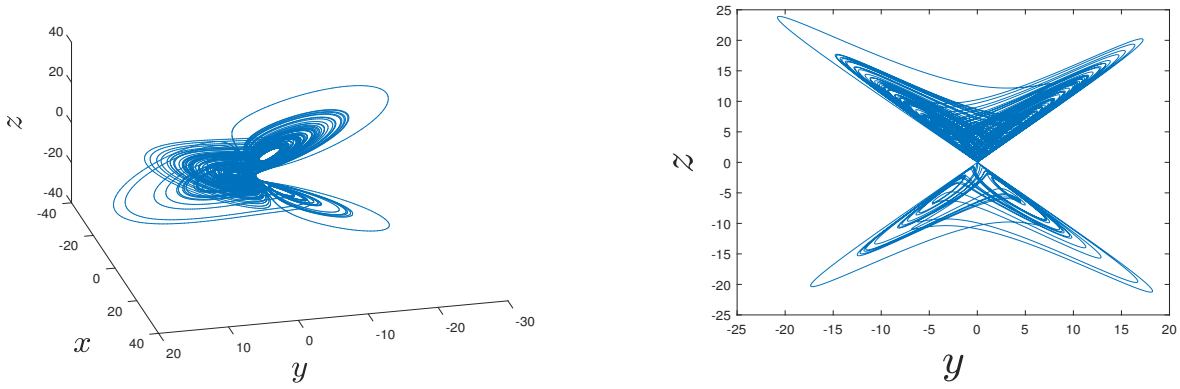

(a) **(b)**

Figure 8. $(x - y - z)$ and $(y - z)$ plane with the order $\alpha = 0.97$ for Eqs. (5)-(7).

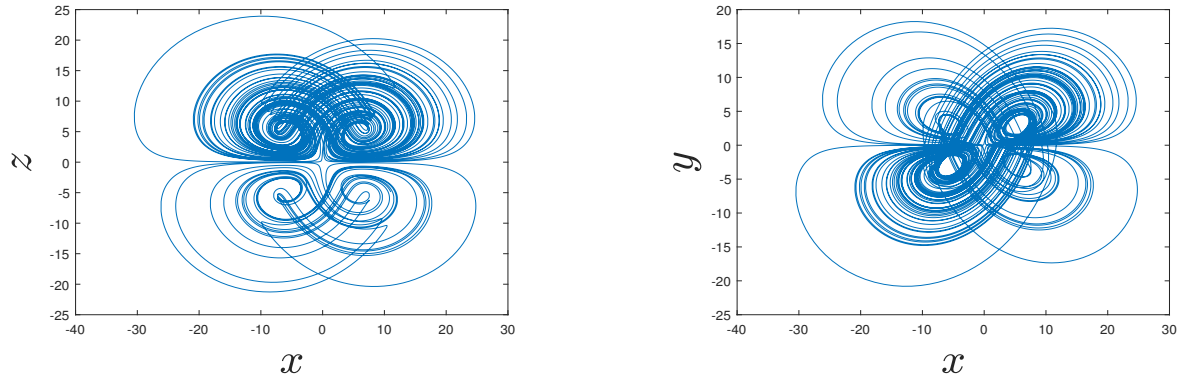

(a) **(b)**

Figure 9. $(x - y)$ and $(x - z)$ planes with the order $\alpha = 0.97$ for Eqs. (5)-(7).

be consecrated to observe the coexisting attractors via the bifurcations maps. We will also represent some phase portraits to support the findings of this section. We start with the variation of the parameter a. The coexisting bifurcation map according to the variation of the parameter a into the interval $(8, 11)$ with the initial condition $(1, 1, 1)$ and $(-1, -1, -1)$ are represented in Figure 19. We consider large intervals to observe clearly the coexisting attractor.

Via the bifurcation map, we can observe according to the variation of the parameter a, the system admits coexisting attractors into the interval $(8.8, 9.5)$. Into this interval, the pair of attractors can not be confused contrary to the interval

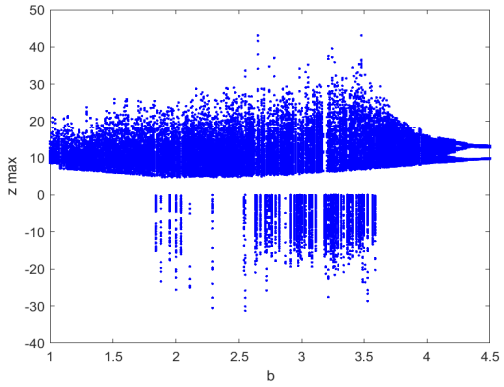

Figure 10. Bifurcation map according to the parameter b at order $\kappa = 0.97$.

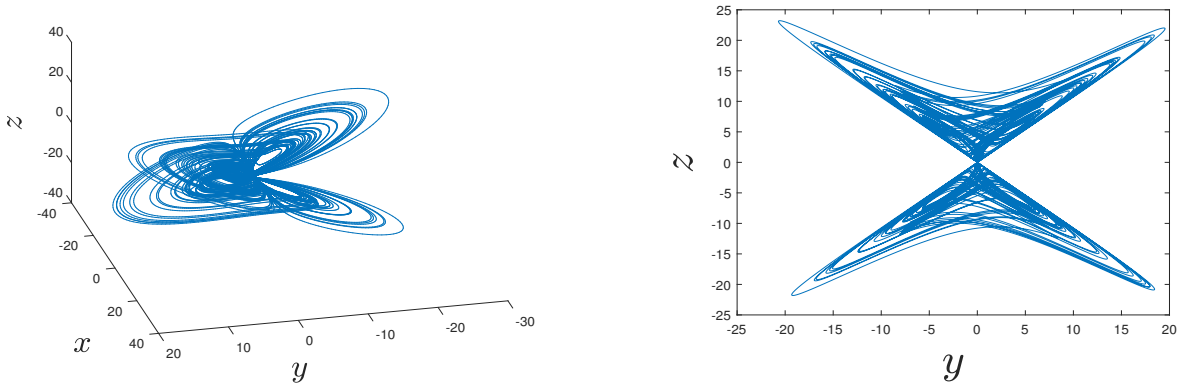

(a) **(b)**

Figure 11. $(x - y - z)$ and $(y - z)$ plane with the order $\alpha = 0.97$ for Eqs. (5)-(7).

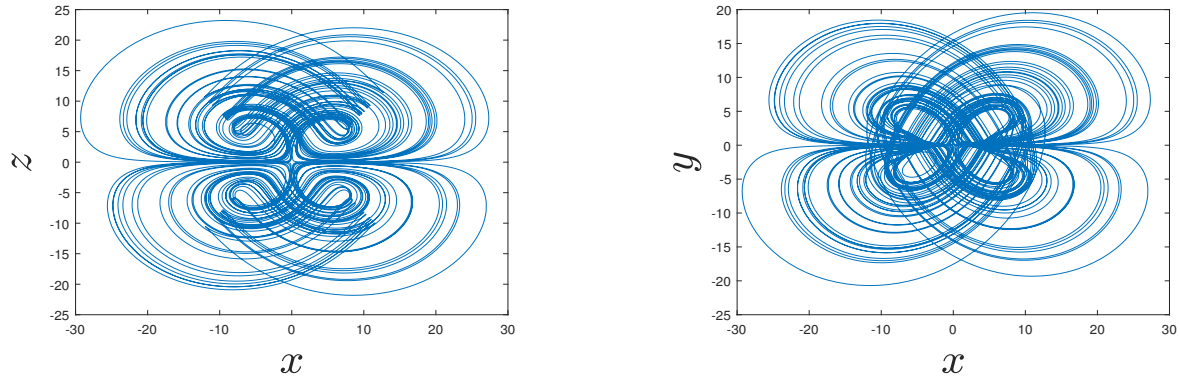

(a) **(b)**

Figure 12. $(x - y)$ and $(x - z)$ planes with the order $\alpha = 0.97$ for Eqs. (5)-(7).

$(9.5, 11)$ where there exist coexisting attractors, but the attractors are confused. For illustrations of the coexisting attractors, we consider $a = 9.2$ and $a = 10$.

In Figures 20a-20b, 21a-21b we are in the region where the coexisting attractors are clearly visible. We mean the region $(8.8, 9.5)$. After this interval, the coexisting attractors are confused, as can be seen in the following figures at $a = 10$.

Similarly, we can provide the coexisting attractors for the other parameters of the model b and c. We finish this section by providing the coexisting attractors with the parameter b. Therefore we depict the coexisting bifurcation map according to the variation of the parameter b and taken at two different initial conditions $(1, 1, 1)$ and $(-1, -1, -1)$. The considered interval for the

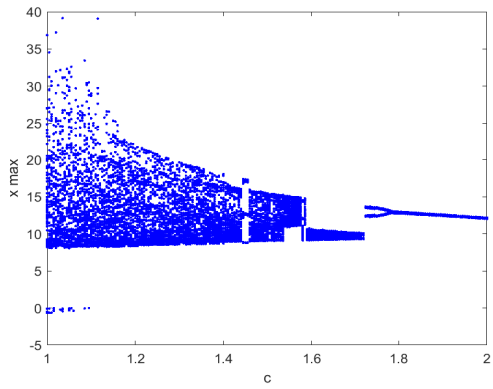

Figure 13. Bifurcation map according to the parameter c at order $\kappa = 0.97$.

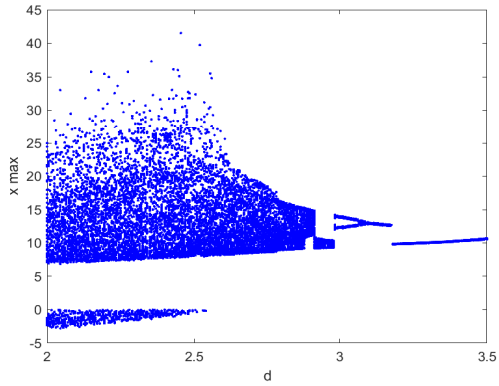

Figure 14. Bifurcation map according to the parameter d at order $\kappa = 0.97$.

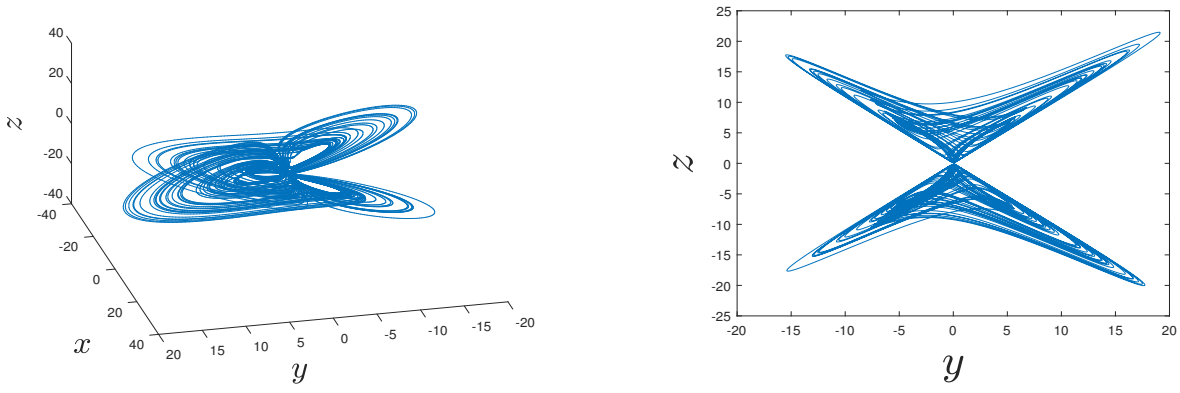

(a) **(b)**

Figure 15. Portrait of phase with the order $\alpha = 0.97$ and $a = 2.65$.

variation of parameter b is extended into the interval $(1, 4.5)$ for more visibility.

In Figure 23, we can observe the coexisting attractors are more visible. That means into the chaotic region $(1, 4.2)$ the pair of attractors are visible and can not be confused. For illustrations we can select arbitrary $b = 3.5$. The existence of pair of attractors are represented in the following Figures 24a-24b,25a-25b.

7. Stability analysis of the equilibrium points

In this section, we trait the stability analysis of the equilibrium points of the considered model (5)-(7). We will use the Jacobian matrix of the system to give the values of the Lyapunov exponents. For the stability, we consider the Matignon criterion to prove the local stability of all the equilibrium points of the system (5)-(7). To obtain

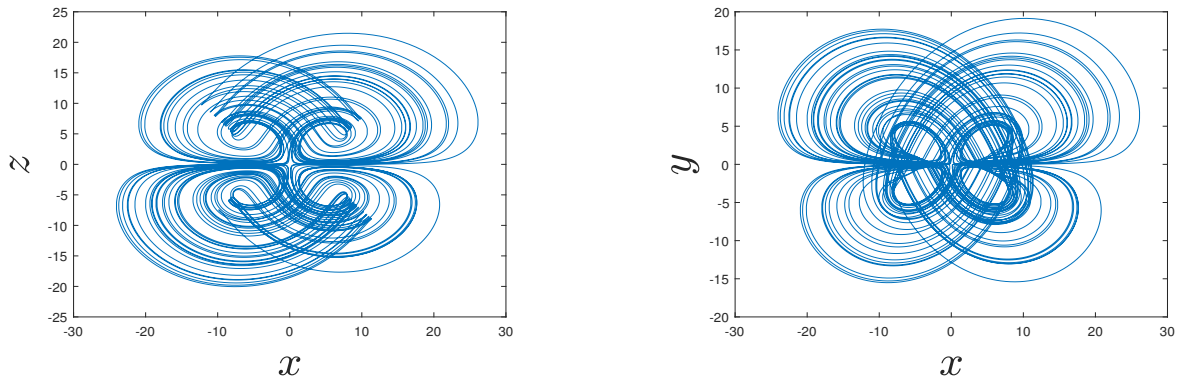

(a) **(b)**

Figure 16. Portrait of phase with the order $\alpha = 0.97$ and $a = 2.65$.

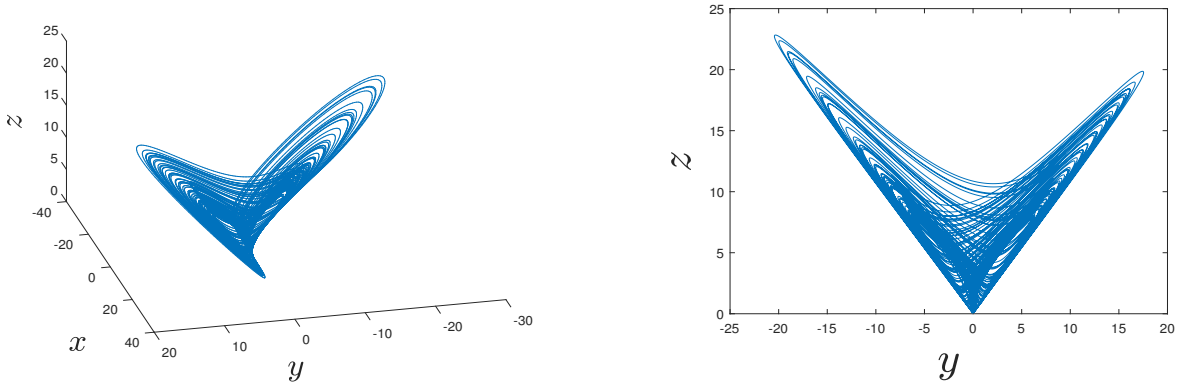

(a) **(b)**

Figure 17. Portrait of phase with the order $\alpha = 0.97$ and $a = 2.65$.

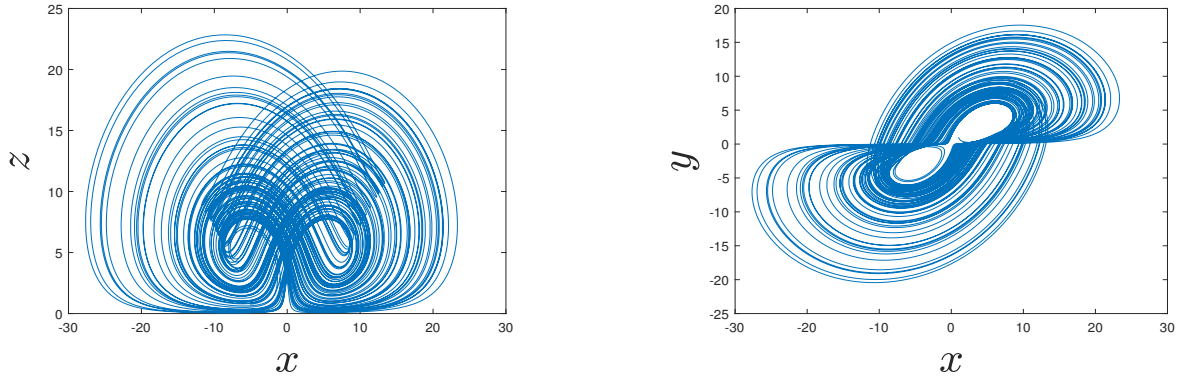

(a) **(b)**

Figure 18. Portrait of phase with the order $\alpha = 0.97$ and $a = 2.65$.

the equilibrium points, we solve the fractional differential equation described by the following equations

$$\begin{aligned} dx - yz &= 0, \\ e - ay + xz + cy &= 0, \\ -bz + xy &= 0, \end{aligned} \tag{41}$$

with $a = 9$, $b = 4$, $c = 1.5$, $d = 2.85$, and $e = 0.2$. The equilibrium points are given as: $A(-5.45, 3.38, -4.60)$, $B(5.50, -3.37, -4.64)$ and $C(0, 0.03, 0)$. The following matrix describes the Jacobian matrix of the chaotic system (5)-(7)

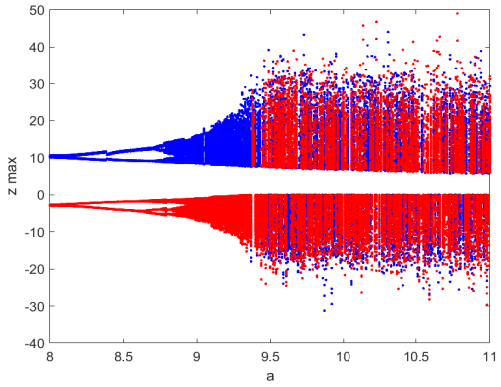

Figure 19. Coexisting bifurcation map according to the parameter a at order $\alpha = 0.97$.

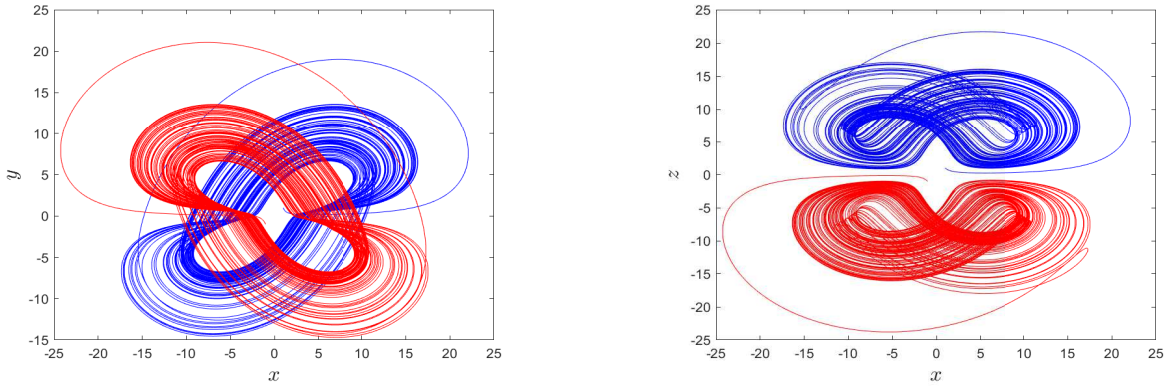

(a) **(b)**

Figure 20. Coexisting attractors in (x, y) and (x, z) with the order $\alpha = 0.97$ and $a = 9.2$.

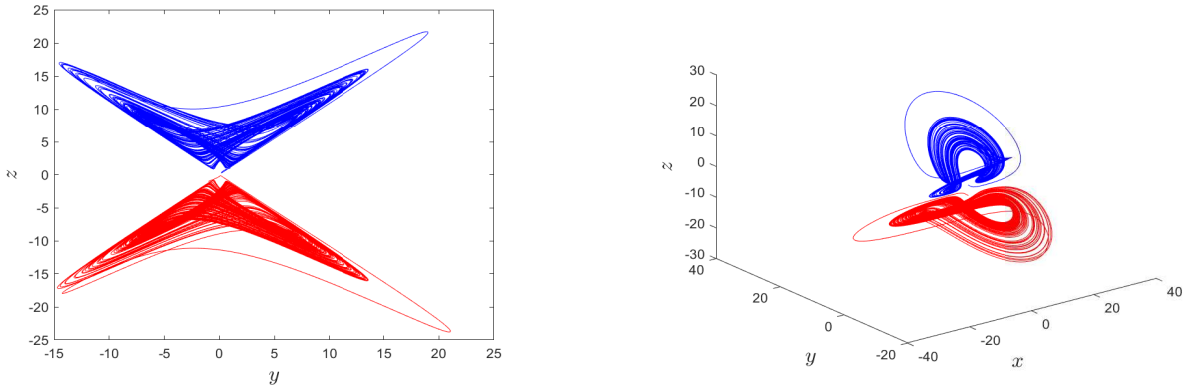

(a) **(b)**

Figure 21. Coexisting attractors in (y, z) and (x, y, z) with the order $\alpha = 0.97$ and $a = 9.2$.

$$J = \begin{pmatrix} 2.85 & -z & -y \\ z & -7.5 & x \\ y & x & -4 \end{pmatrix}. \qquad (42)$$

The objective is to evaluate the Jacobian matrix at the different equilibrium points. With the first equilibrium point A, the Jacobian matrix can be represented as the following form

$$J(A) = \begin{pmatrix} 2.85 & 4.60 & -3.38 \\ -4.60 & -7.5 & -5.45 \\ 3.38 & -5.45 & -4 \end{pmatrix}. \qquad (43)$$

The eigenvalues of the matrix defined by $J(A)$ are represented as the following forms $\lambda_1 = 1.3233 + 5.3154i$, $\lambda_2 = 1.3233 - 5.3154i$ and $\lambda_3 = -11.2966$.

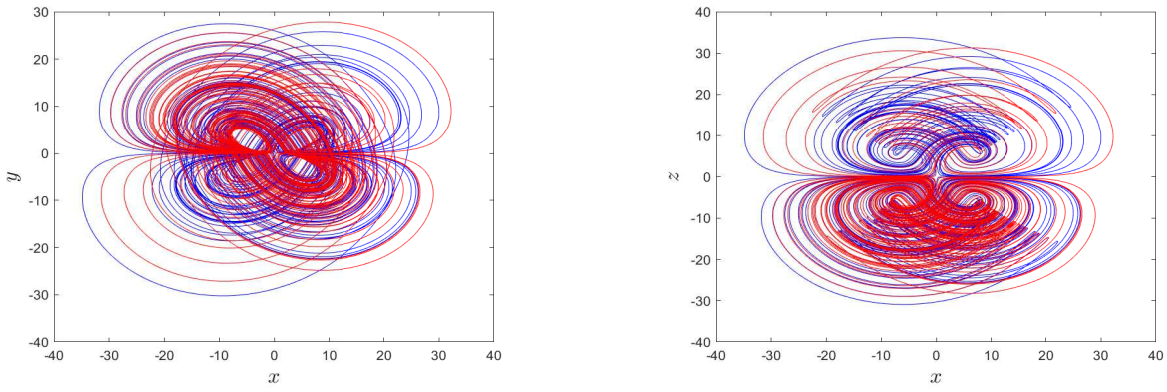

(a) **(b)**

Figure 22. Coexisting attractors in (x, y) and (x, z) with the order $\alpha = 0.97$ and $a = 10$.

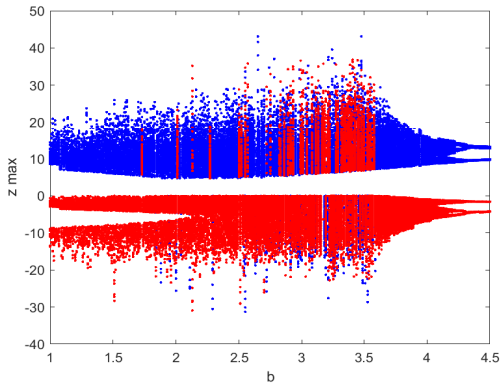

Figure 23. Coexisting bifurcation map according to the parameter b at order $\alpha = 0.97$.

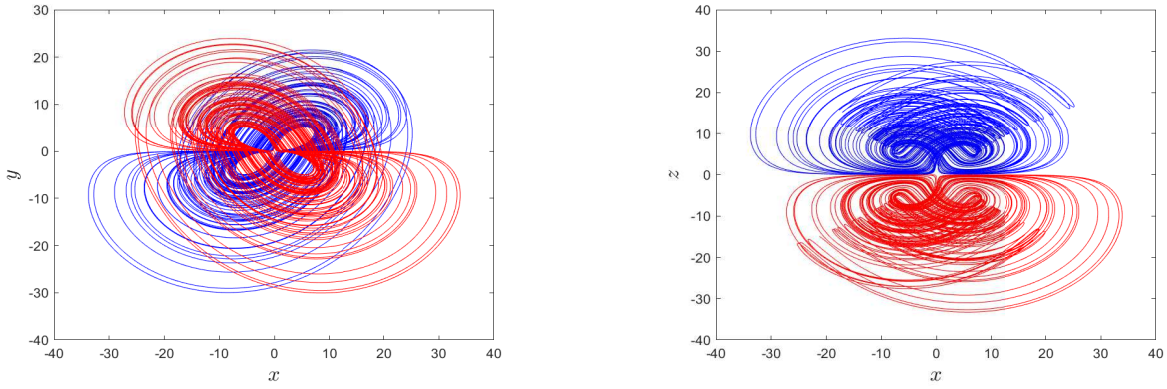

(a) **(b)**

Figure 24. Coexisting attractors in (x, y) and (x, z) with the order $\alpha = 0.97$ and $b = 2.5$.

We can notice the last eigenvalue satisfies the Matignon criterion given by $|\arg(\lambda_3)| = \pi > \alpha\pi/2$ for all orders of the Caputo derivative. The first and the second eigenvalues satisfy the condition $|\arg(\lambda_{1,2})| = 19\pi/45 > \alpha\pi/2$, for all orders satisfying that $\alpha \in (0, 0.84)$. Thus the point A is not stable when the order of the Caputo derivative is into the interval $(0.84, 1)$.

We now consider the second point B, the Jacobian matrix at this point is represented as the form

$$J(B) = \begin{pmatrix} 2.85 & 4.67 & 3.37 \\ -4.64 & -7.5 & 5.50 \\ -3.37 & 5.50 & -4 \end{pmatrix}. \qquad (44)$$

We determine the eigenvalues of the matrix $J(B)$ given as $\lambda_1 = 1.3441 + 5.3418i$, $\lambda_2 = 1.3441 -$

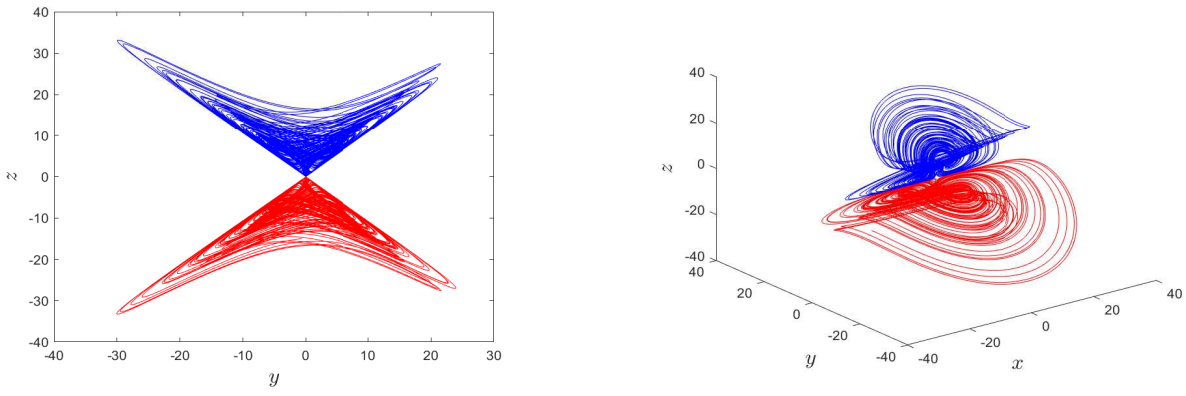

(a) **(b)**

Figure 25. Coexisting attractors in (y, z) and (x, y, z) with the order $\alpha = 0.97$ and $b = 2.5$.

$5.3418i$ and $\lambda_3 = -11.3382$. The next step consists to verify the Matignon criterion for all our eigenvalues. Note that the third eigenvalue respect the condition $|\arg(\lambda_3)| = \pi > \alpha\pi/2$. We can notice the first and the last eigenvalues are conjugate and satisfies the condition $|\arg(\lambda_{1,2})| = 75.9\pi/180 > \alpha\pi/2$ for the order of the Caputo derivative obeying to $\alpha \in (0, 0.84)$. Thus the point B is not stable when the order describes the interval $(0.84, 1)$.

The third part consists to investigate the local stability of the point C. The Jacobian matrix at the point C is given by the following matrix

$$J(C) = \begin{pmatrix} 2.85 & 0 & -0.03 \\ 0 & -7.5 & 0 \\ 0.03 & 0 & -4 \end{pmatrix}. \qquad (45)$$

The eigenvalues of the above matrix are summarized as the values $\lambda_1 = -7.5$, $\lambda_2 = -4.0001$ and $\lambda_3 = 2.8501$. The first and the second eigenvalues satisfy the matignon criterion because they are negative. The last eigenvalue obeys to $|\arg(\lambda_3)| = 0 > \alpha\pi/2$ for all order of the Caputo derivative. Thus, the point C is not stable. The final conclusion about the stability analysis the equilibrium points of the fractional differential considered in this section; they are not stable into the interval $(0.84, 1)$ which is probably the chaotic region of our considered system. The investigation about the chaotic region will be analyzed later for confirmation.

8. Lyapunov exponents for chaos characterization

In this section, we calculate the Lyapunov exponents associated with the different orders used in this paper to characterize the nature of the chaos. There are many types of behaviors, but we are interested in the chaotic, hyperchaotic, limit cycles behaviors, and convergence to an equilibrium point. For brief rappel, in the context of integer order derivative, the system's behavior is considered to describe limit cycle when all the Lyapunov exponents are negative, the same characterization in the context of the convergence of the solution and equilibrium point. The chaotic behavior is obtained when one of the Lyapunov exponents is negative. The hyperchaotic context follows when at least we have two positive Lyapunov exponents. In the context of fractional order derivative, the above cite characterizations are not adequate. Danca provided this assumption. He stipulates the determination of the Lyapunov exponents in fractional context is complex, and the number of positive Lyapunov exponents is not adequate to characterize hyperchaotic behaviors. There exist hyperchaotic behaviors with one positive Lyapunov exponents; see in [25]. The method of the determination use the Jacobian matrix, and the numerical scheme, the method of the determination can be found in [28], we have the following matrix

$$J = \begin{pmatrix} 2.85 & -z & -y \\ z & -7.5 & x \\ y & x & -4 \end{pmatrix}. \qquad (46)$$

For the Lyapunov exponents to validate the chaotic behaviors of the phase portraits depicted in Section 4, we calculate the Lyapunov exponents; we consider the first the order $\alpha = 0.86$. We have the following values

$$L1 = 0.7241, L2 = 0, L3 = -14.0315. \qquad (47)$$

First of all, we can observe the sum of the Lyapunov exponents is negative, which means the considered system in this study is dissipative. We can also see our system has chaotic behaviors at the order $\alpha = 0.86$ because one of the Lyapunov

exponents is positive. We finish by its associated Kaplan Yorke dimension given by the following

$$dim(L) = 2 + \frac{L1 + L2}{|L3|} = 2.0516. \quad (48)$$

We have the same analysis with the order $\alpha = 0.94$. We calculate the Lyapunov exponents. We have the following numbers

$$L1 = 0.5720, L2 = 0, L3 = -11.2740. \quad (49)$$

We also have the chaotic behaviors at the considered order because one of the Lyapunov exponents is negative. The system stays dissipative in this order because the sum of the Lyapunov exponents is negative. For the order, $\alpha = 0.94$, the Kaplan Yorke dimension obtained from the Lyapunov exponents is given by the following

$$dim(L) = 2 + \frac{L1 + L2}{|L3|} = 2.0507. \quad (50)$$

For the order $\alpha = 0.97$, we repeat the same procedure of calculations. The values of the Lyapunov exponents are given by the numbers

$$L1 = 0.4911, -L2 = 0, L3 = -10.2542, \quad (51)$$

its associated dimension is given by

$$dim(L) = 2 + \frac{L1 + L2}{|L3|} = 2.0479. \quad (52)$$

With Eq. (51), we conclude our system is dissipative and has chaotic behaviors. We dress Table of Lyapunov exponents for the confirmation of the chaotic behaviors into the region $(0.84, 1)$ obtained in the stability analysis.

Table 1. Lyapunov exponents.

α	$LE1$	$LE2$	$LE3$
0.84	0.9121	0	-14.8723
0.86	0.7241	0	-14.0315
0.88	0.7581	0	-13.3461
0.90	0.6173	0	-12.5491
0.92	0.5518	0	-11.8962
0.94	0.5720	0	-11.2740
0.95	0.5623	0	-10.9520
0.96	0.5893	0	-10.6669
0.97	0.4911	0	-10.2542
0.98	0.5333	0	-10.0306
0.99	0.4993	0	-9.6960

With Table **??**, we can observe the fractional system (5)-(7) considered in the region $(0.84, 1)$ has chaotic behaviors due to the fact there are one positive Lyapunov exponents at all orders in this interval. We can also observe the system is dissipative in this region. The Table previously presented confirm that our interval obtained in the stability investigations is our chaotic region.

9. Circuit realization of the uncommensurate fractional-order system

We finish this paper by realizing the circuit obtained by the fractional chaotic system considered in this section. To arrive at our objective, we draw the circuit from the system (5)-(7), and we simulate the model using Multisim. The interest of this procedure is to compare the phase portraits obtained with Matlab and the phase portraits obtained after simulation in Multisim. We will observe the results are in good agreement. This section plays an important role in the real applications of fractional calculus in engineering. For the rest of this section, we consider the order $\alpha = 0.97$. First of all, we recall the third approximation of fractional integrator, which we will use; it is given by the following relationship

$$\frac{1}{s^{0.98}} \approx \frac{1.2234s^2 + 1463.28s + 4893.2}{(s + 0.0106)(s + 3.7716)(s + 1341.4)}. \quad (53)$$

The above approximation will be compared to the transfer function associated with the fractional integrator given by the form

$$F(s) = \frac{\frac{1}{C_a}}{s + \frac{1}{R_a C_a}} + \frac{\frac{1}{C_b}}{s + \frac{1}{R_b C_b}} + \frac{\frac{1}{C_c}}{s + \frac{1}{R_c C_c}}. \quad (54)$$

Comparing Eq. (53) and Eq. (54), we get the following values for the Resistors and the Capacitors $C_a = 1.0656nF$, $C_b = 8.5245n$, $C_c = 7.596n$, $R_a = 91.17M\Omega$,$R_b = 32.046k\Omega$, and $R_c = 101.12\Omega$. The second part consists of drawing the circuit associated with the fractional chaotic system (5)-(7). We first use the Capacitors and Resistors to rewrite Eqs. (5)-(7) we have the following system

$$x' = \frac{1}{C_1 R_1}x - \frac{1}{C_1 R_2}yz, \quad (55)$$

$$y' = \frac{V}{C_2 R_5} - \frac{1}{C_2 R_3}y + \frac{1}{C_2 R_4}xz, \quad (56)$$

$$D_c^{\alpha} z = -\frac{1}{C_3 R_6}z + \frac{1}{C_3 R_7}xy, \quad (57)$$

where, we set the following values for the Capacitors $C_1 = C_2 = C_3 = 1nF$, and the values of the resistors are $R_1 = 87.719k\Omega$, $R_2 = 25k\Omega$, $R_3 = 33.33k\Omega$, $R_4 = 6.25k\Omega$, $R_5 = 100000k\Omega$,

$R_6 = 250k\Omega$, $R_7 = 6.25k\Omega$ and we set $V = -1V$. These values are obtained by calibrating Eq. (5)-(7) and the previous Eqs. (55)-(57). The phase portraits obtained after simulation in the Multisim, we have the following outputs.

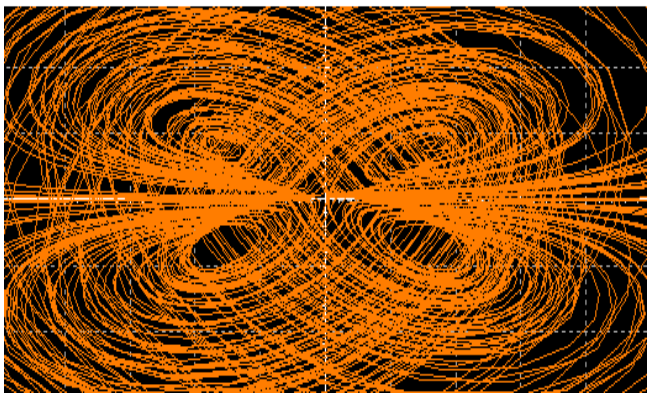

Figure 26. Dynamics evolution in the oscilloscope thought (x, y) plane.

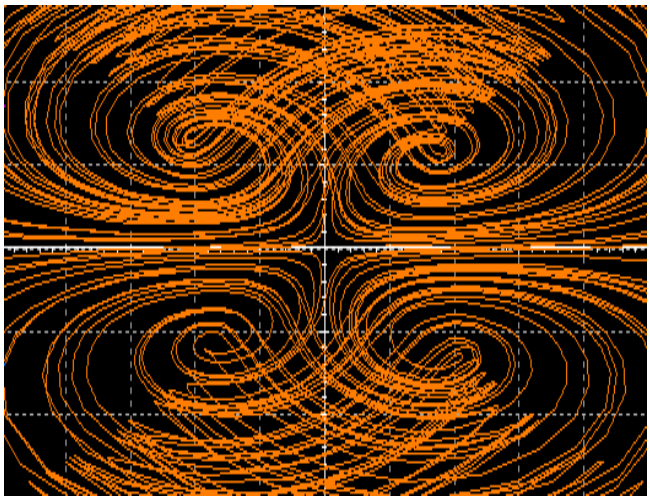

Figure 27. Dynamics evolution in the oscilloscope thought (x, z) plane.

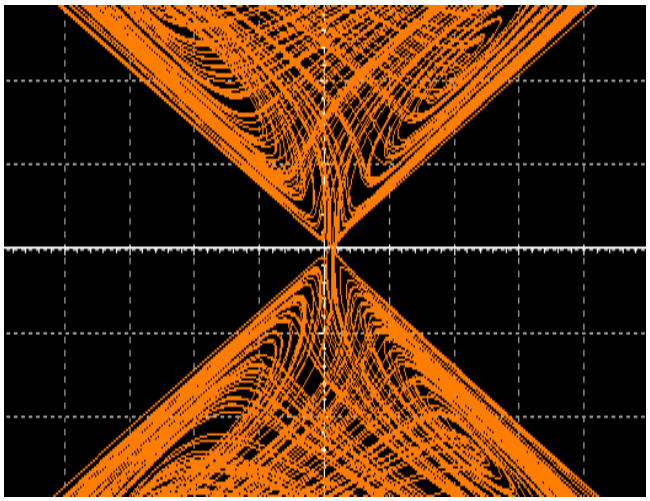

Figure 28. Dynamics evolution in the oscilloscope thought (y, z) plane.

For confirmation of the results in the oscilloscopes, we consider its corresponding fractional system and depict the portraits using the numerical scheme previously exposed in this paper. Thus, we consider the following system

$$\begin{aligned} x' &= dx - yz, && (58)\\ y' &= e - ay + xz + cy, && (59)\\ D_c^{\alpha} z &= -bz + xy. && (60) \end{aligned}$$

We maintain the same initial conditions which are presented as follows

$$x(0) = x_0 = 1, y(0) = y_0 = 1, z(0) = z_0 = 1. \quad (61)$$

We suppose the order $\alpha = 0.98$ and we depict the portraits of system (58)-(60) in the following Figures 29a-29b,30a-30b.

We can finally observe the results obtained after stimulation of the fractional chaotic (55)-(57) in Multisim are in good agreement with the results established for the model (58)-(60). This section also proves fractional calculus can be used in modeling electrical chaotic circuits.

10. Conclusion

In this paper, we have presented the bifurcation, Lyapunov exponents to characterize the chaos, the stability analysis of the equilibrium points, and the coexisting attractors for a class of fractional chaotic system described by the Caputo derivative. To arrives at our end, the fundamental tool for the effectiveness of this paper is the numerical procedure which is crucial for obtaining the phase portraits of the chaotic system. Our fractional chaotic system is simulated by Matlab; we have also proposed the circuit schematic for our considered fractional-order chaotic system. From the fact, we have not the materials to simulate the electrical chaotic circuit, we have simulated our model virtually by considering Mutlisim software. With the simulation in Multisim, we have proved the results in Matlab are in good agreement with the results simulated in the Multisim.

References

[1] Kilbas, A. A., Srivastava, H. M., & Trujillo, J. J. (2006). *Theory and applications of fractional differential equations*. Vol. 204. Elsevier.

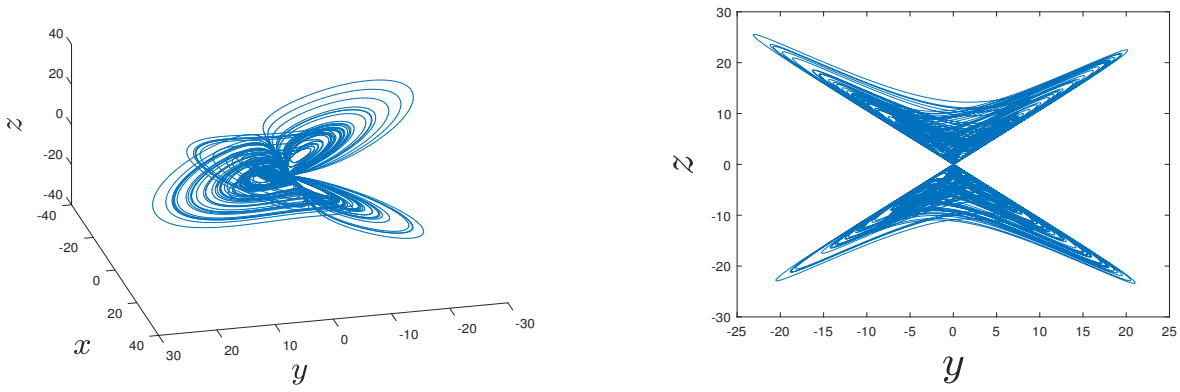

(a) **(b)**

Figure 29. $(x-y-z)$ and $(y-z)$ plane with the order $\alpha = 0.98$ for Eqs. (58)-(60).

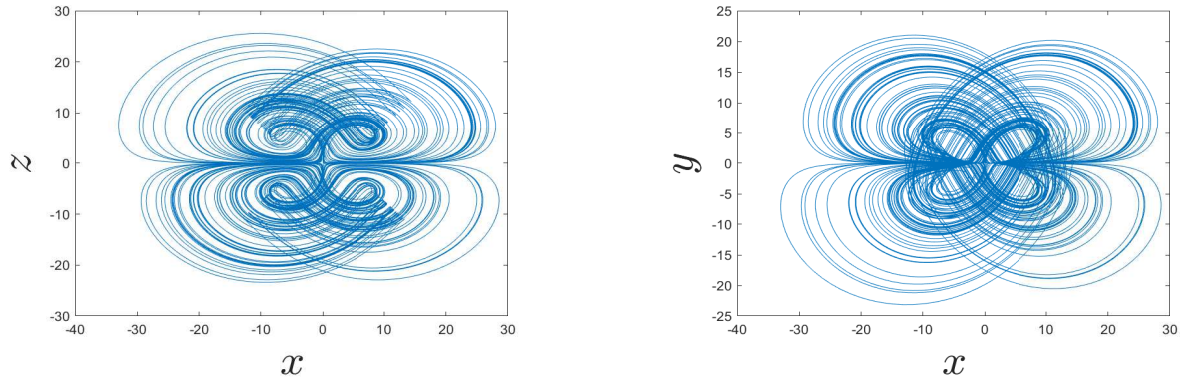

(a) **(b)**

Figure 30. $(x-y)$ and $(x-z)$ planes with the order $\alpha = 0.98$ for Eqs. (58)-(60).

[2] Yavuz, M. (2019). Characterizations of two different fractional operators without singular kernel. *Mathematical Modelling of Natural Phenomena*, 14(3), 302.

[3] Khan, A., Li, Y., Shah, K., & Khan, T. S. (2017). On coupled-laplacian fractional differential equations with nonlinear boundary conditions. *Complexity*, p.9.

[4] Zafar, Z. U. A., Sene, N., Rezazadeh, H., & Esfandian, N. (2021). Tangent nonlinear equation in context of fractal fractional operators with nonsingular kernel. *Mathematical Sciences*, 1-11.

[5] Sene, N. (2020). Second-grade fluid model with Caputo–Liouville generalized fractional derivative. *Chaos, Solitons & Fractals*, 133, 109631.

[6] Mansal, F., & Sene, N. (2020). Analysis of fractional fishery model with reserve area in the context of time-fractional order derivative. *Chaos, Solitons & Fractals*, 140, 110200.

[7] Jarad, F., Abdeljawad, T., & Baleanu, D. (2017). On the generalized fractional derivatives and their Caputo modification. *J. Nonlinear Sci. Appl.*, 10, 2607-2619.

[8] Podlubny, I. (1999). *Fractional Differential Equations*, Mathematics in Science and Engineering, Academic Press, New York, NY, USA, 198.

[9] Pérez, J. E. S., Gómez-Aguilar, J. F., Baleanu, D., & Tchier, F. (2018). Chaotic attractors with fractional conformable derivatives in the Liouville–Caputo sense and its dynamical behaviors. *Entropy*, 20(5), 384.

[10] Gómez-Aguilar, J. F., Abro, K. A., Kolebaje, O., & Yildirim, A. (2019). Chaos in a calcium oscillation model via Atangana-Baleanu operator with strong memory. *The European Physical Journal Plus*, 134(4), 1-9.

[11] Sene, N. (2021). Introduction to the fractional-order chaotic system under fractional operator in Caputo sense. *Alexandria Engineering Journal*, 60(4), 3997-4014.

[12] Akgul, A. (2019). Chaotic oscillator based on fractional order memcapacitor. *Journal*

of Circuits, Systems and Computers, 28(14), 1950239.

[13] Munoz-Pacheco, J. M., Zambrano-Serrano, E., Volos, C., Jafari, S., Kengne, J., & Rajagopal, K. (2018). A new fractional-order chaotic system with different families of hidden and self-excited attractors. *Entropy*, 20(8), 564.

[14] Sene, N. (2020). Analysis of a four-dimensional hyperchaotic system described by the Caputo–Liouville fractional derivative. *Complexity*, 2020.

[15] Khan, A., Gómez-Aguilar, J. F., Abdeljawad, T., & Khan, H. (2020). Stability and numerical simulation of a fractional order plant-nectar-pollinator model. *Alexandria Engineering Journal*, 59(1), 49-59.

[16] Sene, N. (2021). Analysis of a fractional-order chaotic system in the context of the Caputo fractional derivative via bifurcation and Lyapunov exponents. *Journal of King Saud University-Science*, 33(1), 101275.

[17] Sene, N., & Ndiaye, A. (2020). On class of fractional-order chaotic or hyperchaotic systems in the context of the caputo fractional-order derivative. *Journal of Mathematics*, 2020.

[18] Sene, N. (2021). Mathematical views of the fractional Chua's electrical circuit described by the Caputo-Liouville derivative. *Revista Mexicana de Física*, 67(1), 91-99.

[19] Akgul, A., Arslan, C., & Aricioglu, B. (2019). Design of an interface for random number generators based on integer and fractional order chaotic systems. *Chaos Theory and Applications*, 1(1), 1-18.

[20] Akgul, A., Li, C., & Pehlivan, I. (2017). Amplitude control analysis of a four-wing chaotic attractor, its electronic circuit designs and microcontroller-based random number generator. *Journal of Circuits, Systems and Computers*, 26(12), 1750190.

[21] Atangana, A., & Gómez-Aguilar, J. F. (2017). Hyperchaotic behaviour obtained via a nonlocal operator with exponential decay and Mittag-Leffler laws. *Chaos, Solitons & Fractals*, 102, 285-294.

[22] Rajagopal, K., Durdu, A., Jafari, S., Uyaroglu, Y., Karthikeyan, A., & Akgul, A. (2019). Multiscroll chaotic system with sigmoid nonlinearity and its fractional order form with synchronization application. *International Journal of Non-Linear Mechanics*, 116, 262-272.

[23] Rajagopal, K., Guessas, L., Karthikeyan, A., Srinivasan, A., & Adam, G. (2017). Fractional order memristor no equilibrium chaotic system with its adaptive sliding mode synchronization and genetically optimized fractional order PID synchronization. *Complexity*, 2017.

[24] Ávalos-Ruiz, L. F., Zúñiga-Aguilar, C. J., Gómez-Aguilar, J. F., Escobar-Jiménez, R. F., & Romero-Ugalde, H. M. (2018). FPGA implementation and control of chaotic systems involving the variable-order fractional operator with Mittag–Leffler law. *Chaos, Solitons & Fractals*, 115, 177-189.

[25] Danca, M. F. (2018). Lyapunov exponents of a discontinuous 4D hyperchaotic system of integer or fractional order. *Entropy*, 20(5), 337.

[26] Lü, J., Chen, G., & Cheng, D. (2004). A new chaotic system and beyond: the generalized Lorenz-like system. *International Journal of Bifurcation and Chaos*, 14(05), 1507-1537.

[27] Garrappa, R. (2018). Numerical solution of fractional differential equations: A survey and a software tutorial. *Mathematics*, 6(2), 16.

[28] Danca, M. F., & Kuznetsov, N. (2018). Matlab code for Lyapunov exponents of fractional-order systems. *International Journal of Bifurcation and Chaos*, 28(05), 1850067.

Ndolane Sene *was born in Senegal in 1986. He received a Ph.D degree from Cheikh Anta Diop University in June 2017. He currently works on fractional calculus and applications. He is the author of more than 55 research papers since 2018 and be part of more than five books published in Taylor Francis and Springer. His research covers mathematical modeling, applied mathematics, numerical analysis, probability and statistics, and fundamental mathematics. He is nominated as a Review Editor of Frontiers in Applied Mathematics and Statistics and Frontiers in Physics. He was a Lead Guest Editor for a special issue published in the Journal of Mathematics Hindawi.*
https://orcid.org/0000-0002-8664-6464

An International Journal of Optimization and Control: Theories & Applications
ISSN:2146-0957 eISSN:2146-5703
Vol.12, No.1, pp.39-46 (2022)
http://doi.org/10.11121/ijocta.2022.1027

RESEARCH ARTICLE

Comparative assessment of smooth and non-smooth optimization solvers in HANSO software

Ali Hakan Tor*

Abdullah Gül University, Faculty of Computer Science, Department of Mathematics, Kayseri, Turkey
hakan.tor@agu.edu.tr

ARTICLE INFO

Article History:
Received 2 October 2020
Accepted 16 June 2021
Available 27 October 2021

Keywords:
Non-smooth optimization software
BFGS
Gradient sampling algorithm
Hybrid algorithm

AMS Classification 2010:
90C26; 90C30; 65K05; 65K10

ABSTRACT

The aim of this study is to compare the performance of smooth and nonsmooth optimization solvers from HANSO (Hybrid Algorithm for Nonsmooth Optimization) software. The smooth optimization solver is the implementation of the Broyden-Fletcher-Goldfarb-Shanno (BFGS) method and the nonsmooth optimization solver is the Hybrid Algorithm for Nonsmooth Optimization. More precisely, the nonsmooth optimization algorithm is the combination of the BFGS and the Gradient Sampling Algorithm (GSA). We use well-known collection of academic test problems for nonsmooth optimization containing both convex and nonconvex problems. The motivation for this research is the importance of the comparative assessment of smooth optimization methods for solving nonsmooth optimization problems. This assessment will demonstrate how successful is the BFGS method for solving nonsmooth optimization problems in comparison with the nonsmooth optimization solver from HANSO. Performance profiles using the number iterations, the number of function evaluations and the number of subgradient evaluations are used to compare solvers.

1. Introduction

Researchers working in different areas, for instance, in economics, engineering, data mining and machine learning encounter different types of optimization problems including those with smooth, non-smooth, convex or nonconvex objective and/or constraint functions. While these researchers search for an optimal solution of their real-life problems, they need suitable software. Most of existing optimization software and methods contain some user defined parameters and it is not always easy to choose these parameters for a particular problem. The choice of these parameters may strongly depend on the application area. Researchers, who apply optimization methods in their research, prefer optimization software that are robust to the choice of their parameters. For example, in the book [1], optimization problems arising in economics are analyzed and some robust methods for solving them are discussed in [2, 3]. The theory and application of engineering problems can be found in [4], in particular, some genetic engineering problems are discussed in [5, 6]. In the areas such as data mining, machine learning and control theory the sources [7–9] are very useful and important for readers. In addition, you can find all the mathematical theory and application related to the nonsmooth optimization theory in the book [10], which used as a guide book while preparing this study. On the other hand, it is possible to increase the examples in the application area, but it is useful to talk about HANSO software as soon as possible without going beyond our purpose.

In this paper, we provide a comparative assessment of two nonsmooth optimization solvers.

*Corresponding Author

Both these solvers are available in HANSO software [11]. The first solver is the implementation of the BFGS method (Broyden-Fletcher-Goldfarb-Shanno method). The second solver is called HANSO (Hybrid Algorithm for Non-Smooth Optimization). This solver is the combination of the BFGS and Gradient Sampling Algorithm (GSA). Implementations of both algorithms are available in [11]. There are two main reasons to carry out this comparison. The BFGS is the smooth optimization algorithm, however the GSA is developed specifically for solving nonconvex nonsmooth optimization problems. This research will, in particular, show how comparable is smooth optimization solver for solving nonsmooth optimization problems. On the other side, BFGS is a part of HANSO algorithm. Our computational results will demonstrate how much the BFGS can improve the performance of the GSA.

We use the collection of 36 academic test problems to test algorithms. This collection contains convex and nonconvex nonsmooth optimization test problems and they different number of variables. The detailed description of these problems can be found in [10].

The rest of the paper is organized as follows. In the following Section 2, we provide the necessary information about the algorithms in HANSO software. In Section 3, the academic test problems used in this study are described. Summary of computational results is presented in Section 4. Discussion of computational results using performance profiles is given in Section 5. Some concluding remarks are provided in the final Section 6.

2. HANSO (Hybrid Algorithm for Non-Smooth Optimization)

Version 2.2 of HANSO developed by Michael Overton is used in this study. It has General Public License (GNU) as published by the Free Software Foundation, so anybody can redistribute it and/or modify it under the terms of this license.

HANSO is intended to seek a minimum value of non-smooth, non-convex functions, but also applicable to functions that are smooth, convex or both. It is based on the BFGS algorithm and GSA. You can find some details about BFGS and GSA in the following subsections.

2.1. BFGS Algorithm

BFGS algorithm suggested independently by Broyden, Fletcher, Goldfarb, and Shanno, in 1970 uses the Quasi-Newton algorithm which is a generalization of the secant method. The main difference between BFGS and Quasi-Newton algorithms is that it uses and maintains different properties of the matrix when updating formulas. In BFGS, the Hessian matrix is not calculated. Instead of this calculation, BFGS uses inverse Hessian matrix approximation using information from gradient evaluation. BFGS is normally used for optimizing smooth, not necessarily convex, functions, for which the convergence rate is generically superlinear. However, BFGS has acceptable performance even for non-smooth optimization problems, typically with a linear convergence rate as long as a weak Wolfe line search is used. This version of BFGS will work well both for smooth and non-smooth functions and has a stopping criterion that applies for both cases [12].

The weak Wolfe line search is far less complicated than the standard strong Wolfe line search. In addition to this fact, there is no disadvantage to using the weak Wolfe line search compared to the strong Wolfe line search when Newton or BFGS methods are used for smooth problems and BFGS or bundle methods are used for non-smooth problems. Thus, HANSO prefers to use the weak Wolfe line search with parameter $c_1 = 0$ for the sufficient decrease condition and parameter $c_2 = 0.5$ for the weak condition on the directional derivative. As indicated in the code [11],

> "For usual convergence theory for smooth functions, normally one requires $0 < c_1 < c_2 < 1$, but $c_1 = 0$ is fine in practice. May want $c_1 = c_2 = 0$ for some non-smooth optimization algorithms such as Shor or bundle, but not BFGS. Setting $c_2 = 0$ may interfere with superlinear convergence of BFGS in smooth case."

In this context, we can say that we can change the c_2 parameter, but it is not appropriate to make it 0. In our calculations, the code was not intervened and the results were obtained with the aforementioned parameters.

There are several options for the stopping criterion of BFGS algorithm in HANSO. First of all, it is possible to adjust the tolerance of a decent direction. If its norm is less than the given tolerance, the code is terminated. In this study, the default tolerance 10^{-6} is used. Another stopping criterion is that the distance of the gradient vector calculated in each step from the current iteration point is greater than the given tolerance value. The default tolerance value 10^{-4} is used in this

study again. Other stopping criteria are related to change of function values, the magnitude of the current iteration point and CPU time, but in this study numerical results have been obtained without any restrictions on them.

2.2. Gradient Sampling Algorithm (GSA)

Gradient sampling idea was used in [13,14] for the first time. Later, the gradient sampling method was used to approximate the Clarke subdifferential for locally Lipschitz functions in [15] and it was improved for non-smooth non-convex problems in [16], which is used in HANSO Software. Later, other versions of gradient sampling methods for some special optimization problems was developed such as [17–19].

GSA is intended for non-convex and locally Lipschitz functions that are differentiable almost everywhere, in other words, they are not differentiable on a set of the measure zero, so the subgradient at a randomly selected point is uniquely determined as the gradient at that point. Therefore, in GSA, gradients are computed on a set of randomly generated nearby points at current iteration. Consequently, by using gradient sampling, a local information of the function is obtained and the quadratic subproblem is formed. The ϵ-steepest descent direction is constructed by solving this quadratic subproblem, where ϵ is the sample radii.

The stopping criterion of GSA in HANSO is on descent directions. If the norm of the descent direction at current iteration is less then given tolerance, the algorithm is terminated. HANSO's default values 10^{-6} is used as a tolerance in this study.

3. Test Problem

The efficiency of HANSO was tested on the well-known non-smooth optimization academic test problems taken in [10]. Hanso's performance was discussed on this academic test problem according to the type of the non-smooth problems namely convex and non-convex. In Table 1, some information can be found for convex problems. n_{var} denotes the number of variables ,and f_{opt} denotes the optimal value of indicated problem.

Table 1. List of Convex Problems

Problem	n_{var}	f_{opt}
CB2	2	1,9522245
CB3	2	2
DEM	2	-3
QL	2	7,2
LQ	2	-1,4142136
Mifflin 1	2	-1
Wolfe	2	-8
Rosen_Suzuki	4	-44
Polak6	4	-44
Davidon 2	4	115,70644
Shor	5	22,600162
Wong 1	7	680,63006
Wong 2	10	24,306209
Polak 2	10	54,598150
Maxquad	10	-0,8414083
Polak 3	11	3,70348
Wong 3	20	93,90525
Watson	20	$0,14743027 \times 10^{-7}$
Maxq	20	0
Maxl	20	0
Gofflin	50	0
MXHILB	50	0
L1HILB	50	0

Similarly, some information can be found for non-convex problems In Table 2.

Table 2. List of Non-Convex Problems

Problem	n_{var}	f_{opt}
WF	2	0
SPIRAL	2	0
Rosenbrock	2	0
Crescent	2	0
Mifflin 2	2	-1
EVD52	3	3,5997193
OET5	4	$0,26359735 \times 10^{-2}$
OET6	4	$0,20160753 \times 10^{-2}$
El-Attar	6	0,5598131
Gill	10	9,7857721
Osborne 2	11	$0,48027401 \times 10^{-1}$
Steiner 2	12	16,703838
Shell Dual	15	32,348679

HANSO allows us to use the specified starting point or randomly generated starting point. However, in this study, 20 randomly generated starting points were used. Since the HANSO code was not suitable for running 20 different points, this code was modified to use these randomly generated 20 points by reading our starting point files. These numerical results are presented in the next section.

4. Numerical Results

Since it is not possible to give all of the 20 results obtained for each of the 36 test problems mentioned in the previous section, we first give the table below, which presents HANSO and BFGS solves how many problems related to the starting points successfully.

We can observe that there is no difference in the number of solving problems between HANSO and BFGS from Tables 3 and 4. On the other hand, looking at the values of the problems CB3, DEM, Polak 3, Wong 3, WF, SPIRAL, El-Attar, and Gill from Tables 3 and 4., one can observe that both HANSO and BFGS were able to solve them for some starting points. This means that the success of both software depends on the starting point. This is quite normal for non-smooth solvers. In addition, when there were 20 starting points for 36 test problems, in other words, these algorithms worked 720 times, they were successful in only %50 of these works.

Table 3. Number of convex problems solved successfully

Problem	HANSO	BFGS
CB2	20	20
CB3	14	14
DEM	1	1
QL	20	20
LQ	20	20
Mifflin 1	0	0
Wolfe	20	20
Rosen_Suzuki	0	0
Polak6	0	0
Davidon 2	20	20
Shor	20	20
Wong 1	0	0
Wong 2	20	20
Polak 2	0	0
Maxquad	20	20
Polak 3	5	5
Wong 3	10	10
Watson	0	0
Maxq	20	20
Maxl	20	20
Gofflin	20	20
MXHILB	20	20
L1HILB	20	20
TOTAL	290	290

Table 4. Number of non-convex problems solved successfully

Problem	HANSO	BFGS
WF	2	2
SPIRAL	18	18
Rosenbrock	20	20
Crescent	0	0
Mifflin 2	0	0
EVD52	20	20
OET5	0	0
OET6	0	0
El-Attar	8	8
Gill	3	3
Osborne 2	0	0
Steiner 2	0	0
Shell Dual	0	0
TOTAL	71	71

In particular, the rate of successfully solved attempts approximately is %63 and %27 for convex problems and non-convex problems respectively. This means that the number of iterations, function evaluations and gradient evaluations for these softwares should be compared for a more effective comparison. The reason that there is no comparison on CPU time in this study is HANSO software does not provide CPU time information. Of course, CPU time could be calculated by modifying the code, but it has not been done since the program ended in less than 2 seconds for both HANSO and BFGS. The reason that the program terminated such a short time is that HANSO's default maximum number of iterations is 1000, and this default number was used in the calculation.

5. Discussion by using Performance Profile

In order to compare the HANSO and BFGS effectively, as stated in the previous section, it is necessary to compare the numbers of iterations, function evaluations, and gradient evaluations obtained from numerical experiments. Because there is too much data in the numerical results, it is impossible to compare these data for each starting point of each problem. Therefore, the concept of performance profile presented to benchmark optimization software (see [20]) is used to compare HANSO and BFGS.

5.1. Performance Profile

The results are shown in Figures 1 and 2 by using the performance profiles introduced in [20]. In this section, the efficiency of the softwares are discussed in terms of performance measures,

which are iteration, function evaluation and gradient evaluation. The performance profile denoted by $\rho_s(\tau)$,where s is either software HANSO or BFGS, is a following

$$\rho_s(\tau) = \frac{\text{no. of the problems where } r_{p,s} \leq \tau}{\text{total no. of the problems}} \times 100 \tag{1}$$

where $r_{p,s}$ denotes the performance ratio. If software s fails to solve problem p, the performance ratio is sufficiently large number (or infinity), otherwise

$$r_{p,s} = \frac{n_{p,s}}{\min\{n_{p,s} | \text{s is either HANSO or BFGS}\}} \tag{2}$$

where $n_{p,s}$ is the number of the performance measure for the software s for the problem p. In other word, $n_{p,s}$ is the number of the iteration (or function evaluation, gradient evaluation) for the software s for the problem p according to performance measure. One can easily observe from Equation 2 that the performance ratio is 1 for at least one of these two softwares and $r_{p,s} \geq 1$. If the value of $n_{p,s}$ in both softwares are equal, $r_{p,s}$ become 1 for both.

For both software HANSO and BFGS in terms of each of three aforementioned performance measures, graphs of the performance profiles $\rho_s(\tau)$ are given in Figures 1 and 2.

In the performance profiles, the value of $\rho_s(1)$ gives the percentage of test problems for which software s is the best. In other words, it uses the least performance measures, for example, least iteration number, function evaluations or gradient evaluations. If both software have the same values, both are considered the best.

The value of $\rho_s(\tau)$ at the rightmost abscissa gives the percentage of test problems that the corresponding solver can solve successfully, that is, the reliability of the solver. Moreover, the relative efficiency of each software can be directly seen from the performance profiles. The corresponding software of the higher curve is the better.

5.2. Discussion on Convex Problems

Performance profile graphs of the numerical results obtained by using 20 different starting points with 23 Convex problems given in Table 1 are given in Figure 1. Using 20 different starting points on 23 convex problems, 460 results were obtained, which means that the total number of problems in the denominator of the performance profile function which is Equation 1 is 460.

When looking at the performance profile graphs according to 3 different performance measures in Figure 1, we can say that HANSO is more reliable than BFGS in terms of these three measures, since the performance profile graph of HANSO (shortly the graph of HANSO) is above from the performance profile graph of BFGS (shortly the graph of BFGS).

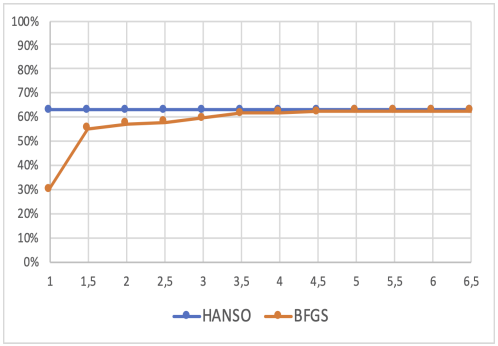

(a) Number of Iterations

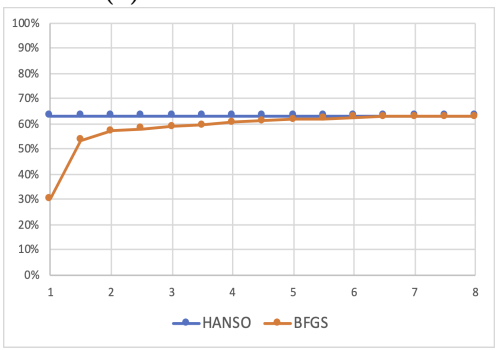

(b) Number of Function Evaluations

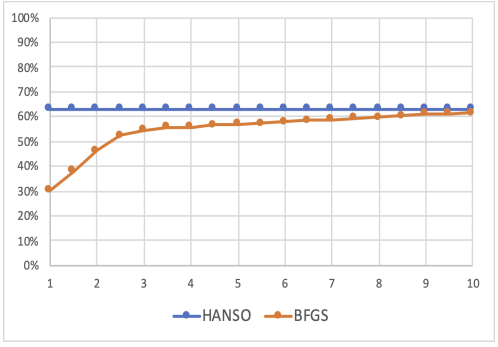

(c) Number of Gradient Evaluations

Figure 1. Performance Profiles for Convex Problems

On the other hand, it is possible to observe that both softwares have successfully solved an equal number of problems, which is %63. When we look at the $rho_s(1)$ value for both softwares, we can see that HANSO has the least number of iterations, functions, and gradients evaluations in all successfully solved problems. Similarly, when we look at the value of $rho_s(1)$ for BFGS, it can be said that BFGS has the least numbers in %30 of the successfully solved problems. This means that HANSO and BFGS have the same values for

all of these %30 problems. So there is no difference between HANSO and BFGS for this %30 problem solved successfully. One can observe that the graph of HANSO in these three graphs is a straight line. This means that for all convex problems, HANSO either has the same evaluation numbers as the BFGS or better.

5.3. Discussion on Non-convex Problems

It can be said that the total number of problems in the performance profile function is 260 with 13 different problems for the non-convex case.

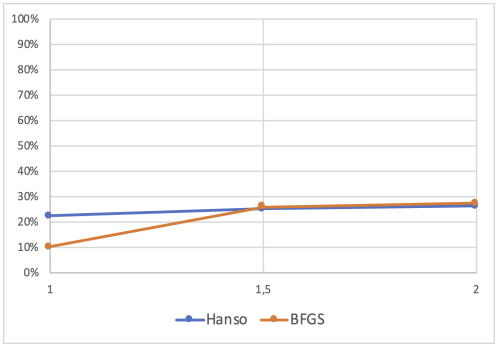

(a) Number of Iterations

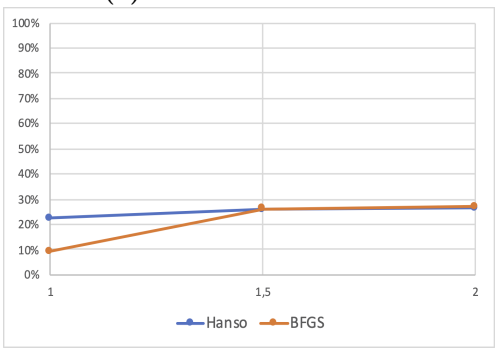

(b) Number of Function Evaluations

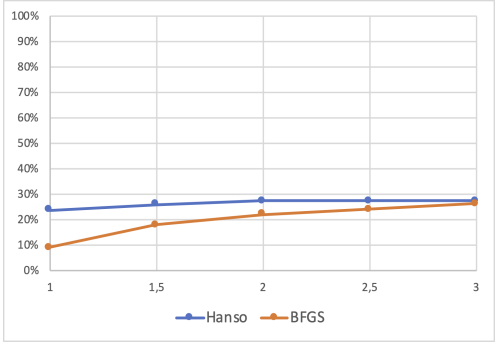

(c) Number of Gradient Evaluations

Figure 2. Performance Profiles for Non-convex Problems

When making a similar discussion for non-convex problems as It has done for convex problems, we will need to look at the graphs given in Figure 2. We can again say that HANSO is more reliable than BFGS for non-convex problems. However, this time the percentage %27 of successfully solving problems for both softwares is very low. Apart from this remarkable percentage of solving success, we see that the graph of HANSO is not a straight line. The reason for this is that some problems are solved by the BFGS by making less iteration, function and gradient evaluation.

On the other hand, the meaning of the abscissa value 2 in Figures 2a and 2b is that the iteration and function evaluation numbers for these two softwares are at most 2 times higher compared to the other. This shows that there is not a huge improvement between HANSO and BFGS in terms of either performance measure. Similarly, this value is 3 in Figure 2c and the number of gradient evaluations has decreased by the factor 3 at most.

6. Conclusion

In this study, some information about HANSO software developed by Michael Overton and coded in MATLAB is presented. The parameters that HANSO uses in the line search algorithm are given and the stopping criteria of the algorithm to find the minimum value are specified. Afterwards, numerical results were obtained to compare HANSO and BFGS softwares by using some academic test problems. According to all these numerical results, it can be said that HANSO, which is a hybrid method, does not give very different results from BFGS in terms of accuracy, but it reduces the number of iterations and calculations efforts to some extent. On the other hand, when we look at the results obtained with different starting points, it can be said that for many problems, both HANSO and BFGS are sensitive to the starting point, that is, neither of them is robust. Nevertheless, this free software can be used for academic studies. Of course, when using this software, it would be more appropriate to use more than one starting point instead of one starting point for academic study. Finally, there is no need to use HANSO and BFGS separately to get results. The results obtained with only HANSO are sufficient.

It will be very useful to compare HANSO with other non-smooth solvers in the literature to shed light on academic studies. Another point not included in this study is how HANSO will give results when it comes to large-scale problems. However, this study demonstrated how HANSO software differs from BFGS by numerical calculations and discussion.

Acknowledgments

I would like to thank the anonymous referees, who contributed greatly to the increase of the quality of this work with their valuable suggestions. Without their support, it was impossible to present this study in this quality.

References

[1] Outrata, J., Kocvara, M., & Zowe, J. (2013). *Nonsmooth approach to optimization problems with equilibrium constraints: theory, applications and numerical results* (Vol. 28). Springer Science & Business Media.

[2] Özmen, A. & Weber, G-W. (2012). Robust conic generalized partial linear models using rcmars method-a robustification of cgplm. In *AIP Conference Proceedings*, vol.1499, 337–343.

[3] Özmen, A., Weber, G-W., Batmaz, İ. & Kropat, E. (2011). Rcmars: Robustification of cmars with different scenarios under polyhedral uncertainty set. *Communications in Nonlinear Science and Numerical Simulation*, 16(12), 4780–4787.

[4] Mistakidis, E.S. & Stavroulakis, G.E. (2013). *Nonconvex optimization in mechanics: algorithms, heuristics and engineering applications by the FEM*, volume 21. Springer Science & Business Media.

[5] Weber, G-W., Alparslan-Gök, Z.S. & Öyler, B.S. (2009). A new mathematical approach in environmental and life sciences: gene–environment networks and their dynamics. *Environmental Modeling & Assessment*, 14(2), 267–288.

[6] Weber, G-W., Tezel, A., Taylan, P., Soyler, A. & Çetin, M. (2008). Mathematical contributions to dynamics and optimization of gene-environment networks. *Optimization*, 57(2), 353–377.

[7] Bagirov, A.M., Karmitsa, N., & Taheri, S. (2020). *Partitional Clustering via Nonsmooth Optimization: Clustering via Optimization*. Springer Nature.

[8] Demyanov, V.F., Bagirov, A.M. & Rubinov, A.M. (2002). A method of truncated codifferential with application to some problems of cluster analysis. *Journal of Global Optimization*, 23(1), 63–80.

[9] Clarke, F.H., Ledyaev, Y.S., Stern, R.J. & Wolenski, P.R. (2008). *Nonsmooth analysis and control theory*, volume 178. Springer Science & Business Media.

[10] Bagirov, A.M., Karmitsa, N. & Mäkelä, M.M. (2014). *Introduction to Nonsmooth Optimization*. Theory, Practice and Software. Springer, Cham.

[11] Overton, M.L. Hanso: Hybrid algorithm for non-smooth optimization. `https://cs.nyu.edu/faculty/overton/software/hanso/index.html`. Accessed: 2020-08-15.

[12] Lewis, A.S. & Overton, M.L. (2013). Nonsmooth optimization via quasi-newton methods. *Mathematical Programming*, 141(1-2), 135–163.

[13] Ermoliev, Y.M. (1982). Methods of nondifferentiable and stochastic optimization and their applications. In *Progress in nondifferentiable optimization*, volume 8 of *IIASA Collaborative Proc. Ser. CP-82*, pages 5–27. International Institute for Applied Systems Analysis, Laxenburg.

[14] Shor, N.Z. (1985). *Minimization methods for nondifferentiable functions*, volume 3 of *Springer Series in Computational Mathematics*. Springer-Verlag, Berlin. Translated from the Russian by K. C. Kiwiel and A. Ruszczyński.

[15] Burke, J.V., Lewis, A.S. & Overton, M.L. (2002). Approximating subdifferentials by random sampling of gradients. *Mathematics of Operations Research*, 27(3), 567–584.

[16] Burke, J.V., Lewis, A.S. & Overton, M.L. (2005). A robust gradient sampling algorithm for nonsmooth, nonconvex optimization. *SIAM Journal on Optimization*, 15(3), 751–779.

[17] Burke, J.V., Henrion, D., Lewis, A.S. & Overton, M.L. (2006). Stabilization via nonsmooth, nonconvex optimization. *Institute of Electrical and Electronics Engineers. Transactions on Automatic Control*, 51(11), 1760–1769.

[18] Burke, J.V., Lewis, A.S. & Overton, M.L. (2004). Pseudospectral components and the distance to uncontrollability. *SIAM Journal on Matrix Analysis and Applications*, 26(2), 350–361 (electronic).

[19] Kiwiel, K.C. (2007). Convergence of the gradient sampling algorithm for nonsmooth nonconvex optimization. *SIAM Journal on Optimization*, 18(2), 379.

[20] Dolan, E.D. & Moré, J.J. (2002). Benchmarking optimization software with performance profiles. *Mathematical Programming. A Publication of the Mathematical Programming Society*, 91(2, Ser. A), 201–213.

Ali Hakan Tor *is an assistant professor at the Department of Mathematics, Abdullah Gul University, Kayseri, Turkey. He received his PhD degree from the Middle East Technical University, Ankara, Turkey in 2013. His research interests include non-smooth optimization theory and numerical non-smooth optimization.*

https://orcid.org/0000-0003-3193-5004

An International Journal of Optimization and Control: Theories & Applications (http://ijocta.balikesir.edu.tr)

An International Journal of Optimization and Control: Theories & Applications
ISSN: 2146-0957 eISSN: 2146-5703
Vol.12, No.1, pp.47-55 (2022)
https://doi.org/10.11121/ijocta.2022.1025

RESEARCH ARTICLE

An EOQ model for deteriorating items analyzing retailer's optimal strategy under trade credit and return policy with nonlinear demand and resalable returns

Mamta Kumari and Pijus Kanti De*

Department of Mathematics, National Institute of Technology Silchar, Silchar -788010, India
mamta_rs@math.nits.ac.in, pkde@math.nits.ac.in

ARTICLE INFO

Article history:
Received: 30 September 2020
Accepted: 1 December 2021
Available Online: 2 January 2022

Keywords:
Inventory
Trade credit policy
Resalable returns
Deteriorating item
Refund

AMS Classification 2010:
90B05, 90B06

ABSTRACT

This paper presents an EOQ model where demand is dependent upon time and selling price. In the proposed model of inventory, the retailer allows its unsatisfied customers to return their product whereas the manufacturer offers a full trade credit policy to the retailer. To make our model realistic, we have assumed that the product returned can be resold with the same selling price. Number of returns is a function of demand. In this proposed inventory model considering deterioration, the retailer does not fully reimburse its customers for the returned product. The primary purpose of this inventory model is to determine the optimal selling price, optimal order quantity, and optimal replenishment cycle length in order to maximize the retailer's total profit earned per unit time. A numerical example is also presented and a sensitivity analysis is carried to highlight the findings of the suggested inventory model.

1. Introduction

Return policies are offered as an attractiveness pill to drag customers by the seller. The return policy allows consumers who are unsatisfied with their purchase to return the product and get a refund either in terms of money or some gift vouchers as stated by the company in its policies. In today's competitive market, many companies offer return policies to their consumers in order to increase sales. Bechwati and Siegel [1] concluded from their research that customers consider return policy as a signal for purchasing products from a store.

Owing to the return policies, customer returns are growing drastically in the past few decades since customers are taking advantage of their strength which can be understood by the retail industry slogan that "consumers are king". Gentry [2] concluded that the rate of product return can be as high as 35% of the initial stock. Mostard et al. [3] observed that return rate can be larger than 18% in the case of mail orders and it can even reach to 74% for fashion products. Due to the high return rate, it becomes difficult for the retailer to handle its inventory and associated cost. Palmquist [4] concluded that product returns cost US retailers and manufacturers approximately 100$ billion annually in reverse logistics.

Many research works have been done in the past decades to analyze whether offering a return policy is beneficial to the seller or not. Recent research recommends to follow a restrictive return policy in order to reduce consumer abuse of leniency of return policies, manage reverse logistic costs and increase profitability [5-8]. Peterson and Kumar [9] studied whether product return is a necessary evil? It's antecedent and consequences. Then, Janakiraman et al. [10] examined the effect of leniency of return policies on consumer behavior towards return and purchase decisions by conducting a review of 21 papers. After that, Khouja et. al. [11] studied retailer's performance under the effect of price adjustment policies and returns. Many research works have also appeared in the literature on deteriorating items with the return policy. Wang et al. [12] formulated an EOQ model with resalable returns for deteriorating items. Ghoreishi et al. [13] framed an EOQ model under inflation to determine the pricing and ordering strategy of deteriorating items under customer returns. Similarly, many relevant research work has been done on EOQ model considering different situations [14-

* Corresponding author

17]. Deterioration refers to decay, evaporation, spoilage, decay, and loss of utility of the product. In full trade credit policy, buyer does not need to pay immediately upon receipt of merchandise and has the opportunity to settle the amount at the end of the delay time. If he fails to pay the money at the end of credit time, then he is bound to pay interest on the unpaid amount.

If we have a glance at the literature, plenty of works have been done on deteriorating items employing trade credit policy under different circumstances [18-19]. However, until now, no research work has been done in the past, which jointly analyzes the effect of return and trade credit terms on deteriorating items with resalable returns. There is a research gap lying on jointly studying the impact of both return policy and trade credit policy in the business of management of inventory. In this paper, according to the best of author knowledge, first attempt has been made to fill this research gap by jointly analyzing the impact of both trade credit and return policy in the supply chain that contributes to the past literature. Both trade credit policy and return policy importance is growing day by day in the supply chain, so it becomes necessary to analyze the impact of jointly considering the aforementioned policies on the pricing and inventory decisions in the supply chain.

Specifically, this paper studies a manufacturer – retailer – customer business relationship with the following features: (a) retailer is offered a full trade credit period by the manufacturer, (b) retailer also offers a return policy to its buyer to generate sales, (c) demand is dependent upon selling price as well as time, (d) deterioration occurs, and (e) rate of return is observed to be dependent upon selling price as well as time. This research work intends to determine the optimal replenishment cycle length and the optimal selling price in order to maximize the total profit earned by the retailer per unit time. A numerical example is also demonstrated to highlight the findings and a sensitivity analysis is carried out to discuss the results.

Further, this paper is organized as follows: Section 2 demonstrates the notations and assumptions used in order to establish the EOQ model mathematically. Thereafter, Section 3 develops the mathematical model considering demand, return and trade credit policy. Section 4 illustrates a numerical example to highlight the findings. Finally, Section 5 depicts a sensitivity analysis and highlights some results. Lastly, Section 6 ends up with few remarkable conclusions and future research directions.

2. Assumptions and notations

2.1 Notations

Table 1. Notations that are used in formulating the inventory model

Notation	Units	Description	Notation	Units	Description
o	\$/order	ordering cost per order	I_e	% /unit time	interest earned by the retailer
c	\$/unit	purchase price per unit	I_p	% /unit time	interest paid by the retailer to the manufacturer
h	\$/unit/unit time	holding cost per unit item per unit time			
θ		constant deterioration rate, $0 < \theta < 1$	***Decision variables:***		
M	unit time	trade credit period offered by the manufacturer to the retailer	p	\$/unit	selling price per unit
			T	unit time	time at which inventory level reaches to zero
t_1	unit time	time at which deterioration starts	$TP(p, T)$	\$/unit time	total profit per unit time

2.2 Assumptions

1. Planning horizon of the inventory system is assumed to be infinite.
2. Single item with non-instantaneous deterioration is considered.
3. Instantaneous replenishment rate, where lead-time is considered negligible.
4. Shortages are not permitted.
5. Demand rate is given by:

$$D(p,t) = (a - bp)e^{\lambda t} \text{ where } a > 0, b > 0$$

It is a linearly decreasing function of price and increases (decreases) exponentially with time as $\lambda > 0$ ($\lambda < 0$).

6. A full trade credit policy is offered by the manufacturer to the retailer.
7. It is assumed that customer return increases with the goods sold. So,

$$R(p,t) = \alpha D(p,t) \qquad \text{where } 0 \leq \alpha < 1$$

Customers are allowed to return the product during any phase of the length of the replenishment cycle. Products returned can be resold at the same selling price. The retailer does not return the full amount to its customers for the returned goods. He just offers

50% of the initial amount of the product.

3. Model formulation

This section derives, in detail, an inventory model with trade credit and return policy. Initially, $\boldsymbol{Q}$ units of goods exist in the inventory model. During the time interval from $\mathbf{0}$ to $\boldsymbol{t_1}$, no deterioration takes place. During this time, the level of inventory changes due to returns and demand. From time t = $\boldsymbol{t_1}$, deterioration of items at the rate $\boldsymbol{\theta}$ starts taking place. From time $\boldsymbol{t_1}$ to $\boldsymbol{T}$, inventory level changes because of returns, deterioration and demand. At time t = $\boldsymbol{T}$, the level of inventory demises to zero. Thereafter, a replenishment order of $\boldsymbol{Q}$ units is placed. The change in inventory level with the passage of time is shown in Figure 1. The arrival of the ordered goods marks the beginning of the next cycle. The retailer is offered a trade credit period of $\boldsymbol{M}$ to settle the account by the manufacturer.
The retailer also allows its customers to return products, during any time of the replenishment cycle with a condition. The condition is that the retailer will refund only 50% of the initial amount of the product. The inventory situation is best governed by the following differential equations:

$$\frac{dI}{dt} = -(a - bp)e^{\lambda t} + \alpha(a - bp)e^{\lambda t}, \quad 0 \le t \le t_1 \tag{1}$$

$$\frac{dI}{dt} = -(a - bp)e^{\lambda t} + \alpha(a - bp)e^{\lambda t} - \theta I(t), \quad t_1 \le t \le T \tag{2}$$

with the boundary conditions $I(0) = Q$ and $I(T) = 0$.

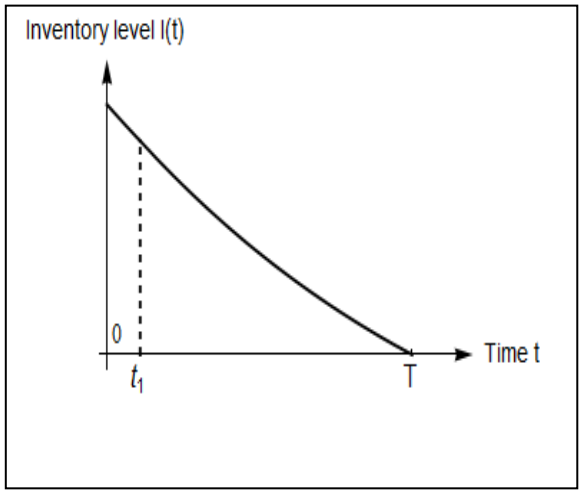

Figure 1. Inventory level at any time t

Solving the differential equations (1) and (2) along with the above-mentioned boundary conditions we get,

$$I(t) = Q + \frac{(\alpha-1)(a-bp)(e^{\lambda t}-1)}{\lambda}, \quad 0 \le t \le t_1 \tag{3}$$

$$I(t) = \frac{(a-bp)(\alpha-1)e^{-\theta t}}{(\lambda+\theta)}\left[e^{(\lambda+\theta)t} - e^{(\lambda+\theta)T}\right], \quad t_1 \le t \le T \tag{4}$$

Using the continuity condition from the equation (3) and (4) at the point $t = t_1$, we get

$$Q = \left[\frac{(a-bp)(\alpha-1)e^{-\theta t_1}}{(\lambda+\theta)}\left[e^{(\lambda+\theta)t_1} - e^{(\lambda+\theta)T}\right]\right] - \left[\frac{(\alpha-1)(a-bp)(e^{\lambda t_1}-1)}{\lambda}\right] \tag{5}$$

Various costs associated with this model are defined as follows:

1. Ordering cost = o (6)
2. Purchasing cost = cQ (7)
3. Sales revenue collected over the cycle (SR)

$$= p\left[\int_0^T D(p,t)dt - \int_0^T \frac{R(p,t)}{2}dt\right]$$
$$= p\left[\int_0^T (a-bp)e^{\lambda t}dt - \int_0^T \frac{\alpha(a-bp)e^{\lambda t}}{2}dt\right]$$
$$= \left[\frac{p(a-bp)(e^{\lambda T}-1)}{\lambda}\right]\left[1 - \frac{\alpha}{2}\right] \tag{8}$$

4. Deterioration cost over the cycle (DC)

$$= c\int_{t_1}^T \theta I(t)dt$$
$$= c\int_{t_1}^T \theta\left[\frac{(a-bp)(\alpha-1)e^{-\theta t}}{(\lambda+\theta)}\right]\left[e^{(\lambda+\theta)t} - e^{(\lambda+\theta)T}\right]dt$$
$$= \left[\left[c(a-bp)(\alpha-1)[(\theta+\lambda)e^{\lambda T} - \theta e^{\lambda t_1} - \lambda e^{(\lambda+\theta)T}e^{-\theta t_1}]\right]/[\lambda(\lambda+\theta)]\right] \tag{9}$$

5. Holding cost over the cycle (HC)

$$= h\left[\int_0^{t_1} I(t)dt + \int_{t_1}^T I(t)dt\right]$$
$$= h\left[\int_0^{t_1}\left[Q + \frac{(\alpha-1)(a-bp)(e^{\lambda t}-1)}{\lambda}\right]dt + \int_{t_1}^T\left[\frac{(a-bp)(\alpha-1)e^{-\theta t}}{(\lambda+\theta)}\left[e^{(\lambda+\theta)t} - e^{(\lambda+\theta)T}\right]\right]dt\right]$$
$$= h\left[Qt_1 + \left[\frac{(\alpha-1)(a-bp)(e^{\lambda t_1} - \lambda t_1 - 1)}{\lambda^2}\right] - \left[\frac{(a-bp)(\alpha-1)}{\theta\lambda(\theta+\lambda)}\right]\left[\theta e^{\lambda t_1} - (\theta+\lambda)e^{\lambda T} + \lambda e^{(\theta+\lambda)T}e^{-\theta t_1}\right]\right] \tag{10}$$

6. Trade credit:
Manufacturer offers the retailer a delay period of M. According to the values of M, t_1 and T three subcases arise:
(1) $0 \le M \le t_1$
(2) $t_1 \le M \le T$
(3) $M \ge T$

6.1. $0 \le M \le t_1$

In this case, the credit period offered by the manufacturer to the retailer is less than the time at which deterioration starts in the inventory. After the end of credit period M, the retailer is subject to interest charges and needs to pay interest during the time interval $[M, T]$. Therefore, interest paid is calculated as follows:

$$\begin{aligned}\text{IP} &= cI_p\left[\int_M^{t_1} I(t)dt + \int_{t_1}^{T} I(t)dt\right] \\ &= cI_p\left[\int_M^{t_1}\left[Q + \frac{(\alpha-1)(a-bp)(e^{\lambda t}-1)}{\lambda}\right]dt + \right. \\ &\quad \left.\int_{t_1}^{T}\left[\frac{(a-bp)(\alpha-1)e^{-\theta t}}{(\lambda+\theta)}\left[e^{(\lambda+\theta)t} - \right.\right.\right. \\ &\quad \left.\left.\left. e^{(\lambda+\theta)T}\right]\right]dt\right] \\ &= cI_p\left[Q(t_1 - M) + \left[\frac{(\alpha-1)(a-bp)}{\lambda}\right]\left[M - \right.\right. \\ &\quad t_1 + ((e^{\lambda t_1} - e^{\lambda M})/\lambda)\Big] + \\ &\quad [(\alpha - 1)(a - bp)/(\lambda + \theta)]\left[\frac{e^{\lambda T}}{\theta\lambda}(\theta + \right. \\ &\quad \left.\left.\lambda) - \frac{e^{\lambda t_1}}{\lambda} - \frac{e^{(\lambda+\theta)T}e^{-\theta t_1}}{\theta}\right]\right] \qquad (11)\end{aligned}$$

The retailer also earns interest from time period 0 to M. It is calculated as follows:

$$\begin{aligned}\text{IE} &= pI_e\left[\int_0^M\int_0^t (a-bp)e^{\lambda u}dudt - \right. \\ &\quad \left.\int_0^M\int_0^t \frac{\alpha(a-bp)e^{\lambda u}}{2}dudt\right] \\ &= pI_e\left[\frac{(a-bp)}{\lambda^2}\right]\left[e^{\lambda M} - \lambda M - 1\right]\left[1 - \frac{\alpha}{2}\right] \qquad (12)\end{aligned}$$

The total profit per unit time is calculated as follows:

$$TP_1(p,T) = \frac{SR+IE-o-IP-HC-DC-PC}{T}$$

Therefore,

$$\begin{aligned}TP_1(p,T) &= [1/T]\left[\left[\frac{p(a-bp)(e^{\lambda T}-1)}{\lambda}\right]\left[1-\frac{\alpha}{2}\right] + \right. \\ &\quad pI_e\left[\frac{(a-bp)}{\lambda^2}\right]\left[e^{\lambda M} - \lambda M - 1\right]\left[1-\frac{\alpha}{2}\right] - o - \\ &\quad cI_p\left[Q(t_1 - M) + \left[\frac{(\alpha-1)(a-bp)}{\lambda}\right]\left[M - t_1 + \right.\right. \\ &\quad \left.\left(\frac{e^{\lambda t_1}-e^{\lambda M}}{\lambda}\right)\right] + \left[\frac{(\alpha-1)(a-bp)}{\lambda+\theta}\right]\left[\frac{e^{\lambda T}}{\theta\lambda}(\theta+\lambda) - \right. \\ &\quad \left.\left.\frac{e^{\lambda t_1}}{\lambda} - \frac{e^{(\lambda+\theta)T}e^{-\theta t_1}}{\theta}\right]\right] - h\left[Qt_1 + \right. \\ &\quad \left[\frac{(\alpha-1)(a-bp)(e^{\lambda t_1}-\lambda t_1-1)}{\lambda^2}\right] - \\ &\quad \left[\frac{(a-bp)(\alpha-1)}{\theta\lambda(\theta+\lambda)}\right]\left[\theta e^{\lambda t_1} + \lambda e^{(\lambda+\theta)T}e^{-\theta t_1} - \right. \\ &\quad \left.\left.(\theta+\lambda)e^{\lambda T}\right]\right] - \\ &\quad \left[\frac{c(a-bp)(\alpha-1)\left[(\theta+\lambda)e^{\lambda T} - \theta e^{\lambda t_1} - \lambda e^{(\lambda+\theta)T}e^{-\theta t_1}\right]}{[\lambda(\lambda+\theta)]}\right] - \\ &\quad c\left[\left[\frac{(a-bp)(\alpha-1)e^{-\theta t_1}}{(\lambda+\theta)}\left[e^{(\lambda+\theta)t_1} - e^{(\lambda+\theta)T}\right]\right] - \right. \\ &\quad \left.\left.\left[\frac{(\alpha-1)(a-bp)(e^{\lambda t_1}-1)}{\lambda}\right]\right]\right] \qquad (13)\end{aligned}$$

Problem – 1:

Maximize $TP_1(p,T) = \frac{W_1}{T}$

where $W_1 = SR + IE - o - IP - HC - DC - PC$

subject to $0 \le M \le t_1$

6.2. $t_1 \le M \le T$

In this subcase, the credit period offered to the retailer by the manufacturer is greater than the time at which deterioration starts and less than the time by which the inventory level reaches zero. After the end of credit period M, the retailer is subject to interest charges and needs to pay interest during the time interval $[M, T]$. It is calculated as follows:

$$\begin{aligned}\text{IP} &= cI_p\left[\int_M^T I(t)dt\right] \\ &= cI_p\left[\int_M^T\left[\frac{(a-bp)(\alpha-1)e^{-\theta t}}{(\lambda+\theta)}\left[e^{(\lambda+\theta)t} - \right.\right.\right. \\ &\quad \left.\left.\left. e^{(\lambda+\theta)T}\right]\right]dt\right] \\ &= cI_P\left[[(\alpha-1)(a-bp)/(\lambda + \right. \\ &\quad \left.\left.\theta)]\left[\frac{e^{\lambda T}}{\theta\lambda}(\theta + \lambda) - \frac{e^{\lambda M}}{\lambda} - \frac{e^{(\lambda+\theta)T}e^{-\theta M}}{\theta}\right]\right] \qquad (14)\end{aligned}$$

The retailer also earns interest from time period 0 to M. It is calculated as follows:

$$\begin{aligned}\text{IE} &= \left[\int_0^M\int_0^t (a-bp)e^{\lambda u}dudt - \right. \\ &\quad \left.\int_0^M\int_0^t \frac{\alpha(a-bp)e^{\lambda u}}{2}dudt\right] \\ &= pI_e\left[\frac{(a-bp)}{\lambda^2}\right]\left[e^{\lambda M} - \lambda M - 1\right]\left[1 - \frac{\alpha}{2}\right] \qquad (15)\end{aligned}$$

The total profit per unit time is calculated as follows:

$$TP_2(p,T) = \frac{SR+IE-o-IP-HC-DC-PC}{T}$$

Therefore,

$$\begin{aligned}TP_2(p,T) &= [1/T]\left[\left[\frac{p(a-bp)(e^{\lambda T}-1)}{\lambda}\right]\left[1-\frac{\alpha}{2}\right] + \right. \\ &\quad pI_e\left[\frac{(a-bp)}{\lambda^2}\right]\left[e^{\lambda M} - \lambda M - 1\right]\left[1-\frac{\alpha}{2}\right] - o - \\ &\quad cI_P\left[\left[\frac{(\alpha-1)(a-bp)}{\lambda+\theta}\right]\left[\frac{e^{\lambda T}}{\theta\lambda}(\theta+\lambda) - \frac{e^{\lambda M}}{\lambda} - \right.\right.\end{aligned}$$

$$\frac{e^{(\lambda+\theta)T}e^{-\theta M}}{\theta}\Bigg] - h\Bigg[Qt_1 + \left[\frac{(\alpha-1)(a-bp)(e^{\lambda t_1}-\lambda t_1-1)}{\lambda^2}\right] - \left[\frac{(a-bp)(\alpha-1)}{\theta\lambda(\theta+\lambda)}\right]\left[\theta e^{\lambda t_1} + \lambda e^{(\lambda+\theta)T}e^{-\theta t_1} - (\theta+\lambda)e^{\lambda T}\right]\Bigg] - \left[\frac{c(a-bp)(\alpha-1)\left[(\theta+\lambda)e^{\lambda T}-\theta e^{\lambda t_1}-\lambda e^{(\lambda+\theta)T}e^{-\theta t_1}\right]}{[\lambda(\lambda+\theta)]}\right] - c\Bigg[\left[\frac{(a-bp)(\alpha-1)e^{-\theta t_1}}{(\lambda+\theta)}\left[e^{(\lambda+\theta)t_1} - e^{(\lambda+\theta)T}\right]\right] - \left[\frac{(\alpha-1)(a-bp)(e^{\lambda t_1}-1)}{\lambda}\right]\Bigg] \quad (16)$$

Problem 2:

Maximize $TP_2(p,T) = \frac{W_2}{T}$

where $W_2 = SR + IE - o - IP - HC - DC - PC$

subject to $t_1 \le M \le T$

6.3. $M \ge T$

In this subcase, the delay period offered by the retailer to the manufacturer is greater than the time by which level of inventory drops down to zero. By this time the retailer clears all his debt. Hence,

$$\text{IP} = 0 \quad (17)$$

The retailer earns interest from time period 0 to M. It is calculated as follows:

$$\begin{aligned}\text{IE} = {} & pI_e\Bigg[\int_0^T\int_0^t (a-bp)e^{\lambda u}dudt - \int_0^T\int_0^t \frac{\alpha(a-bp)e^{\lambda u}}{2}dudt + (M-T)\int_0^T (a-bp)e^{\lambda t}dt - (M-T)\int_0^T \frac{\alpha(a-bp)e^{\lambda t}}{2}dt\Bigg] \\ = {} & pI_e\left[\left[\frac{(a-bp)(M-T)(e^{\lambda T}-1)}{\lambda}\right]\left[1-\frac{\alpha}{2}\right] + \left[\frac{(a-bp)(e^{\lambda T}-T\lambda-1)}{\lambda^2}\right]\left[1-\frac{\alpha}{2}\right]\right] \end{aligned} \quad (18)$$

The total profit per unit time is calculated as follows:

$$TP_3(p,T) = \frac{SR+IE-o-IP-HC-DC-PC}{T}$$

Therefore,

$$TP_3(p,T) = [1/T]\Bigg[\left[\frac{p(a-bp)(e^{\lambda T}-1)}{\lambda}\right]\left[1-\frac{\alpha}{2}\right] + \Bigg[pI_e\left[\left[\frac{(a-bp)(M-T)(e^{\lambda T}-1)}{\lambda}\right]\left[1-\frac{\alpha}{2}\right] + \left[\frac{(a-bp)(e^{\lambda T}-T\lambda-1)}{\lambda^2}\right]\left[1-\frac{\alpha}{2}\right]\right] - o - h\Bigg[Qt_1 + \left[\frac{(\alpha-1)(a-bp)(e^{\lambda t_1}-\lambda t_1-1)}{\lambda^2}\right] - \left[\frac{(a-bp)(\alpha-1)}{\theta\lambda(\theta+\lambda)}\right]\left[\theta e^{\lambda t_1} - (\theta+\lambda)e^{\lambda T} + \lambda e^{(\lambda+\theta)T}e^{-\theta t_1}\right]\Bigg] - \left[\frac{c(a-bp)(\alpha-1)\left[(\theta+\lambda)e^{\lambda T}-\theta e^{\lambda t_1}-\lambda e^{(\lambda+\theta)T}e^{-\theta t_1}\right]}{[\lambda(\lambda+\theta)]}\right] - c\Bigg[\left[\frac{(a-bp)(\alpha-1)e^{-\theta t_1}}{(\lambda+\theta)}\left[e^{(\lambda+\theta)t_1} - e^{(\lambda+\theta)T}\right]\right] - \left[\frac{(\alpha-1)(a-bp)(e^{\lambda t_1}-1)}{\lambda}\right]\Bigg]\Bigg] \quad (19)$$

4. Numerical example

A numerical example has been presented to illustrate the proposed inventory model. The main objective is to determine the optimal price p^* and optimal cycle length T^* which maximizes total profit per unit time earned by the retailer. The values of different parameters are as follows:

$a = 200$; $b = 4$; $t_1 = \frac{1}{12}$year; $I_e = 10\%$/year; $I_p = 15\%$/year; $M = 0.01$ year; $\alpha = 0.1$; $\theta = 0.08$; $c =$ \$20/unit; $o =$ \$200/order; $\lambda = -0.98$; $h =$ \$1/ unit/year.

Since $M < t_1$, it falls into the category of subcase 6.1. Hence, the following results are obtained:

$p^* = 35.5357$; $T^* = 0.765714$; $Q^* = 28.6351$; ${TP_1}^* = 300.394$.

It can be observed from Figure 2 that the profit function plot is concave in nature.

5. Sensitivity analysis

Based on the above numerical example, a sensitivity analysis is executed to understand the influence of overestimation or underestimation of input parameters on the optimal values of p, T, Q, and total profit gained per unit time. The values of input parameters are changed from -30% to 30% to carry out the process. The results are determined by keeping the other parameters constant and transforming one parameter at a time. The following results are obtained from Table 2.

(i) With the increment in the value of I_e, the total profit gained per unit time is observed to increase. As I_p increases, decrement in the total profit earned per unit time is observed. With the increment in trade credit time M, profit earned per unit time increases since now the retailer has the opportunity to settle its payment after a longer period of time. With the increase in trade credit time, the

retailer has the opportunity to sell most of its stock and needs to pay interest on a smaller number of left items.

(ii) With the increase in the purchasing price c, optimal cycle length T and optimal price p increases whereas total profit per unit time decreases. It is obvious that if the retailer buys goods at a higher price and if sells them at a lower price, he will incur loss. Since, demand is dependent upon selling price p, with the increase in selling price, demand decreases. Hence, cycle length increases and total profit per unit time decreases.

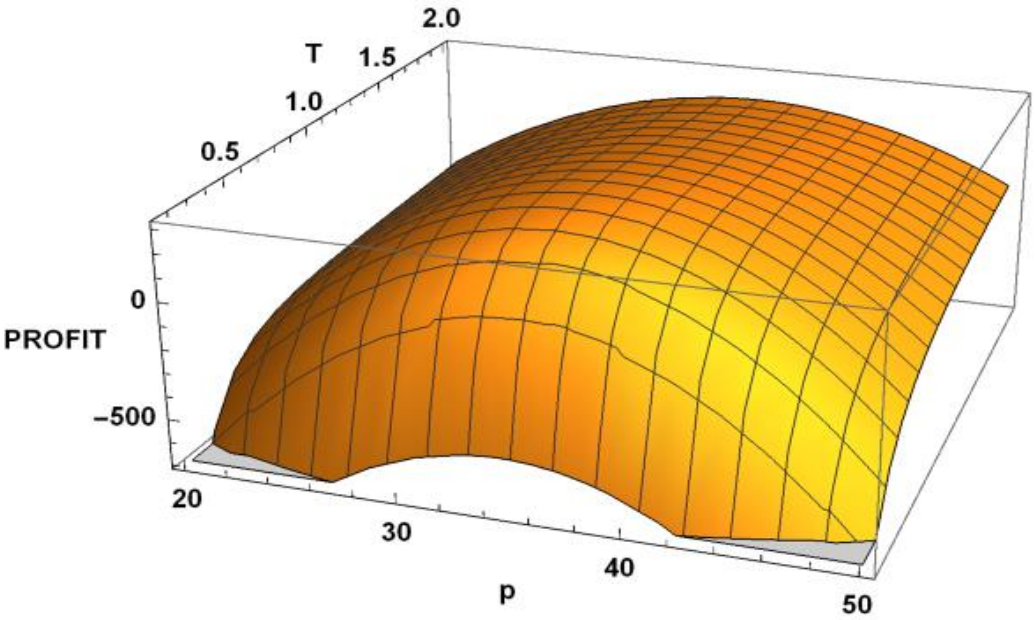

Figure 2. A three-dimensional plot showing the total profit function for the above numerical example

Table 2. Sensitivity analysis with respect to input parameters

Parameters	% Change in parameters	Change in optimal values			
		TP^*	p^*	T^*	Q^*
I_e	-30	300.391	35.5357	0.765714	28.6351
	-20	300.392	35.5357	0.765714	28.6351
	-10	300.393	35.5357	0.765714	28.6351
	10	300.396	35.5357	0.765714	28.6351
	20	300.397	35.5357	0.765714	28.6351
	30	300.398	35.5357	0.765714	28.6351
I_p	-30	311.323	35.5357	0.765714	28.6351
	-20	307.68	35.5357	0.765714	28.6351
	-10	304.037	35.5357	0.765714	28.6351
	10	296.752	35.5357	0.765714	28.6351
	20	293.109	35.5357	0.765714	28.6351
	30	289.466	35.5357	0.765714	28.6351
M	-30	300.057	35.5357	0.765714	28.6351
	-20	300.169	35.5357	0.765714	28.6351
	-10	300.282	35.5357	0.765714	28.6351
	10	300.507	35.5357	0.765714	28.6351
	20	300.62	35.5357	0.765714	28.6351
	30	300.733	35.5357	0.765714	28.6351
c	-30	574.261	32.3214	0.628571	30.366
	-20	475.682	33.3929	0.662857	29.6643
	-10	384.27	34.4643	0.731429	29.7851
	10	223.775	36.6071	0.8	27.3258
	20	154.945	37.6786	0.902857	27.2466
	30	93.9067	38.75	0.971429	26.0645

Table 2. *Cont.*

Parameters	% Change in parameters	Change in optimal values			
		TP^*	p^*	T^*	Q^*
o	-30	389.085	35.5357	0.594286	23.822
	-20	357.024	35.5357	0.662857	25.8368
	-10	327.436	35.5357	0.731429	27.731
	10	274.965	35.5357	0.8	29.5118
	20	251.321	35.5357	0.868571	31.1861
	30	229.037	35.5357	0.937143	32.7601
h	-30	304.149	35.5357	0.765714	28.6351
	-20	302.897	35.5357	0.765714	28.6351
	-10	301.646	35.5357	0.765714	28.6351
	10	299.143	35.5357	0.765714	28.6351
	20	297.892	35.5357	0.765714	28.6351
	30	296.64	35.5357	0.765714	28.6351
a	-30	-45.9395	29.1071	2	19.5502
	-20	15.4218	31.25	1.48571	25.6462
	-10	131.364	33.3929	1.00571	27.4763
	10	519.239	37.6786	0.628571	29.7525
	20	786.702	40.3571	0.56	30.9182
	30	1102.86	42.5	0.491429	31.9772
b	-30	975.374	45.7143	0.491429	28.8302
	-20	677.305	41.4286	0.56	26.5333
	-10	460.794	38.2143	0.662857	27.8781
	10	180.989	33.3929	0.868571	28.6064
	20	92.5807	31.7857	1.04	28.6474
	30	28.5492	30.1786	1.28	29.2753
θ	-30	310.018	35.5357	0.765714	28.4561
	-20	306.821	35.5357	0.765714	28.5155
	-10	303.613	35.5357	0.765714	28.5752
	10	297.165	35.5357	0.765714	28.6952
	20	293.924	35.5357	0.765714	28.7555
	30	290.741	35.5357	0.731429	27.8973
λ	-30	356.155	35.5357	0.8	32.806
	-20	336.532	35.5357	0.8	31.6531
	-10	318.01	35.5357	0.765714	29.6094
	10	283.553	35.5357	0.765714	27.7056
	20	267.562	35.5357	0.731429	26.0377
	30	252.308	35.5357	0.731429	25.2459
α	-30	295.011	35.5357	0.765714	29.5896
	-20	296.806	35.5357	0.765714	29.2715
	-10	298.6	35.5357	0.765714	28.9533
	10	302.189	35.5357	0.765714	28.317
	20	303.983	35.5357	0.765714	27.9988
	30	305.778	35.5357	0.765714	27.6806
t_1	-30	297.756	35.5357	0.765714	28.6853
	-20	298.649	35.5357	0.765714	28.6683
	-10	299.529	35.5357	0.765714	28.6516
	10	301.246	35.5357	0.765714	28.6189
	20	302.084	35.5357	0.765714	28.6031
	30	302.908	35.5357	0.765714	28.5874

(iii) As ordering cost o increases, simultaneously replenishment cycle length T and order quantity Q start increasing. It is to be observed that the total profit per unit time decreases since cycle length is increasing. With the increment in holding cost h, total profit per unit time decreases.

(iv) With the increase in the value of a, it is observed that optimal values of p, Q, and total profit per unit time increases whereas the optimal replenishment cycle T decreases. It can be seen that with the increment in the value of b, optimal price p and total profit per unit time decreases whereas replenishment cycle length T increases.

(v) As the value of θ i.e., deterioration rate increases, a decrease in total profit per unit time earned by the retailer is detected. With the increase in the deterioration rate, items get deteriorated faster, so total profit earned per unit time decreases

(vi) It can be seen that with the increase in the value of λ, order quantity Q, cycle length T and total profit earned per unit time decreases. With the increment in the value of α, optimal order quantity Q decreases whereas an increment in total profit earned per unit time is observed. As the number of returns are increasing, some are resold to satisfy demand, so order quantity Q decreases and total profit increases. With the increase in t_1, the time at which deterioration starts, optimal order quantity Q decreases whereas total profit earned per unit time increases.

6. Conclusion

An inventory model with a single item is developed for a single period under both return policy and trade credit policy. If we have a glance at the literature, plenty of works on inventory model considering deteriorating items have been done. Lot of work has also been done on inventory model with trade credit policy. Some researchers have also formulated inventory models considering resalable returns for deteriorating items. Recent research recommends to follow a restrictive return policy. Nowadays, many companies offer return policies to their customers to attract them. Seller often offers buyer trade credit terms which is beneficial for the business of both of them. Till now, according to the best of author knowledge, no research work has been done which jointly studies the impact of both trade credit policy and return policy. In this paper, an attempt has been made to fill this research gap. The analysis of the impact of these two aforementioned policies in the supply chain is the main contribution of this research work. In the proposed model for deteriorating items, demand is considered to be a function of selling price and time. Retailer is offered a full trade credit period by the manufacturer whereas customers are offered with a return policy by the retailer. The returns are allowed at any time in a period. The returned product can be resold at the same selling price. Customers are not fully reimbursed for the returned product in the inventory model. Number of returns is a function of demand.

The following guidelines are recommended for future research directions: it can be extended to partial trade credit policy, a full refund of the initial amount or returning a fraction of the initial amount, an extension on multi-item and multi-period.

Acknowledgement

The authors are thankful to the anonymous reviewers and the editor for their constructive comments and suggestions. This paper has been revised in light of their suggestions and comments.

References

[1] Bechwati, N.N., Siegal, W.S. (2005). The impact of the pre-choice process on product returns. *J. Market. Res*., 42(3), 358–367.

[2] Gentry, C.R. (1999). Reducing cost of returns. *Chain store Age*, 75, 124-126.

[3] Mostard, J., Teunter, R., Koster, R.D. (2005). The distribution-free newsboy problem with resalable returns. *International Journal of Production Economics*, 97, 329-342.

[4] Palmquist, M. (2015). The unexpected benefits of product returns. Available from ⟨http://www.strategy-business.com/blog/The-Unexpected-Benefits-of-Product-Returns?gko=b808b⟩. Accessed 18 november 2020.

[5] Boyd, E., Bahn, K.D. (2014). Information and its impact on consumer's reaction to restrictive return policies. *Journal of Retailing and Consumer Services*, 21, 415-423.

[6] Harris, L.C. (2010). Fraudulent consumer returns: exploiting retailer's return policies. *Eur. J. Marketing*, 44(6), 730–747.

[7] Harris, L.C. (2008). Fraudulent return proclivity: an empirical analysis. *J. Retailing*, 84(4), 461-476.

[8] Yao, D.Q., Yue, X., Wang, X., Liu, J.J. (2005). The impact of information sharing on a returns policy with the addition of a direct channel. *International Journal of Production Economics*, 97(2), 196-209.

[9] Petersen, J.A., Kumar, V. (2009). Are product returns a necessary evil? Antecedents and consequences. *J. Market*., 73(3), 35–51.

[10] Janakiraman, N., Syrdal, H.A., Freling, R. (2016). The effect of return policy leniency on consumer purchase and return decisions: a meta-analytic review. *J. Retail.*, 92(2), 226-235.

[11] Khouja, M., Ajjan, H., Liu, X. (2019). The effect of return and price adjustment policies on a retailer's performance. *European Journal of Operations Research*, 276, 466-482.

[12] Wang, K.H., Tung, C.T., & Lee, Y.J. (2010). EOQ model for deteriorating items with resalable returns. *Journal of information and Optimization Sciences*, 31(1), 189-204.

[13] Ghoreishi, M., Mirzazadeh, A., & Weber, G.W. (2014). Optimal pricing and ordering policy for non-instantaneous deteriorating items under inflation and customer returns. *Optimization*, 63(12), 1785-1804.

[14] Al-Salamah, M., Alsawafy, O. (2011). Economic order quantity for items with two types of imperfect

quality. *An International Journal of Optimization and Control: Theories and Applications*, 2(1), 73-82.

[15] Ekren, B.Y., Arslan, B. (2020). Simulation based lateral transshipment policy optimization for s, S inventory control problem in a single-echelon supply chain network. *An International Journal of Optimization and Control: Theories and Applications*, 10(1), 9-16.

[16] Gurkan, M.E., Tunc, H. (2021). A fix-and-optimize heuristic for the capacitated multi-item stochastic lot-sizing problem. *An International Journal of Optimization and Control: Theories and Applications*, 11(1), 41-51.

[17] Uddin, F.M., Sano, K. (2012). Coordination and optimization: the integrated supply chain analysis with non-linear price-sensitive demand. *An International Journal of Optimization and Control: Theories and Applications*, 2(1), 83-94.

[18] Mahata, G.C. (2012). An EPQ-based inventory model for exponentially deteriorating items under retailer partial trade credit policy in supply chain. *Expert Syst. Appl.*, 39(3), 3537–3550.

[19] Min, J., Zhou, Y. W., Liu, G. Q., & Wang, S. D. (2012). An EPQ model for deteriorating items with inventory-level-dependent demand and permissible delay in payments. *International Journal of Systems Science*, 43(6), 1039–1053.

Mamta Kumari *has obtained her B.Sc. degree from Banaras Hindu University. She has obtained her M.Sc. degree from National Institute of Technology Durgapur. She is currently carrying out her doctoral research at National Institute of Technology Silchar. Her research area includes Operations Research, Inventory Management and Supply Chain Management.*

http://orcid.org/0000-0002-7308-7405

Pijus Kanti De *has obtained his M.Sc. and B.T. degrees from the University of Kalyani and received his M. Phil and Ph. D. degrees in Applied Mathematics from Indian School of Mines, Dhanbad (presently IIT Dhanbad). Presently he is employed as an Associate Professor in Mathematics in the National Institute of Technology Silchar. Before joining to NIT Silchar, Dr. De was employed in many other institutions like C-MMACS, National Aerospace Laboratories Bangalore, KIET Ghaziabad, Delhi College of Engineering (presently Delhi Technological University) and Banasthali University as a Senior Research Fellow, Lecturer, Sr Lecturer, Reader and Associate Professor. Dr. De has supervised several thesis at doctoral and master's level. Also Dr. De has adjudicated several doctoral thesis from different Universities. He has published many research articles and written a book, 'Computer Based Numerical Methods and Statistical Techniques'. His research areas include Operations Research, Optimization Techniques, Fuzzy Logic & Belief Theory, Fuzzy Optimization, Fuzzy Mathematics, Mathematical Modelling, Elasto-Dynamics and Numerical Methods.*

http://orcid.org/0000-0003-3361-9371

An International Journal of Optimization and Control: Theories & Applications
ISSN: 2146-0957 eISSN: 2146-5703
Vol.12, No.1, pp.56-65 (2022)
https://doi.org/10.11121/ijocta.2022.1084

RESEARCH ARTICLE

Multi-objective regression modeling for natural gas prediction with ridge regression and CMARS

Ayşe Özmen *

Department of Mathematics, TED University, Turkey
Department of Mathematics and Statistics, University of Calgary, Canada
ayseozmen19@gmail.com

ARTICLE INFO

Article history:
Received: 17 February 2021
Accepted: 23 November 2021
Available Online: 1 January 2022

Keywords:
Ridge Regression
(C)MARS
CQP
Interior Point
Prediction of Natural Gas Consumption

AMS Classification 2010:
90C30, 90C51, 90C90

ABSTRACT

Residential customers are the main users generally need a great quantity of natural gas in distribution systems, especially, in the wintry weather season since it is particularly consumed for cooking and space heating. Hence, it ought to be non-interruptible. Since distribution systems have a restricted ability for supply, reasonable planning and prediction through the whole year, especially in winter seasons, have emerged as vital. The Ridge Regression (RR) is formulated mainly to decrease collinearity results through shrinking the regression coefficients and reducing the impact in the model of variables. Conic multivariate adaptive regression splines ((C)MARS) model is constructed as an effective choice for MARS by using inverse problems, statistical learning, and multi-objective optimization theories. In this approach, the model complexity is penalized in the structure of *RR* and it is constructed a relaxation by utilizing continuous optimization, called *Conic Quadratic Programming* (*CQP*). In this study, CMARS and RR are applied to obtain forecasts of residential natural gas demand for local distribution companies (LDCs) that require short-term forecasts, and the model performances are compared by using some criteria. Here, our analysis shows that CMARS models outperform RR models. For one-day-ahead forecasts, CMARS yields a MAPE of about 4.8%, while the same value under RR reaches 8.5%. As the forecast horizon increases, it can be seen that the performance of the methods becomes worse, and for a forecast one week ahead, the MAPE values for CMARS and RR are 9.9% and 18.3%, respectively.

1. Introduction

Local Distribution Companies (LDCs) are the service carriers of private natural gas purchasers within a particular transportation structure. When LDCs target unbalanced gas consumption from Transmission System Operator (TSO) pipelines, regulations, and related policies impose fairly high costs on them in the form of penalties. So correct forecasting is crucial here, as LCD demand is met through spot markets and much of the total demand is organized with global supply contracts through pipelines or liquefied natural gas. The operation must be flexible to compensate for fluctuations in demand. The fluctuation adjustment of energy demand under the constraints of system operation should be realized by predictive models organized for individual types of customers. For LCDs, a unique one-day and one-week forecast gives a discount to cost operations and elimination of penalties that occur due to unbalanced demand-supply quantities [1,2].

A problem is described as an ill-posed problem if a solution is not unique, present, or stable under perturbation on data. This means that if a small perturbation of the data may bring about a large perturbation of the solution. Ridge Regression is one of the most well-known structures to make these problems regular and stable [3, 4]. It is also known as Tikhonov Regularization. In the statistical literature, there exist some approaches such as principal components regression, partial least squares, least absolute shrinkage and selection operator (LASSO), and ridge regression (RR) to prevent collinearity in traditional linear regression models. Here, RR and LASSO are regularization/penalization strategies that impose a constraint on the regression coefficients while principal components and partial least squares regression are

*Corresponding author

variable subset decision strategies that employ linear combinations of the independent variables in the regression model. RR is formulated mainly to decrease collinearity results by shrinking the regression coefficients and reducing the impact in the model of variables. Here, it seems that shrinking the coefficient estimates may extensively decrease their variance [5].

MARS creates flexible models by employing piecewise linear functions. This continuous model gives a high-quality way to model nonlinearities [6]. Nowadays, as a nonparametric model, MARS is efficiently applied to many areas of technology and science. Here, Conic Multivariate Adaptive Regression Splines (CMARS) model [7-10] is evolved for the backward stage of MARS. It is obtained as a model-based alternative and an effective choice to MARS. In this algorithm, a *Penalized Residual Sum of Squares* (*PRSS*) is applied for MARS as *RR* problem and it is worked out by *Conic Quadratic Programming* (*CQP*). So, Interior Point Methods [11, 12] and their codes, e.g., MOSEK [13] can be applied by the technique of CMARS. In this paper, we represent natural gas forecasts for one day and one week in advance for a transmission system operator by using RR and CMARS.

In this study, two multi-objective regression models are developed for short-term natural gas demand prediction using RR and CMARS for one day, and one week ahead with daily forecasting intervals. Here, the minimum temperature, the maximum temperature, and heating degree days of the daily average temperature are taken into consideration as different input variables. The MAPE values of CMARS reach 4.8 % and 8.5 for one day, and one week ahead forecasts, respectively. On the other hand, RR gives MAPE values of around 9.9% and 18.3%. We reveal that CMARS performs better than RR in terms of the main performance criteria.

The rest of the paper is organized into four parts. In Sections 2 and 3, we provide a brief review of the models applied in this study. In Section 3, we present our mathematical models. The numerical results of the model are presented and discussed in Section 4. We conclude our study with a discussion of the results and giving future research in Section 5.

2. Ridge regression

The subset determination strategies include applying the least-squares to fit a linear model which involves a subset of the predictors. As an alternative to subset selection, we may fit a model including all *k* predictors utilizing a procedure that contracts the coefficient estimates towards zero, or equivalently, that compels or regularizes the coefficient estimates [4, 14]. The shrinkage strategies become smaller the regression coefficients by implying a penalty on their size. These techniques bias the estimator of the regression coefficients to decrease the variance in addition to the mean squared error of the estimator and to forestall the model from overfitting [15]. The least-squares fitting procedure estimates $\alpha_0, \alpha_1, \ldots, \alpha_k$ using the values that minimize the Residual Sum of Square (RSS)

$$\sum_{i=1}^{n} y_i - \alpha_0 - \left(\sum_{j=1}^{k} \alpha_j x_{ij} \right)^2 .$$

The coefficients of RR are the values that minimize the quantity

$$\sum_{i=1}^{n} \left(y_i - \alpha_0 - \sum_{j=1}^{k} \alpha_j x_{ij} \right)^2 + \phi \sum_{j=1}^{k} \alpha_j^2 . \qquad (1)$$

Here, $\phi \geq 0$ is a *penalty parameter* and it is defined separately. In this method, there is a **tradeoff** between two different criteria (bias and variance). RR search coefficients that match the data well, by decreasing the RSS. Here, the second term, $\phi \sum_{j=1}^{k} \alpha_j^2$, known as a *shrinkage penalty*, is small if $\alpha_1, \ldots, \alpha_k$ are close to zero. Therefore, it affects the estimates of α_j towards zero. The penalty parameter, ϕ, controls the relative effect of these two criteria on the estimation of regression coefficient in (1). When $\phi = 0$, RR produces the least-squares estimates and the penalty term does not affect the model [4, 15]. The penalty term is also known as ℓ_2 penalty and the ℓ_2 norm of a coefficient vector $\boldsymbol{\alpha}$ is provided by $\|\boldsymbol{\alpha}\|_2 = \sqrt{\sum_{j=1}^{k} \alpha_j^2}$.

3. Conic multivariate adaptive regression splines

In general, with the CMARS algorithm, implementation of spline function acquires extreme and very important benefits especially in the modeling of dynamics. For both MARS and CMARS, considering a one-dimensional case (input variable), splines are piecewise polynomials. MARS obeys the following general model assumed to exist between the variables [6, 15]:

$$Y = f(\boldsymbol{x}) + \varepsilon, \qquad (2)$$

where $\boldsymbol{x} = \left(x_1, x_2 \ldots, x_k \right)^T$ is a vector of predictor, *Y* is the dependent variable and ε is an error that is supposed to have 0 mean and finite variance. MARS obtains reflected pairs for each input x_j $(j = 1, 2, ..., k)$ with *k*-dimensional knots $\vartheta_i = (\vartheta_{i,1}, \vartheta_{i,2}, ..., \vartheta_{i,k})^T$ at each input data vector $\boldsymbol{x}_i = (x_{i,1}, x_{i,2}, ..., x_{i,k})^T$ $(i = 1,2,...,N)$. Here, each function is piecewise linear with a knot value, ϑ. Therefore, in MARS, the Basis Functions (BFs) are determined as [15]

$$C := \left\{ (x_j - \vartheta)_+, \ (\vartheta - x_j)_+ \ \middle| \ \begin{array}{l} \vartheta \in \{x_{1,j}, x_{2,j}, ..., x_{N,j}\}, \\ j \in \{1, 2, ..., k\} \end{array} \right\}.$$

Here, $f(\boldsymbol{x})$ in (2) can be closer represented by a successively constructed linear combination of

functions obtained from the set *C* and *Y* takes the following form:

$$Y = \alpha_0 + \sum_{m=1}^{M} \alpha_m \delta_m(\boldsymbol{x}) + \varepsilon, \tag{3}$$

where α_0 is the intercept, α_m is the unknown coefficient for the *m*th BF (*m* = 1,2,...,*M*), and δ_m presents either a function or product of more than one function from the set C. The form of *m*th BF is represented as follows [15]:

$$\delta_m(\boldsymbol{x}_i) := \prod_{j=1}^{K_m} (x_{i\kappa_j^m} - \vartheta_{\kappa_j^m})_{\pm} \quad (i = 1,2,...,N). \tag{4}$$

Here, $\vartheta_{\kappa_j^m}$ is the corresponding knot value of the variable $x_{\kappa_j^m}$ and, $x_{i\kappa_j^m}$ is the corresponding input variable for the *j*th truncated linear function in the *m*th BF. Moreover, K_m is the interaction degree of the *m*th BF [16]. To construct the model, the MARS forward stepwise algorithm begins with the constant function $\delta_0(\boldsymbol{X}^0) = 1$ to estimate α_0, and all functions in the set C are considered as candidate functions. A lack-of-fit criterion is used to compare the possible BFs that has the form [16,17]:

- 1,
- x_a,
- $[x_a - \tau_j]_+$,
- $x_a x_b$, and
- $[x_a - \tau_j]_+ [x_b - \tau_k]_+$.

The BFs above employ different input variables, x_a and x_b, with their knots, τ_j and τ_k as input variables cannot be the same for each BF in the MARS algorithm. At each step, with one of the reflected pair in set C, all products of a function $\delta_m(\boldsymbol{X}^m)$ in the model set are taken into account as a new function pair and added the term to the model set. This term has the following form

$$\alpha_{M+1}\delta_a(\boldsymbol{X}^a)\cdot[X_k - \tau]_+ + \alpha_{M+2}\delta_a(\boldsymbol{X}^a)\cdot[\tau - X_k]_+$$

where α_{M+1} and α_{M+2} are coefficients that are estimated by least-squares with all other *M*+1 coefficients. Then the "winning" products are added into the model and then, for example, the possible candidates for BFs as follows [17]:

- 1,
- x_a,
- $[x_a - \tau_j]_+$, if x_a is in the model already,
- $x_a x_b$, if x_a and x_b are in the model already,
- $[x_a - \tau_j]_+ [x_b - \tau_k]_+$, if $[x_a - \tau_j]_+ x_b$ and $[x_b - \tau_k]_+ x_a$ are in the model already.

The model obtained by forward stage overfits the data. Therefore, a backwards-pruning procedure is applied to find BFs that contribute least to model fit, and then these BFs are progressively deleted. This iterative process continues until an optimal number of terms are presented in the final model [18, 19]. Here, MARS used a modified recursive partitioning strategy to simplify high-dimensional problems. The sequence of models generated from this procedure is evaluated by using generalized cross-validation (GCV), and the model with the best predictive fit is selected. Consequently, an estimated best model $\hat{f}_\beta$ of each number of terms, β, is found at the end of that process. In MARS model, generalized cross-validation is applied to define the optimal number of terms, μ, and it also shows the lack of fit. The GCV criterion defined by Friedman [4] is given by

$$LOF(\hat{f}_\beta) \;=\; GCV(\beta) := \frac{\sum_{i=1}^{N}(y_i - \hat{f}_\beta(\boldsymbol{x}_i))^2}{(1 - M(\beta)/N)^2}.$$

Here, *N* is the number of sample observations, and $M(\beta)$ represents the effective number of parameters in the model.

In the CMARS method, firstly, the large model provided by the forward MARS algorithm is built up and addressed. Instead of the backward stage algorithm of MARS, the *PRSS* with $M_{\max}$ BFs is employed as a refinement of the least-squares estimation (LSE) to control the lack of fit from the viewpoint of the tradeoff between goals of *complexity* and *stability* to estimate and assess the function $f(\boldsymbol{x})$ in (2). Consequently, PRSS can be summed up during the forward stage of MARS and written as [6]:

$$\begin{aligned} PRSS \;&:= \sum_{i=1}^{N}(y_i - \boldsymbol{\alpha}^T \boldsymbol{\delta}(\boldsymbol{b}_i))^2 \\ &+ \sum_{m=1}^{M_{\max}} \phi_m \sum_{\substack{|\boldsymbol{\theta}|=1 \\ \boldsymbol{\theta}^T=(\theta_1,\theta_2)}}^{2} \sum_{\substack{r<s \\ r,s\in V(m)}} \int_{Q^m} \alpha_m^2 \left[D_{r,s}^{\boldsymbol{\theta}} \delta_m(\boldsymbol{t}^m) \right]^2 d\boldsymbol{t}^m, \end{aligned} \tag{5}$$

Here, $\boldsymbol{\delta}(\boldsymbol{b}_i) := \left(1, \delta_1(\tilde{\boldsymbol{x}}_i^1), \delta_2(\tilde{\boldsymbol{x}}_i^2), ..., \delta_m(\tilde{\boldsymbol{x}}_i^{M_{\max}})\right)^T$; $V(m) := \{\kappa_j^m \mid j = 1,2,...,K_m\}$ is the variable set related to the *m*th BF, δ_m; $\boldsymbol{t}^m = (t_{m_1}, t_{m_2}, ..., t_{m_{K_m}})^T$ presents the vector of variables contributing to the *m*th BF, δ_m; $\phi_m \geq 0$ are *penalty parameters* (m = 1,2,..., $M_{\max}$); $\boldsymbol{\alpha}$ is a $((M_{\max}+1)\times 1)$-parameter vector to be estimated by using the data points [16]. Furthermore, Q^m is some appropriate integration domains in K_m-dimensional parallel-pipe. After a discretization is employed to approximate the multi-dimensional integral

$\int \alpha_m^2 \left[D_{r,s}^{\boldsymbol{\theta}} \delta_m(\boldsymbol{t}^m) \right]^2 d\boldsymbol{t}^m$ and only one penalty parameter $\left(\phi = \phi_m := \lambda^2\right)$ is used rather than applying distinct penalty parameters for each derivative in (5), the new approximate form of PRSS can be written as follows (we refer to [2,7-9,16,20] for more details):

$$PRSS \approx \left\| \boldsymbol{y} - \boldsymbol{\delta}(\tilde{\boldsymbol{b}})\boldsymbol{\alpha} \right\|_2^2 + \phi \left\| \boldsymbol{L}\boldsymbol{\alpha} \right\|_2^2 . \tag{6}$$

Here, L is to be assigned an $((M_{\max}+1)\times(M_{\max}+1))$-diagonal matrix. Then, the *PRRS* problem looks like a classical *RR problem* with $\phi > 0, \phi = \lambda^2$ for some $\lambda \in \mathbb{R}$, and this problem in (6) is expressed as a CQP [21]. So, based on a suitable selection of the bound K, the optimization problem in (6) can be rearranged [16]:

$$\begin{aligned} &\underset{t,\boldsymbol{\alpha}}{\text{minimize}}\ t \\ &\text{subject to } \left\| \boldsymbol{\varsigma}(\boldsymbol{b})\boldsymbol{\alpha} - \boldsymbol{y} \right\|_2 \le t, \\ &\qquad \left\| \boldsymbol{L}\boldsymbol{\alpha} \right\|_2 \le \sqrt{K}. \end{aligned} \tag{7}$$

At this point, we state that a careful learning process has to be followed for the choice of K.

4. Natural gas demand modeling by RR and CMARS

In this study, we consider two multi-objective models which use ℓ_2 norm regularization in linear and nonlinear modeling for the prediction of natural gas demand. Here, the advantage of regularization is to decrease the risk of overfitting, which usually occurs in high-dimensional learning. The primary goal of the regularization technique is to make the machine learning algorithm "learn" but "not memorize" by penalizing the algorithm to decrease its generalization error to avoid the risk of overfitting. As a consequence, the variance of the model may be considerably declined, without losing any important properties in the data. Moreover, since regularization is a kind of robustification, these kinds of models can also be called robust models.

4.1. Data

In this study, the data set comprising of daily natural gas demand data from 2004 to 2013 are provided by Baskentgaz, the LDC of Ankara. To check the performance of our models, we draw on the validation technique. We divide the dataset into two subsets as training and testing sets. Here, the dataset is not divided randomly since it includes a time series of natural gas and meteorological variables. Instead, the first six years (from 2004 to 2009) of each variable under consideration are selected as the training dataset, while the last four years of the series are selected as the test dataset. In this study, demand for residential customers of Baskentgaz is modeled by applying RR and CMARS algorithms.

Our dataset contains some meteorological variables namely heating degree day (average temperature), relative humidity, wind speed, daily maximum and minimum temperatures. in this study, the meteorological variables used are proved by the Turkish State Meteorological Service. Indeed, energy consumption, especially natural gas, is highly dependent on weather conditions. If the temperature drops below a certain value of the heating threshold, households use more energy owing to the excessive need for space heating [1,2].

Here, firstly, the model details are given and then their performances are discussed for each forecasting time horizon. In the application of RR, the MATLAB regularization toolbox is utilized. In applications of CMARS, Salford MARS [19] is utilized to obtain BFs for the large model provided by the forward MARS algorithm. Afterward, MOSEK optimization software and MATLAB are used to solve the CQP problem and estimate unknown parameters.

4.2. Criteria for performance evaluations

Here, we tested the prediction accuracy of two specific prediction methods on real-time data. The main performance indicator for checking the accuracy of the models is the mean absolute percentage error (MAPE). In addition to MAPE, we also evaluate the multiple coefficient of determination (R^2), correlation coefficient (r), average absolute error (AAE), and root mean square error (RMSE) to check the performances of proposed models. These measures and their formulas are presented in Table 1.

Table 1. Performance measures and their formulas.

Abbreviation	Formula
MAPE	$MAPE := \frac{1}{N}\sum_{k=1}^{N}\left\lvert\frac{(y_k - \hat{y}_k)}{y_k}\right\rvert$
R^2	$R^2 := 1 - \left(\frac{\sum_{k=1}^{N}(y_k - \hat{y}_k)^2}{\sum_{k=1}^{N}(y_k - \bar{y}_k)^2} \right).$
AAE	$AAE := \frac{1}{N}\sum_{k=1}^{N}\lvert y_k - \hat{y}_k\rvert$
RMSE	$RMSE := \sqrt{\frac{1}{N}\sum_{k=1}^{N}(y_k - \hat{y}_k)^2}$
r	$r := \frac{\sum_{k=1}^{N}(y-\bar{y})(\hat{y}-\bar{\hat{y}})}{(N-1)\sqrt{s(y)^2 s(\bar{y})^2}}$

4.3. RR models

In the RR algorithm, first, many different models were obtained based on different penalty parameters, ϕ , by using the MATLAB regularization toolbox. Here, the penalty parameter, ϕ, controlled the relative effect of both criteria (bias and variance) on the estimation of regression coefficient in (1). Then, the penalty parameter that tries to minimize two criteria in a balanced manner was selected. So, the following RR model based on selected penalty value provided the best solution for complexity and accuracy in (1).

4.3.1. One-day-ahead prediction

Day-ahead forecast is generally used to reduce operational costs and eliminate the drawbacks that can occur owing to the imbalance between supply and demand quantities. The system operator requires to identify the supply security issues that may exist the next day. The RR model for one-day-ahead forecasting can be represented as follows:

$$\begin{aligned}\hat{Y}_t &= 0.22 + 0.91X_1 - 0.11X_2 - 0.01X_3 + 0.01X_4 \\ &\quad - 0.04X_5 + 0.04X_6 + 0.02X_7 + 0.09X_8 + 0.09X_9 \\ &\quad - 0.03X_{10} + 0.04X_{11} + 0.05X_{12}.\end{aligned}$$

Here, for RR and CMARS models based on one-day ahead and one-week ahead, X_1, X_2, X_3, X_4, X_5, X_6, X_7, and X_8 represents the first-order lagged, second-order lagged, third-order lagged, fourth-order lagged, fifth-order lagged, sixth-order lagged, seventh-order lagged and fourteenth-order lagged natural gas consumption, respectively. Hence, the RR and CMARS models obtained are "lag" models since they involve lagged dependent variables. Furthermore, X_9, X_{10}, X_{11}, and X_{12} are the heating degree days, maximum temperature, minimum temperature, and wind speed, respectively.

4.3.2. One-week-ahead prediction

One-week-ahead forecast is usually used for generating unit production schedules for the next week. This gives companies insight into generation and consumption trends as well as assisting them to plan their weekly generation schedules. The RR model for a one-week forecast can be stated as follows:

$$\begin{aligned}\hat{Y}_t &= 0.007 + 0.061X_1 + 0.06X_2 + 0.06X_3 + 0.06X_4 \\ &\quad + 0.06X_5 + 0.06X_6 + 0.06X_7 + 0.6X_8 + 0.16X_9 \\ &\quad + 0.03X_{10} - 0.02X_{11} + 0.01X_{12}.\end{aligned}$$

Here, RR models find all variables to be significant as expected.

4.4. CMARS Models

In the CMARS algorithm, first of all, using original data, the MARS algorithm is run via Salford MARS [22] and many MARS models were developed changing the number of BF and interaction. After selecting the optimal model for MARS among obtained models, the set of BFs in the forward part of MARS in the optimal MARS model was taken for the CMARS model. After the greatest models are constructed with the selected BFs and the *L* matrices in (7) are obtained, the PRSS in (6) is reformulated as a CQP problem. Here, based on different $\sqrt{K}$ values in (7), several different CQP models in (7) were solved individually via MOSEK [11]. Here, MOSEK applies an interior point algorithm [12,13] to treat the CQP problems CMARS yields many solutions. Finally, the CQP model that has the minimum value of approximate PRSS was selected and the unknown parameters were estimated for the CMARS model. Here, this point tries to minimize the criteria, $\|\boldsymbol{\varsigma}(\boldsymbol{b})\boldsymbol{\alpha} - \boldsymbol{y}\|_2$ and $\|\boldsymbol{L}\boldsymbol{\alpha}\|_2$, in a balanced manner and the chosen value provides the best solution for complexity and accuracy based on PRSS. Here, we should note that the knot values of BFs in the CMARS model are selected differently but extremely close to the corresponding input data to avoid non-differentiability in the optimization problem.

4.4.1. One-day ahead prediction

In the CMARS algorithm, using the MARS software [22], the highest degree of interactions and $M_{\max}$ are found by the forward MARS algorithm. For this data set, $M_{\max}$ is 23 and the highest degree of interaction is 2. So, the largest model constructed by the forward MARS stage includes the following BFs.

$$\psi_1(\boldsymbol{x}) = \max\{0,\ X_1 - 6.249\},$$

$$\psi_2(\boldsymbol{x}) = \max\{0,\ 6.249 - X_1\},$$

$$\psi_3(\boldsymbol{x}) = \max\{0,\ X_9 - 8.001\},$$

$$\psi_4(\boldsymbol{x}) = \max\{0,\ 8.001 - X_9\},$$

$$\psi_5(\boldsymbol{x}) = \max\{0,\ X_{11} - 7.801\},$$

$$\psi_6(\boldsymbol{x}) = \max\{0,\ 7.801 - X_{11}\},$$

$$\psi_7(\boldsymbol{x}) = \max\{0,\ X_6 - 9.925\},$$

$$\psi_8(\boldsymbol{x}) = \max\{0,\ 9.925 - X_6\},$$

$$\psi_9(\boldsymbol{x}) = \max\{0,\ X_9 - 10.301\} \cdot \max\{0,\ 9.925 - X_6\},$$

$$\psi_{10}(\boldsymbol{x}) = \max\{0,\ 10.301 - X_9\} \cdot \max\{0,\ 9.925 - X_6\},$$

$$\psi_{11}(\boldsymbol{x}) = \max\{0,\ X_1 - 2.502\} \cdot \max\{0,\ 9.925 - X_6\},$$

$$\psi_{12}(\boldsymbol{x}) = \max\{0,\ 2.502 - X_1\} \cdot \max\{0,\ 9.925 - X_6\},$$

$$\psi_{13}(\boldsymbol{x}) = \max\{0,\ X_{11} - 5.601\} \cdot \max\{0,\ 6.249 - X_1\},$$

$$\psi_{14}(\boldsymbol{x}) = \max\{0,\ 5.601 - X_{11}\} \cdot \max\{0,\ 6.249 - X_1\},$$

$$\psi_{15}(\boldsymbol{x}) = \max\{0,\ X_6 - 7.336\} \cdot \max\{0,\ X_9 - 8.001\},$$

$$\psi_{16}(\boldsymbol{x}) = \max\{0,\ 7.336 - X_6\} \cdot \max\{0,\ X_9 - 8.001\},$$

$$\psi_{17}(\boldsymbol{x}) = \max\{0,\ X_1 - 4.685\} \cdot \max\{0,\ X_9 - 8.001\},$$

$$\psi_{18}(\boldsymbol{x}) = \max\{0,\ 4.685 - X_1\} \cdot \max\{0,\ X_9 - 8.001\},$$

$$\psi_{19}(\boldsymbol{x}) = \max\{0,\ X_{11} - 8.901\} \cdot \max\{0,\ X_9 - 8.001\},$$

$$\psi_{20}(\boldsymbol{x}) = \max\{0,\ 8.901 - X_{11}\} \cdot \max\{0,\ X_9 - 8.001\},$$

$$\psi_{21}(\boldsymbol{x}) = \max\{0,\ X_1 - 8.402\} \cdot \max\{0,\ X_9 - 8.001\},$$

$$\psi_{22}(\boldsymbol{x}) = \max\{0,\ 8.402 - X_1\} \cdot \max\{0,\ X_9 - 8.001\},$$

$$\psi_{23}(\boldsymbol{x}) = \max\{0,\ X_9 - 0.001\} \cdot \max\{0,\ X_6 - 9.925\}.$$

CMARS model for the one-day-ahead forecast is stated as follows:

$$\begin{aligned}\hat{Y} &= \alpha_0 + \sum_{m=1}^{23} \alpha_m \psi_m(\boldsymbol{x}) \\ &= 5.30 + 0.77\psi_1(\boldsymbol{x}) - 0.61\psi_2(\boldsymbol{x}) - 0.27\psi_3(\boldsymbol{x}) - 0.09\psi_4(\boldsymbol{x}) \\ &\quad + 0.10\psi_5(\boldsymbol{x}) - 0.01\psi_6(\boldsymbol{x}) - 0.19\psi_7(\boldsymbol{x}) - 0.08\psi_8(\boldsymbol{x}) \\ &\quad + 0.01\psi_9(\boldsymbol{x}) + \alpha_{10}\psi_{10}(\boldsymbol{x}) - 0.002\psi_{11}(\boldsymbol{x}) - 0.01\psi_{12}(\boldsymbol{x}) \\ &\quad - 0.02\psi_{13}(\boldsymbol{x}) - 0.01\psi_{14}(\boldsymbol{x}) + 0.01\psi_{15}(\boldsymbol{x}) - 0.02\psi_{16}(\boldsymbol{x}) \\ &\quad + 0.05\psi_{17}(\boldsymbol{x}) - 0.09\psi_{18}(\boldsymbol{x}) + 0.01\psi_{19}(\boldsymbol{x}) + 0.02\psi_{20}(\boldsymbol{x}) \\ &\quad - 0.06\psi_{21}(\boldsymbol{x}) + 0.07\psi_{22}(\boldsymbol{x}) - 0.02\psi_{23}(\boldsymbol{x}).\end{aligned}$$

For the CMARS model based on one-day ahead forecasting, the first-order lagged natural gas consumption (X_1), the sixth-order lagged natural gas consumption (X_6), the heating degree days (X_9), and minimum temperature (X_{11}) are significant.

4.4.2. One-week ahead prediction

For this natural gas data set based on one-week ahead forecasting, $M_{\max}$ is 27 and the highest degree of interaction is 2. So, the largest model constructed by the forward MARS algorithm includes the following BFs.

$$\psi_1(\boldsymbol{x}) = \max\{0,\ X_9 - 7.001\},$$

$$\psi_2(\boldsymbol{x}) = \max\{0,\ 7.001 - X_9\},$$

$$\psi_3(\boldsymbol{x}) = \max\{0,\ X_1 - 10.221\},$$

$$\psi_4(\boldsymbol{x}) = \max\{0,\ 10.221 - X_1\},$$

$$\psi_5(\boldsymbol{x}) = \max\{0,\ X_{10} - 20.801\},$$

$$\psi_6(\boldsymbol{x}) = \max\{0,\ 20.801 - X_{10}\},$$

$$\psi_7(\boldsymbol{x}) = \max\{0,\ X_{10} - 19.201\} \cdot \max\{0,\ 10.221 - X_1\},$$

$$\psi_8(\boldsymbol{x}) = \max\{0,\ 19.201 - X_{10}\} \cdot \max\{0,\ 10.221 - X_1\},$$

$$\psi_9(\boldsymbol{x}) = \max\{0,\ X_1 - 2.217\} \cdot \max\{0,\ X_9 - 7.001\},$$

$$\psi_{10}(\boldsymbol{x}) = \max\{0,\ 2.217 - X_1\} \cdot \max\{0,\ X_9 - 7.001\},$$

$$\psi_{11}(\boldsymbol{x}) = \max\{0,\ X_3 - 1.572\} \cdot \max\{0,\ 10.221 - X_1\},$$

$$\psi_{12}(\boldsymbol{x}) = \max\{0,\ 1.572 - X_1\} \cdot \max\{0,\ 10.221 - X_1\},$$

$$\psi_{13}(\boldsymbol{x}) = \max\{0,\ X_8 - 6.032\} \cdot \max\{0,\ 10.221 - X_1\},$$

$$\psi_{14}(\boldsymbol{x}) = \max\{0,\ 6.032 - X_8\} \cdot \max\{0,\ 10.221 - X_1\},$$

$$\psi_{15}(\boldsymbol{x}) = \max\{0,\ X_{12} - 1.601\} \cdot \max\{0,\ X_9 - 7.001\},$$

$$\psi_{16}(\boldsymbol{x}) = \max\{0,\ 1.601 - X_{12}\} \cdot \max\{0,\ X_9 - 7.001\},$$

$$\psi_{17}(\boldsymbol{x}) = \max\{0,\ X_{12} - 1.601\} \cdot \max\{0,\ 20.801 - X_{10}\},$$

$$\psi_{18}(\boldsymbol{x}) = \max\{0,\ 1.601 - X_{12}\} \cdot \max\{0,\ 20.801 - X_{10}\},$$

$$\psi_{19}(\boldsymbol{x}) = \max\{0,\ X_3 - 10.937\},$$

$$\psi_{20}(\boldsymbol{x}) = \max\{0,\ 10.937 - X_3\},$$

$$\psi_{21}(\boldsymbol{x}) = \max\{0,\ X_1 - 1.733\} \cdot \max\{0,\ 10.937 - X_3\},$$

$$\psi_{22}(\boldsymbol{x}) = \max\{0,\ 1.733 - X_1\} \cdot \max\{0,\ 10.937 - X_3\},$$

$$\psi_{23}(\boldsymbol{x}) = \max\{0,\ X_6 - 6.287\} \cdot \max\{0,\ X_9 - 7.001\},$$

$$\psi_{24}(\boldsymbol{x}) = \max\{0,\ 6.287 - X_6\} \cdot \max\{0,\ X_9 - 7.001\},$$

$$\psi_{25}(\boldsymbol{x}) = \max\{0,\ X_7 - 3.521\} \cdot \max\{0,\ X_9 - 7.001\},$$

$$\psi_{26}(\boldsymbol{x}) = \max\{0,\ 3.521 - X_7\} \cdot \max\{0,\ X_9 - 7.001\},$$

$$\psi_{27}(\boldsymbol{x}) = \max\{0,\ X_{10} + 7.401\} \cdot \max\{0,\ 7.001 - X_9\}.$$

CMARS model for the one-week-ahead forecast is stated as follows:

$$\begin{aligned}\hat{Y} &= \alpha_0 + \sum_{m=1}^{23} \alpha_m \psi_m(\boldsymbol{x}) \\ &= 5.24 + 0.43\psi_1(\boldsymbol{x}) + 0.65\psi_2(\boldsymbol{x}) + 0.44\psi_3(\boldsymbol{x}) + 1.07\psi_4(\boldsymbol{x}) \\ &\quad - 0.20\psi_5(\boldsymbol{x}) + 0.04\psi_6(\boldsymbol{x}) + 0.01\psi_7(\boldsymbol{x}) - 0.02\psi_8(\boldsymbol{x}) \\ &\quad - 0.01\psi_9(\boldsymbol{x}) + \alpha_{10}\psi_{10}(\boldsymbol{x}) - 0.18\psi_{11}(\boldsymbol{x}) - 0.18\psi_{12}(\boldsymbol{x}) \\ &\quad + 0.04\psi_{13}(\boldsymbol{x}) - 0.003\psi_{14}(\boldsymbol{x}) - 0.05\psi_{15}(\boldsymbol{x}) - 0.03\psi_{16}(\boldsymbol{x}) \\ &\quad + 0.04\psi_{17}(\boldsymbol{x}) + 0.06\psi_{18}(\boldsymbol{x}) - 0.15\psi_{19}(\boldsymbol{x}) - 1.36\psi_{20}(\boldsymbol{x}) \\ &\quad + 0.15\psi_{21}(\boldsymbol{x}) - 0.24\psi_{22}(\boldsymbol{x}) + 0.004\psi_{23}(\boldsymbol{x}) + 0.002\psi_{24}(\boldsymbol{x}) \\ &\quad - 0.04\psi_{25}(\boldsymbol{x}) + 0.02\psi_{26}(\boldsymbol{x}) - 0.02\psi_{27}(\boldsymbol{x}).\end{aligned}$$

For the CMARS model based on one-week ahead forecasting, the first-order lagged natural gas consumption (X_1), the third-order lagged natural gas consumption (X_3), the sixth-order lagged natural gas consumption (X_6), the seventh-order lagged natural gas consumption (X_7), the fourteenth-order lagged natural gas consumption (X_8), the heating degree days (X_9), maximum temperature (X_{10}), and wind speed (X_{12}) are significant.

4.5. Results

In this study, we propose to model seasonal patterns and trends directly without using any transformations. As shown in Figures 1-8, the presented models capture the seasonality and trend of natural gas consumption. Moreover, with an additional plot, Figures 1-8 display the daily error (residual) time series for each model and let us analyze the residual dynamics. For natural gas demand prediction, the performance of the RR and CMARS models was evaluated using the performance measures presented in Table 1. For the training and test cases of the RR and CMARS models, Table 2 and Table 3 show the performance matrices for the forecasting of one-day-ahead and one-week-ahead, respectively.

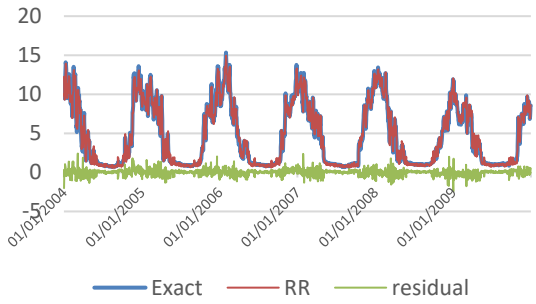

Figure 1. Exact values and RR approximation of natural gas consumption for one-day-ahead prediction based on training data

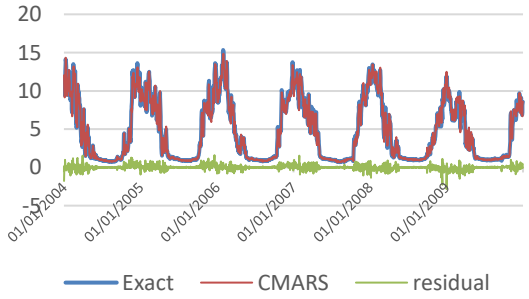

Figure 2. Exact values and CMARS approximation of natural gas consumption for one-day ahead prediction based on training data

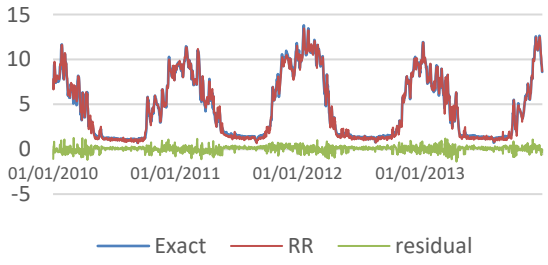

Figure 3. Exact values and RR approximation of natural gas consumption for one-day ahead prediction based on test data

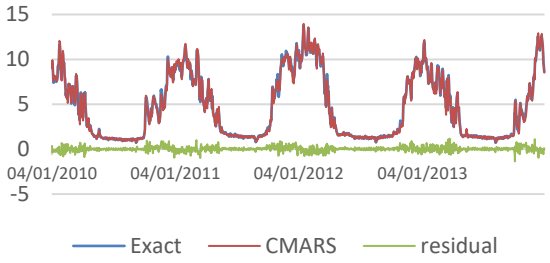

Figure 4. Exact values and CMARS approximation of natural gas consumption for one-day ahead prediction based on test data

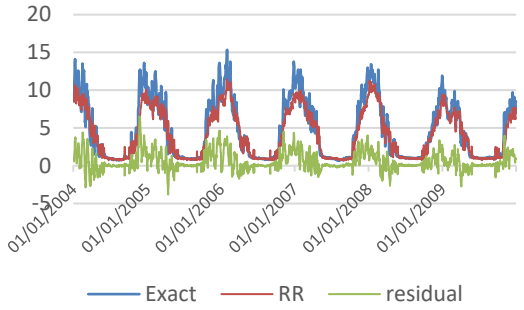

Figure 5. Exact values and RR approximation of natural gas consumption for one-week ahead prediction based on training data

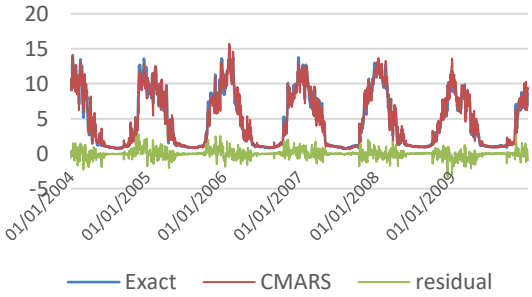

Figure 6. Exact values and CMARS approximation of natural gas consumption for one-week ahead prediction based on training data

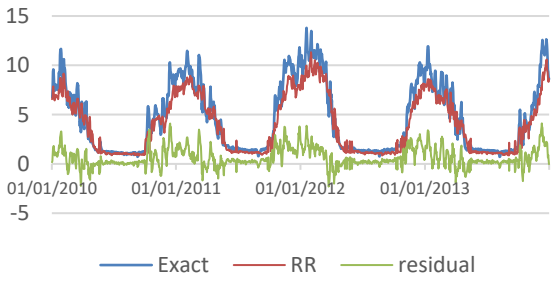

Figure 7. Exact values and RR approximation of natural gas consumption for one-week ahead prediction based on test data

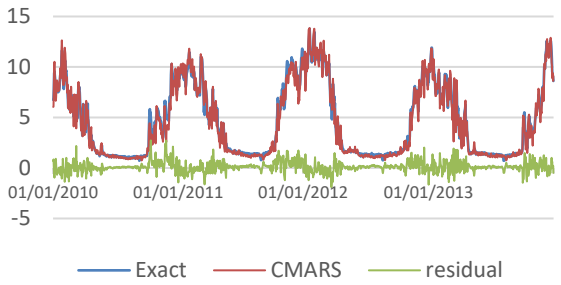

Figure 8. Exact values and CMARS approximation of natural gas consumption for one-week ahead prediction based on test data

Table 2. Performance of RR and CMARS for one-day ahead forecasting

	RR		CMARS	
	train	**test**	**train**	**test**
R^2	0.989	0.991	0.994	0.994
AAE	0.28	0.253	0.195	0.18
RMSE	0.405	0.333	0.313	0.264
r	0.995	0.996	0.997	0.997
MAPE	**0.094**	**0.085**	**0.046**	**0.048**

Table 3. Performance of RR and CMARS for one-week ahead forecasting

	RR		CMARS	
	train	**test**	**train**	**test**
R^2	0.885	0.889	0.977	0.976
AAE	0.861	0.827	0.383	0.368
RMSE	1.324	1.165	0.596	0.538
r	0.965	0.971	0.988	0.989
MAPE	**0.181**	**0.183**	**0.09**	**0.099**

For the one-day-ahead forecast, Table 2 shows the performances of the RR and CMARS models based on training and test. Depending on the results given in Table 2, the CMARS model outperforms the RR model in terms of all performance measures for training and testing data.

For the one-week-ahead forecast, the performances of RR and CMARS models are compared in Table 3 in terms of training and test cases. Based on the results shown in Table 3, the CMARS model outperforms the RR model in terms of all performance measures for training and test cases. Here, the MAPE performance becomes worse as the prediction horizon increases.

Based on residual, RR and CMARS have similar plots for one-day-ahead forecast whereas CMARS has better results than RR for the one-week-ahead forecast as in terms of training and test cases, as seen in Figures 1-8. Here, the proposed models have very small residuals for one-day-ahead forecasting. However, when the forecasting horizon increases, the residuals of the models become worse as expected.

In this application, the most *essential variables* in the analyzed residential demand models are based on *temperature* since a huge volume of natural gas is needed for space heating in Ankara, Therefore, in cold weather, natural gas usage reduces virtually linearly as the temperature rises. As you can see in Figures 1-7, this event also constructs a large difference between the winter and summer periods of private natural gas demand. Among the presented models, the CMARS model significantly outperforms the RR model in terms of all the training and test case performance criteria presented in Table 1 based on the short-term forecast. Therefore, CMARS should be the preferred model for this particular problem based on the short-term natural gas forecast.

5. Conclusion

In this study, we present two innovative models to short-term natural gas forecasting problems in the energy market. For residential users of LDCs, we evaluate daily and weekly forecasts of natural gas demand with daily intervals. We produce out-of-sample forecasts and compare them to observed data in terms of test datasets to assess the models' prediction accuracy.

The prediction accuracy is assessed for each forecast horizon using the performance criteria listed in Table 1. The proposed models, as illustrated in Figures 1-8, can capture the natural gas demand trend and seasonal pattern. However, it is found that CMARS performs better for one-day-ahead and one-week-ahead forecasts with MAPE values of 4.8% and 9.9%, respectively. Moreover, using CMARS as a substitute for MARS provides an integrated representation of all parameter identification tasks as a model-based optimization model instead of a model-free problem. As a result, in the multicriteria regression models offered, CMARS models should be favored for this particular situation.

However, since the knot selection does not require for the linear parts in CMARS, as further study, Conic Generalized Partial Linear Model (CGPLM) [23] may also be added to the CMARS algorithms so that these semi-parametric algorithms may provide to decrease the complexity of CMARS. Moreover, the same study may be repeated with the robust counterparts being R(C)PLM [24,25] and R(C)MARS [26-31], and then the comparative results may be provided. In future researches, proposed models can be compared to time series models and many other traditional and recent methods.

Acknowledgments

The authors would like to thank the anonymous reviewers for their valuable comments. This work was supported by TUBITAK under the 2219-International Postdoctoral Research Scholarship Programme.

References

[1] Özmen, A., (2021). Sparse regression modeling for short- and long-term natural gas demand prediction. *Annals Operations Research*, DOI: https://doi.org/10.1007/s10479-021-04089-x

[2] Özmen, A., Yılmaz Y., & Weber, G.-W. (2018). Natural Gas Consumption Forecasting Model for Residential User. *Energy Economics*, 70, 357–381.

[3] Aster, R.C., Borchers, B., & Thurber C.H. (2013). *Parameter Estimation and Inverse Problems*. Academic Press, Boston.

[4] James, G., Witten, D., Hastie, T., & Tibshirani, R. (2013). *An introduction of statistical learning*, Springer.

[5] Wheeler, D. (2009). Simultaneous Coefficient Penalization and Model Selection in Geographically Weighted Regression: The Geographically Weighted Lasso. *Environment and Planning A*, 39(3), 722-742.

[6] Friedman, J.H. (1991). Multivariate adaptive regression splines. Annals of Statistics,19,1–67.

[7] Taylan, P., Weber, G.-W., & Beck, A. (2007). A new approach to regression by generalized additive models and continuous optimization for modern applications in finance, science and technology, Optimization. 56, 5-6, 675–698.

[8] Taylan, P., Weber, G. W., & Özkurt, F. Y. (2010). A new approach to multivariate adaptive regression splines by using Tikhonov regularization and continuous optimization. Top, 18(2), 377-395.

[9] Weber, G.-W., Batmaz, İ., Köksal, G., Taylan, P., & Yerlikaya-Özkurt, F. (2012). CMARS: a new contribution to nonparametric regression with multivariate adaptive regression splines supported by continuous optimization. *Inverse Problems in Science and Engineering*, 20(3), 371-400.

[10] Ayyıldız, E., Purutçuoğlu, V., & Weber, G. W. (2018). Loop-based conic multivariate adaptive regression splines is a novel method for advanced construction of complex biological networks. European Journal of Operational Research, 270(3), 852-861.

[11] Roos, C., Terlaky, T., & Vial, J. (1997). *Interior Point Approach to Linear Optimization: Theory and Algorithms*, John Wiley & Sons, New York.

[12] Roos, C., Terlaky, T., & Vial, J. (2006). Interior Point Methods for Linear Optimization. Springer Science, Heidelberg/Boston.

[13] MOSEK; software available at http://www.mosek.com.

[14] Tibshirani, R.(1996). *Regression shrinkage and selection via the lasso*. Journal of the Royal Statistical Soceity B, 267-288.

[15] Hastie, T., Tibshirani, R. & Friedman, J.H. (2001). *The Element of Statistical Learning*. Springer Series in Statistics; New York, USA.

[16] Özmen, A., Kropat, E., & Weber, G.-W. (2014b). Spline regression models for complex multi-modal regulatory networks. *Optimization Methods and Software* (OMS) 29(3), 515-534.

[17] Kriner, M. (2007). *Survival Analysis with Multivariate Adaptive Regression Splines*, Dissertation, LMU Munchen: Faculty of Mathematics, Computer Science and Statistics.

[18] Hastie, T. & Tibshirani, R.J. (1996). Discriminant analysis by Gaussian mixtures, Journal of the Royal Statistical Society (Ser. B) 58, 155–176.

[19] Leathwicka, J.R., Elith, J., & Hastie, T. (1993). Comparative performance of generalized additive models and multivariate adaptive regression splines for statistical modelling of species distributions, Ecological Modelling 199 (2), 188-196.

[20] Kuter, S., Weber, G.-W., Özmen, A.,& Akyürek, Z. (2014). Modern applied mathematics for alternative modelling of the atmospheric effects on satellite images, Modeling, *Optimization, Dynamics and Bioeconomy I, Springer Proceedings in Mathematics & Statistics*, 73, 469-485.

[21] Gürbüz, B., & Sezer, M. (2020). Modified operational matrix method for second-order nonlinear ordinary differential equations with quadratic and cubic terms. *An International Journal of Optimization and Control: Theories & Applications* (IJOCTA), 10(2), 218-225.

[22] Salford Systems-Data Mining and Predictive Analytics Software: MARS software available at http://www.salfordsystems.com.

[23] Weber, G.-W., Çavuşoğlu, Z, & Özmen, A. (2012).Predicting default probabilities in emerging markets by conic generalized partial linear models and their optimization. *Optimization*, 61(4), 443-457.

[24] Özmen A., Weber, G.-W., & Kropat, E. (2012). Robustification of conic generalized partial linear models under polyhedral uncertainty. *International IFNA-ANS scientific Journal* "*Problems of Nonlinear Analysis in Engineering Systems*", 2(38), 104-113.

[25] Özmen, A., Weber, G.-W., Çavuşoğlu, Z., & Defterli, Ö. (2013). The new robust conic GPLM method with an Application to Finance: prediction of credit default. *Journal of Global Optimization* (JOGO), 56 (2), 233-249.

[26] Özmen, A. (2016). Robust optimization of spline models and complex regulatory networks - theory, methods and application. Contribution to Management Science, Springer.

[27] Özmen, A., Weber, G.-W., Batmaz, I., & Kropat, E. (2011). RCMARS: Robustification of CMARS with Different Scenarios under Polyhedral Uncertainty Set. *Communications in Nonlinear Science and Numerical Simulation* (CNSNS) 16 (12), 4780-4787.

[28] Özmen, A., Weber, G.-W., & Karimov, A. (2013). RCMARS: A new optimization supported tool applied on financial data. *Pacific Journal of Optimization* (PJO) 9(3), 535-552.

[29] Özmen, A. & Weber, G.-W. (2014). RMARS: Robustification of Multivariate Adaptive Regression Spline under Polyhedral Uncertainty. *Journal of Computational and Applied Mathematics* (CAM), 259, 914–924.

[30] Özmen, A., Batmaz, I., & Weber, G.-W. (2014). Precipitation Modeling by Polyhedral RCMARS and Comparison with MARS and CMARS. *Environmental Modeling & Assessment*, 19(5), 425-435.

[31] Özmen, A., Kropat, E., & Weber, G.-W. (2017). Robust Optimization in Spline Regression Models for Multi-model Regulatory Networks under Polyhedral Uncertainty. *Optimization*, 66 (12), 2135-2155.

Ayse Özmen *studied Industrial Engineering and also Mathematics and Computer Science as a double major at Çankaya University. She earned her M.S. and Ph.D. degrees in Scientific Computing at the Institute of Applied Mathematics from Middle East Technical University (METU). Her master thesis was honored by the Best Thesis Award of METU in 2012. Then her Ph.D thesis was honored by the Serhat Ozyar Award in 2016. Then, she has been in Canada for 1.5 years as a Post-doctoral Scholar at the University of Calgary, Department of Mathematics and Statistics. Her research field is on Optimization, Network Modeling, Data Science, Machine Learning, and Mathematical Modeling and Programming, Energy Modeling. Dr. Özmen has participated in many research projects from different areas and (co-)authored lots of special issues and articles.*

http://orcid.org/0000-0003-3393-3619

An International Journal of Optimization and Control: Theories & Applications
ISSN: 2146-0957 eISSN: 2146-5703
Vol.12, No.1, pp.66-78 (2022)
https://doi.org/10.11121/ijocta.2022.1137

RESEARCH ARTICLE

Optimization of flexo process parameters to reduce the overall manufacturing cost

Akshay V. Joshi *

Department of Printing Engineering, P. V. G's College of Engineering & Technology and G. K. Pate (Wani) Institute of Management, Pune, India
avj_print@pvgcoet.ac.in

ARTICLE INFO

Article history:
Received: 12 July 2021
Accepted: 23 November 2021
Available Online: 2 January 2022

Keywords:
Flexography
Polyethylene
Design of Experiments
Analysis of Variance
Regression

AMS Classification 2010:
62K05 62K15, 62K86

ABSTRACT

The flexo process parameters play an important role in ink transfer and will lead to wastage of inks, substrate, solvents and printed stocks if not monitored and controlled. The work focuses on optimizing the flexo process parameters for 40 microns 3-layer polyethylene (PE) film with Blue Nitrocellulose (NC) ink to reduce overall manufacturing cost while maintaining the print quality for diaper application. An experimental design was conducted for the response Ink GSM (grams per square meter), ΔE and Print Mottle with factors such as ink viscosity, anilox volume, plate dot shape and substrate opacity. The data was analyzed through Main Effect, Interaction Plot and Analysis of Variance (ANOVA). The regression models were developed for the response to validate the predictive ability of model. The process optimization resulted in reduction of Ink GSM, ΔE and Print Mottle by 18%, 52% and 1% respectively. The ink consumption reduced by 18.26% with minimized print defects, thereby reducing the overall manufacturing cost.

1. Introduction

As per Mordor Intelligence Report [1], the growth of flexography printing market will be 2.44% CAGR within a period from 2021 to 2026 which accounts to 124.61 USD billion from 107.42 USD billion. A large part of the flexography industry clientele remains to be from the industry catering to the needs of people i.e. personal care products like baby diapers. The India Diaper Market Outlook 2021 [2] reports 22.23% CAGR in baby diaper market over past 5 years. There are almost 25 million babies born every year. The hygiene awareness of Indian mothers, rise in income of common people has led to an exponential growth in diaper market. These diapers are packaged in pouches that are printed on Polyethylene (PE) and Cast Polypropylene (CPP) films using NC based inks by Flexo process. The surface anomalies and print defects, plate fill-ups, frequent machine stoppages, shade inconsistency is one of the major challenges during printing these films. This results in print mottle, uneven print density and ink deposition, thereby depreciating the print quality and degrading the selling potential of the product. Furthermore, the overall manufacturing cost inclusive of printing, converting and process scrap cost is high. This demands for optimization with tight control of flexo process parameters to minimize the total manufacturing cost with improved print quality.

2. Flexography printing process

Flexography is a printing process which utilizes a flexible relief plate that adheres to a printing cylinder. The usage of flexible (soft) printing plates and low viscosity inks prints on a wide range of absorbent and non-absorbent substrates such as plastics, metallic films, paper and board. These plates are mounted on sleeves that receive ink from the ink pan through an anilox roller. An anilox roller is a cylinder consisting of fixed number of cells with a definite volume. A doctor blade is used to control the amount of ink transferred to the anilox roller. It wipes out any extra ink is collected back to the ink tray. The anilox roller rotates in the ink tray and carries the ink in its cells to the flexible plate mounted on a sleeve. In this process, ink gets transferred from anilox roller to the raised areas of the plate and thus inking only the image portion. This image area then comes in contact with the substrate and

*Corresponding author

transfers the image onto it by thrusting itself against the impression roller (Figure 1). The pressure between the plate cylinder and the impression roller is termed as kiss pressure and should be just enough to transfer ink from plate to substrate [3].

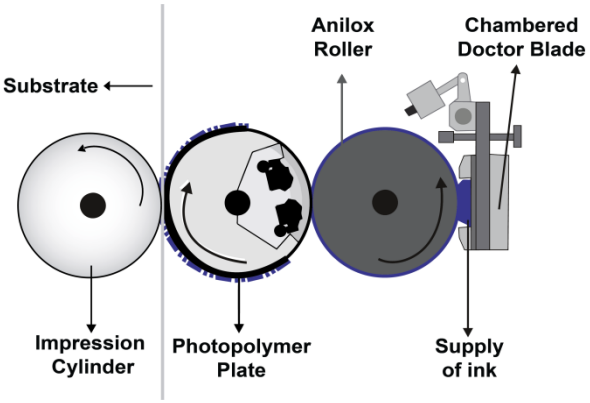

Figure 1. Flexography printing process

3. Flexography process parameters

The parameters that affect ink transfer in flexography and printability include plate, anilox, ink, substrate, solvents, press speed, surface energy of substrate etc. The printability attributes include density, Tone Value Increase, color deviation (Delta E), gloss, ink coat weight (GSM) and print mottle. Several works have been conducted by researchers to obtain the optimum print quality in the flexography print process [4-15]. The cost of print can be easily reduced by increasing the ink mileage and optimizing the flexo process parameters.

The anilox roller is the heart of flexography process and plays a significant role in ink transfer. The 60-deg hexagonal pattern are shallower and accommodates 15% more cells as compared to 30^0 hex,45^0 tri-helical and 70^0 cell angles. The 60^0 hex cells provide better dot support during printing with greater uniformity [4]. The flexo ink transfer is directly proportional to the anilox roller cell volume [5]. A thinner ink film is deposited on the substrate at higher anilox line screen that carries more no. of cells in a given area. This results in less ink transfer due to cell clogging, anilox scoring, and anilox wear. The lower line screen and volume led to a smoother cell surface with consistent ink transfer and print performance. There exists a direct relation between the coating deposit and the volume of the anilox. The ink transfer is governed by type of anilox engraving techniques, inking system and plate-making. These parameters allow to accommodate finer screen volume with lower cell volume [6-9]. The ink film thickness in flexography process depends upon the anilox volume measured in billion cubic microns. The transfer of ink from anilox to plate is almost 50% and further transfers 50% of the ink from plate to the substrate [3, 10]. In order to avoid print defects such as dirty print and dot dipping, banded anilox test should be performed with varying anilox screen and cell volume to identify the right specification of anilox roller for optimal ink transfer [11]. The laser engraved ceramic coated anilox roller has better release properties as compared to mechanically engraved chrome anilox roller. The quality of ink lay-down improves with ceramic coated anilox rollers [12]. The print consistency shall be achieved by the right selection of anilox screen ruling, volume and cell geometry [13].

The type of coating and polarity of substrate has a significant effect on print gloss and density. The coating on the substrate provides higher gloss as compared to uncoated substrate. The print density on uncoated substrate is inconsistent due to the ink deposition on the rough areas of the substrate. The presence of coating on the substrate leads to even lay-down of an ink. The print density increases with higher polarity of the substrate [14].

The ink film thickness and tone value increase in flexography is affected by the type of substrate, ink and viscosity. The print density increases for both solvent and water based flexo inks with the increase in anilox volume. The coated substrate reproduces higher print density with solvent-based inks as compared to water-based inks while the behavior is opposite for uncoated substrate. A higher tone value increase is noted with water-based ink on coated substrate as compared to solvent-based ink which is exactly opposite to uncoated substrate [15].

The solvents have a significant impact on the accuracy of the structures. The flexographic printing plate material must adapt to the solvents in functional fluids to avoid plate swelling due to penetration of solvents in plate [16]. The solvents used in flexographic ink play an important role in printed dot reproduction of both coated and uncoated paper. The dot shape improves with ink having high boiling point solvent and low drying velocity than the ink with low boiling point solvent and high drying velocity [17].

The ink transfer in flexography is governed by the substrate manufacturing processes. The correlation between substrate surface energy and ink surface tension have an impact on ink transfer. The surface treatments increase surface energy of the substrate that reduces the contact angle and improve wettability. The liquids adhere stronger to a surface with high surface energy [18]. The films with higher surface free energy results in higher optical density. A stronger adhesion leads to thicker layer of ink and hence higher optical density. The optical density is greatly affected by polar component of surface energy in water-diluted inks and dispersive component of free surface energy in solvent based inks [19]. The substrate with lower surface energy reduces wettability and results in higher mottle [20]. The non-uniform corona treatment will result in improper wetting on the printing surface and lead to occurrence of uncovered areas in the print [21]. The dot gain is affected by the nip pressure between plate and impression cylinder. The dot size increases with an increase in line screen [22]. The increased plate to

substrate engagement results in reduction in L* values while higher anilox to plate pressure yields higher ink transfer in the mid-tone areas. The rise in press speed initially produces a drop in ink transfer but increases with further increased speed, particularly in the highlights [23]. The type of flexo plate-making has an impact on print quality. The digital plate-making shows significant improvement in print contrast and tonal values as compared to conventional photopolymer plate [24]. The increase in depth of dot, increases dot stability that results in reduced tone value increase. The dot is expanded with an engagement of printing cylinder and impression cylinder. The line rulings on plate affects the image quality if not compensated during pre-press [25].

3.1. Substrate-ink interaction

The substrate surface energy, ink surface tension and interfacial tension between substrate and ink dictates the printability in flexography.

3.1.1. Surface energy of substrate

The measure of break up of inter-molecular bonds occurring at the surface is referred to as surface energy. In simple terms, it is the energy required per unit area to increase the size of surface and measured in mN/m.

In the most basic sense, surface free energy is defined as the adhesive characteristic of the solid, indicating its affinity towards the other materials. The substrate surface energy and ink surface tension are the crucial factors in ink transfer, spreading and adhesion. The difference between the surface energy and the surface tension has larger impact on ink transfer and extent of spreading. Higher the difference lower will be contact angle and better is the ink spreading on the substrate. Nevertheless, very high surface energy may lead to erratic print quality.

Surface free energy can be calculated by contact angle measurement with certain liquids of known surface tension. Contact angle is the angle between a liquid surface and the outline of contact surface of solid. The contact angle of a drop of liquid over a solid surface is determined by Young's Equation. Young described the relation between surface energy of solids, surface tension of liquid and their interfacial surface tension. It is mathematically given by:

$$cos\theta = (\gamma_S - \gamma_{LS})/\gamma_L \quad (1)$$

Where

θ = contact angle of liquid

γ_s = Surface Energy of Solid

γ_L = Surface Tension of Liquid

γ_{SL} = Interfacial Surface Tension between Solid and Liquid

The contact angle can be measured by either by varying the drop volume or with constant drop volume. The factors that affect contact angle other than substrate surface energy are ink surface tension, its viscosity and wetting speed. The contact angle determines liquid's wettability on that surface. Thus higher the contact angle lower will be the wettability.

Two types of PE substrates were selected for the work having an average opacity of 79% and 82%. The surface energy of these substrates were determined by measuring the contact angle of two test liquids viz., Formamide and Glycerol of known polar and dispersive components. Holmarc Contact Angle Meter was used to measure contact angle on both the substrates with 10 samples each.

The geometric mean equation was used to calculate the surface energy of these substrates.

$$\gamma_{SL} = \gamma_S + \gamma_L - 2(\sqrt{\gamma_S^d \gamma_L^d} + \sqrt{\gamma_S^p \gamma_L^p} \quad (2)$$

γ_s = Surface Energy of Solid

γ_L = Surface Tension of Liquid

γ_{SL} = Interfacial Surface Tension between Solid and Liquid

The above equation was replaced by simplified Young's Equation to calculate the surface energy from the contact angle.

$$\gamma_L(1 + cos\theta) = 2[\sqrt{\gamma_L^d \gamma_S^d} + \sqrt{\gamma_L^p \gamma_S^p} \quad (3)$$

Where

$\gamma_S^d = dispersive\ component\ of\ solid$

$\gamma_L^d = dispersive\ component\ of\ liquid$

$\gamma_S^p = polar\ component\ of\ soild$

$\gamma_L^p = polar\ component\ of\ liquid$

γ_s^d of Formamide = 39.5 γ_L^p of Formamide = 18.7

γ_L^d of Glycerol = 34 γ_L^p of Glycerol = 30

γ_L of Formamide = 58.2

γ_L of Glycerol = 64

Substrate 1

$$58.2(1 + \cos 67.51) = 2[\sqrt{39.5 \times \gamma_s^d} + \sqrt{18.7 \times \gamma_s^p}] \quad (4)$$

$$64(1 + \cos 80.78) = 2[\sqrt{34 \times \gamma_s^d} + \sqrt{30 \times \gamma_s^p}] \quad (5)$$

Solving equation (4) and (5), polar and dispersive components of substrate 1 was calculated

$\gamma_s^d = 42.05$ and $\gamma_s^p = 0.0225$

Therefore, Total Surface Energy of PE laminate for Substrate 1

$= \gamma_s^d + \gamma_s^p = 42.26$ mN/m

Substrate 2

$$58.2(1 + cos\ 68.6) = 2[\sqrt{39.5 \times \gamma_s^d} + \sqrt{18.7 \times \gamma_s^p}] \quad (6)$$

$$64(1 + cos\,81.48) = 2[\sqrt{34 \times \gamma_s^d} + \sqrt{30\ \times \gamma_s^p}] \quad (7)$$

The polar and dispersive component of Substrate 2 was hence calculated by solving equation (6) and (7).

$\gamma_s^d = 40.70$ and $\gamma_s^p = 0.00722$

Therefore, total Surface Energy of PE laminate for Substrate 2

$= \gamma_s^d + \gamma_s^p = 40.7$ mN/m

Substrate 1 and Substrate 2 are different in only opacity. The opacity of substrate was varied to check it's effect on print attributes. Both the substrates are 40 µ thickness (37 GSM) with 0.943 density. The gloss of the substrates was 65% @ 60^0. The Coefficient of Friction (CoF) was ranging between 0.3 to 0.4 while Haze between 10% to 15%.

3.1.2. Surface tension of ink

Table 1. Contact angle measurement

Viscosity @22^{0}C (sec)	Left Angle (^{0})	Right Angle (^{0})	Contact Angle (^{0})
20	39.5	41.58	40.54
22	44.13	45.71	44.92
24	45.18	48.22	46.70

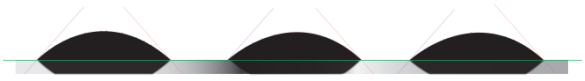

(a) (b) (c)

Figure 2. Contact angle (θ) 20 sec (a), 22 sec (b), 24 sec (c)

The contact angle was found to be lower at 20 sec viscosity (Table 1), thereby resulting in higher ink spread and print mottle (Figure 2).

Surface Tension is defined as the amount of energy required to increase the surface of the liquid by unit area. The surface tension was determined based on Wilhelmy Plate method [26].

$$\gamma = \frac{F}{l\,cos\theta} \quad (8)$$

Where,

F = Force acting on the plate

γ =Surface tension of liquid (ink)

l = Wetted perimeter of the plate

θ = Contact angle with plate

Surface tension measurement was conducted on 10 samples of ink to increase accuracy of measurement. The mean surface tension was found to be 23.98mN/m at 22^0C. The temperature is a crucial factor affecting surface tension. The rise in temperature exerts more molecular vibrations among the liquid molecules, thereby decreasing surface tension. The increase in temperature, increases adhesion and decreases the cohesive forces between liquid molecules. This results in increased contact angle and reduced surface tension. The ink-substrate interaction is critical to print quality. The ink lay-down over the substrate after transfer from the plate has an impact on printability. The ink spreading depends on various printability factors such as circularity, area and perimeter of the dot. Moreover, it reflects directly on print defects such as voids and print mottle. A higher spreading tendency of ink over the substrate leads to better area coverage, reducing void area. On the contrary, spreading yields in scattered distribution of pigment particles with uneven reflectance from the printed substrate, thus leading to higher print mottle over non-absorbent substrates. NC based ink was prepared in a dispenser that comprised of Master Batch, Varnish/Resin, Medium and Solvent. Master Batch is a combination of Pigment, Additives, Varnish and True Solvent (Table 2).

Table 2. Basic composition of NC ink

Ingredients	Proportion (%)
Master Batch	42% - 52%
Vanish	24% - 26%
Medium	5% - 10%
Solvent	17% - 24%
Total	100%

Table 3. Substrate-ink interaction

Substrate Opacity	η (s)	(θ)	γ_s	γ_l	γ_{sl}	w_a	S
Substrate 1 (79%)	20	37	42	24	23	43	-4.9
	22	42	42	24	24	42	-6.0
	24	45	42	24	25	41	-6.9
Substrate 2 (82%)	20	41	41	24	23	42	-5.8
	22	45	41	24	24	41	-7.0
	24	47	41	24	25	40	-7.5

The interfacial tension (γsl), work of adhesion (Wa) and spreading co-efficient (S) was calculated using following formulae:

$$\gamma sl = \gamma s - \gamma l(Cos\theta) \quad (9)$$

$$S = \gamma s - \gamma l - \gamma sl \quad (10)$$

where θ = Contact angle of ink with substrate.

The values of contact angle from Table 3 suggest higher spreading at lower ink viscosity (20 sec) for both the substrates. The higher surface energy of substrate 1 increases the ability of the substrate to bind with ink. Higher surface energy ensures higher spreading as the amount of spreading is directly proportional to the difference in substrate surface energy of substrate and ink surface tension. This difference is found to be greater in substrate 1 and hence the ink spread is more in substrate 1 than substrate 2. Furthermore, the lower contact angle at lower viscosity resulted in higher ink spread and print mottle. A higher adhesion between the

ink and substrate is achieved on substrate 1 as indicated by higher work of adhesion (w_a). The negative values of spreading co-efficient (S) suggest that the spreading does not occur spontaneously. Substrate 2 displayed lower ink spread indicated by higher magnitude of S. Thus, 20 sec ink viscosity on substrate 1 resulted in higher ink spread.

4. Printability analysis

Printability is essential for defining the optimum settings for improving print quality in flexography printing press. Printability in this study is defined as the optimal amalgamation of ink, substrate and process parameters for the responses such as ink gsm (grams per square meter), ΔE*00 and print mottle. The optimization of these responses with minimized defects shall enhance printability and reduce the overall manufacturing cost of a package.

4.1. Plate dot structure

Two plates, with dot structure 1 (circular) and dot structure 2 (square) were used for the study. The plate layout design comprised of logo, solid and halftone patch, surface and reverse text. The solid patch was included to measure and analyze Ink GSM, ΔE*00 and Print Mottle. The halftone patch was used to check the tone value increase. The logo was incorporated in the layout for visual assessment while surface and reverse text to check minimum reproducible text. These plates were mounted on the same sleeve and printing was carried out by keeping the other color parameters constant.

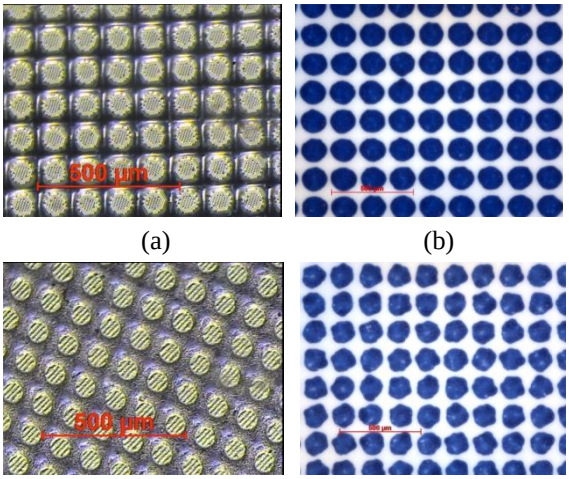

(a) (b)

(c) (d)

Figure 3. Dot shape on Plate 1 (a), Dot reproduction of Plate 1 (b), Dot shape on Plate 2 (c), Dot reproduction of Plate 2 (d).

The dot circularity also referred to as roundness and represented as

$$C = \frac{4\pi A}{P^2} \tag{11}$$

where A = area of dot and P = perimeter or the dot

The ideal dot circularity is 1 and more closer to 1, better is the dot reproduction. The dot circularity of Dot Shape 1 (0.8194) was found to be higher than Dot Shape 2 (0.8163) as indicated by Figure 3.

4.2. Baseline identification

A production run was conducted on 40µ PE substrate with solvent based blue ink at 23s ink viscosity (30^0C and 50% humidity) as measured by B4 Ford cup and diluted with n-propanol and n-propyl acetate in the ratio of 4:1. A anilox cell volume of 5.3 billion cubic microns (BCM), square dot plate and 79% average substrate opacity was used for the run. The other constant parameters set during the press run were 5.83 m/s press speed, 1.7 mm plate thickness, medium backing tape with 0.38 mm thickness and 30^0 reverse angle chambered doctor blade. The assessment of response Ink GSM, Color Deviation (ΔE*00) and Print Mottle was done with 20 printed sheets being considered as sample size for each response. The baseline for Ink GSM and Print Mottle was the mean value of the sample size. The baseline or reference L*a*b* values for the blue color was 14.42L* 36.22a* -66.53b* and the target was set to reduce the color deviation from the baseline for the printed blue sample with ΔE*00 not exceeding 1.5 (Table 4).

Table 4. Baseline for the response

Run	Ink GSM	ΔE*00	Print Mottle
Production Run	0.98	1.07	0.91

The selection of anilox roller cell volume was based on ratio of plate to anilox screen ruling and the available inventory used in daily production run. The plate to anilox screen ruling was kept in a range of 1:5 (5.3 BCM) and 1:7 (4.5 BCM) with plate screen ruling as 133 lpi while anilox screen ruling as 648 lpi and 914 lpi.

Table 5. Design of experiments for the response

Factors	Low Level	Mid Level	High Level
Viscosity (sec)	20	22	24
Anilox Volume (BCM)	4.5	-	5.3
Dot Shape	1	-	2
Substrate Opacity (%)	1	-	2

A general full factorial experimental design was run with 4 factors namely viscosity with 3 levels while anilox volume, dot shape and substrate opacity at 2-levels and 2 replicates, thus totaling to 48 runs (Table 5). The dot shape 1 refers to dot circularity of 0.8194 while dot shape 2 refers to dot circularity of 0.8163. The lower level of substrate opacity represents mean opacity of 79% while higher level represents mean opacity of 82%. The selection of levels for the factors in DOE were considered based on the working levels. A viscosity lower than 20 sec will result in more tone value increase and mottling while viscosity above 24 sec will clog the anilox cells and yield in uneven lay down of an ink. Anilox volume levels were considered

based on ratio of plate to anilox line screen. There are only two types of dot shape available round and square, hence considered. The recommended substrate opacity for the diaper application is normally ranging between 80% to 82%. The substrate opacity below 79% will result in dispersion lines on PE substrate while opacity above 82% will require more addition of master-batch, thereby increasing the production cost. Hence, the two opacity levels of 79% and 82% were considered for the work.

4.3. Ink GSM

Ink GSM is the amount of ink deposited over one square meter of printed substrate. The Ink GSM was measured on solid patch of the printed sample.

The main effect plot (Figure 4) shows that higher ink GSM is obtained at higher viscosity (24 sec) and anilox volume (5.3 BCM) with a circular dot (dot shape 1) on lower substrate opacity. The solid content in the ink is higher at 24 sec viscosity that constitutes higher ink GSM. The anilox volume determines the quantity of ink transfer to the plate and further on to the substrate. Higher the anilox volume, higher the amount of ink deposited and therefore the ink GSM. The larger area coverage on plate with dot shape 1 (circular dot) led to higher ink transfer and ink GSM. The difference between substrate surface energy and ink surface tension played a significant role in ink transfer. The substrate 1 with higher surface energy showed higher difference that led to more ink transfer. A higher surface energy increases the force of adhesion between the ink and the substrate. This force of adhesion pulls more ink from the plate and hence results in a higher ink GSM.

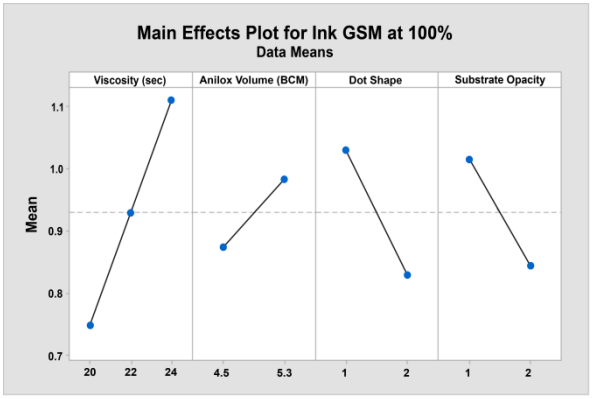

Figure 4. Main effect plot for ink GSM

There is no strong interaction between the factors affecting ink GSM (Figure 5). High ink GSM is obtained when an ink having 24 sec viscosity is used irrespective of the plates, anilox volume and substrate used. Similarly anilox volume of 5.3 BCM, dot shape-1 and substrate opacity-1 yielded maximum ink GSM. Minitab 17 was used to calculate ANOVA (Analysis of Variance) and Regression models for Ink GSM, ΔE and Print Mottle.

The degrees of freedom abbreviated as df (Table 6) are the number of values that can be varied once certain parameters have been established.

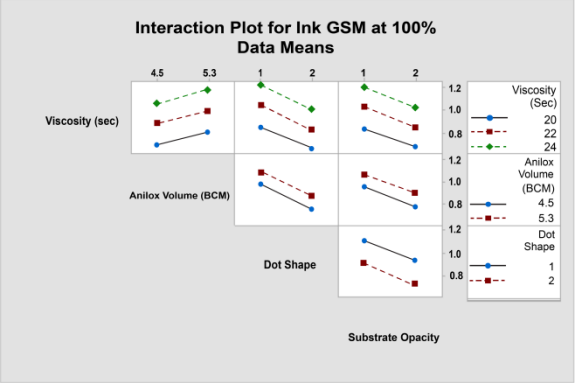

Figure 5. Interaction plot for ink GSM

Table 6. ANOVA for ink GSM

Source	df	Adj SS	Adj MS	F	P
Regression	7	2.030	0.29	2222.15	0.000
Viscosity (sec)	1	1.048	1.048	8024.92	0.000
Anilox Volume (BCM)	1	0.146	0.146	1120.69	0.000
Dot Shape	1	0.486	0.486	3722.94	0.000
Substrate Opacity	1	0.349	0.349	2669.56	0.000
Viscosity* Dot Shape	1	0.0009	0.0009	6.92	0.012
Viscosity* Substrate Opacity	1	0.0007	0.0007	5.39	0.025
Dot Shape * Substrate Opacity	1	0.0006	0.0006	4.61	0.038
Error	40	0.0052	0.0001		
Lack of Fit	16	0.0021	0..0001	0.91	0.568
Pure Error	24	0.0033	0.0001		
Total	47	2.0358			
S=0.0114257			R-sq =99.74%		
R-sq(adj)= 99.70%			R-sq(pred)= 99.63%		

Adjusted Sum of Squares (Adj SS) are measures of variation for different components of the model. Sum of Squares describe the variation due to different sources. Adjusted Mean Square (Adj MS) measures the description of magnitude of variation by the term or model. Adj MS takes into consideration df. The F-value is the test statistic used to determine whether the term is associated with the response. It is the ratio of two sample variances i.e. MS of a particular row divided by MS Error. The p-value is the probability that measures the evidence against the null hypothesis. The lower p-values provide the stronger evidence against null hypothesis. The constants of the regression equation was derived from the coefficients of each term namely Viscosity, Anilox Volume, Dot Shape, Substrate Opacity and interactions between them.

Regression Equation for Ink GSM

InkGSM = -1.542 + 0.10547*Viscosity(sec)*
+ 0.13802*AniloxVolume (BCM)*
-0.0631*DotShape* – 0.046*SubstrateOpacity*(%)
-0.00531*Viscosity*DotShape*
-0.00469*Viscosity*SubstrateOpacity*
-0.01417*DotShape*SubstrateOpacity (12)

The p-values in ANOVA (Table 6) of all the main factors are below α value of 0.05, thereby indicating as significant factors affecting Ink GSM. The lower p-values below α value of 0.05 proves rejection of null hypothesis. The viscosity was found to be of highest significance affecting Ink GSM as indicated by higher F-value. A 99.74% of variability could be explained by the model as indicated by R-Sq. value. The adjusted R-Sq of 99.70% shows significant improvement of the model with selected four factors. As the experimental design involved 2 replicates i.e. having multiple observations with an identical X values, hence lack-of-fit test was performed. The p-value greater than α>0.05 indicates that model correctly specifies the relationship between the response and predictors and the test does not detect lack-of-fit. The model was adequate as the lack of fit (p=0.568) value was greater than α > 0.05.

4.4. Print density

The print density is directly correlated to ink GSM and therefore the trend for Ink GSM and print density is same as indicated by Main Effect Plot.

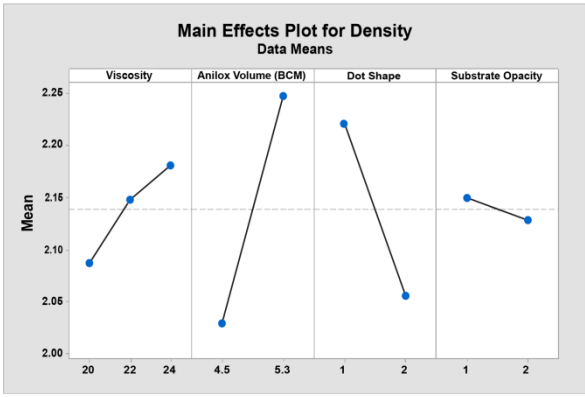

Figure 6. Main effect plot for print density

The main effects plot (Figure 6) shows that higher print density is obtained at higher viscosity, higher anilox volume, a circular dot shape and on a surface with lower opacity. A lower viscosity (20 sec) implies a lower concentration of solid content and hence a lower print density was achieved. A lower anilox volume (4.5 BCM) resulted in a lower print density. This occurred due to the fact that a lower anilox volume will store a less amount of ink and therefore will transfer lesser ink and hence a low print density. The dot shape 1 i.e. circular dots exhibited higher print density than square dotted plate. This can be attributed to the fact that area coverage of circular dot is more than square dot (dot shape 2) and transfers more ink as compared to a square dot. The substrate 1 with lower mean opacity of 79% displayed a higher print density than substrate 2 i.e. mean opacity of 82.4%. A higher ink transfer was observed at lower substrate opacity 1 due to higher surface energy of 42.26mN/m as compared to higher substrate opacity with a lower surface energy of 40.7mN/m that has led to higher print density.

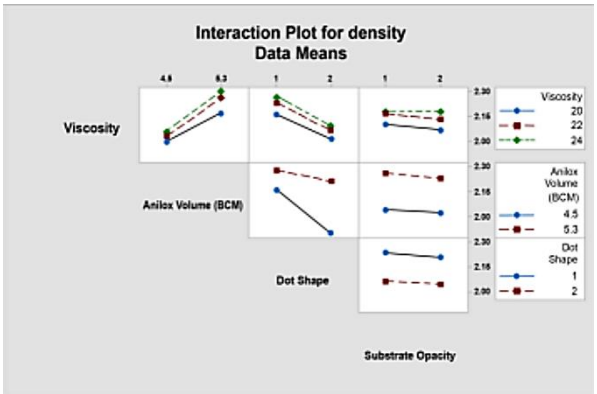

Figure 7. Interaction plot for print density

The interaction plot for density (Figure 7) shows higher density at 24s viscosity, 5.3 BCM anilox volume for a circular dot shape at lower substrate opacity. The interaction of viscosity with anilox volume, dot shape and substrate opacity affects the print density. The higher solid content at 24 sec ink viscosity and more ink carrying capacity of 5.3 BCM anilox volume resulted in high ink deposition on to the substrate; thereby higher print density. The higher area coverage of plate dot 1 and higher viscosity of 24 sec with less ink spread yielded in higher ink film thickness, thus higher print density. The ink with higher viscosity, high anilox BCM and circular dots yield high print densities. The interaction plot shows great inter dependence of circular dots with anilox volume. A sharp rise in print density was observed with circular dots at 4.5 BCM anilox volume as compared to square dots. The higher ink transfer at lower substrate opacity with higher surface energy was achieved at 24 sec ink viscosity.

4.5. Delta E

The color variation or deviation in the print is referred to as Delta E. It involves a 3 dimensional color space where each color occupies unique location according to its color co-ordinates namely L*, a* and b*. The L* refers to lightness and darkness of a color. The a* refers to green and red coordinates while yellow and blue coordinates are represented by b* values.

$$\Delta E2000 = \sqrt{\left(\frac{\Delta L'}{K_L S_L}\right)^2 + \left(\frac{\Delta C'}{K_C S_C}\right)^2 + \left(\frac{\Delta H'}{K_H S_H}\right)^2 + R_T \left(\frac{\Delta C'}{K_C S_C}\right)\left(\frac{\Delta H'}{K_H S_H}\right)} \quad (13)$$

Where,

$\overline{L}' = (L_1 + L_2)/2$

$C_1 = \sqrt{a_1^2 + b_1^2}, \quad C_2 = \sqrt{a_2^2 + b_2^2}$

$\overline{C} = (C_1 + C_2)/2$

$G = \frac{1}{2}\left(1 - \sqrt{\frac{c^{-7}}{c^{-7} + 25^7}}\right)$

$a_1' = a_1(1 + G), \quad a_2' = a_2(1 + G)$

$C_1' = \sqrt{a_1' + b_1^2}, \quad C_2' = \sqrt{a_2' + b_2^2}$

$\overline{C}' = (C_1' + C_2')/2$

$\Delta L' = L_2 - L_1, \quad \Delta C' = C_2' - C_1'$

$\Delta H' = \sqrt[2]{C_1' C_2'} \sin(\Delta h'/2)$

$S_L = 1 + \frac{0.015(\overline{L}' - 50)^2}{\sqrt{20 + (\overline{L}' - 50)^2}}$

$S_C = 1 + 0.045\overline{C}', \quad S_H = 1 + 0.015\overline{C}'T$

$\Delta\theta = 30\exp\left\{-\left(\frac{\overline{H}' - 275°}{25}\right)^2\right\}$

$R_C = \sqrt[2]{\frac{\overline{C}'^7}{\overline{C}'^7 + 25}}, \quad RT = -R_C \sin(2\Delta\theta)$

$K_L = 1$ default, $K_C = 1$ default, $K_H = 1$ default

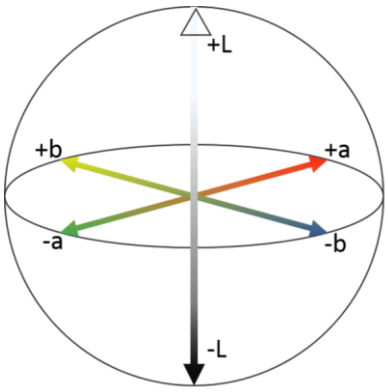

Figure 8. Lab color space

The color values of 14.42L* 36.22a* -66.53b* was considered as reference based on the customer approval. The color deviation was calculated based on CIE ΔE2000 (weighing factor 1:1:1) with M1 measurement mode, D50 illuminant and 2^0 observer angle between reference L*a*b* and L*a*b* values of printed samples measured on the solid patches. The Main Effect plot (Figure 9), depicts lower delta E at higher viscosity and anilox volume with square dot on higher substrate opacity. The plot (Figure 10) indicates an interaction of viscosity with anilox volume and dot shape and anilox volume with dot shape affecting ΔE*00.

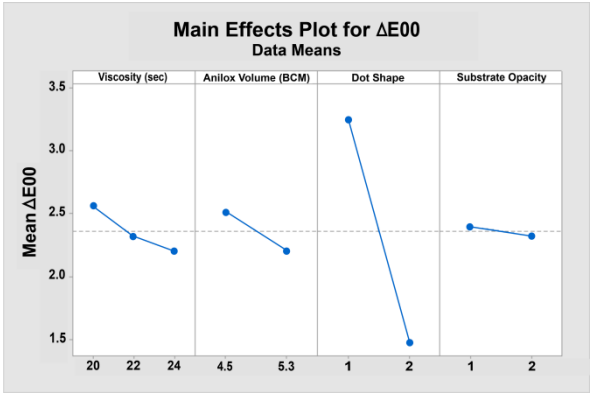

Figure 9. Main effect plot for ΔE*00.

The variation in ΔE2000 was due to the deviation in L* a* b* coordinates.

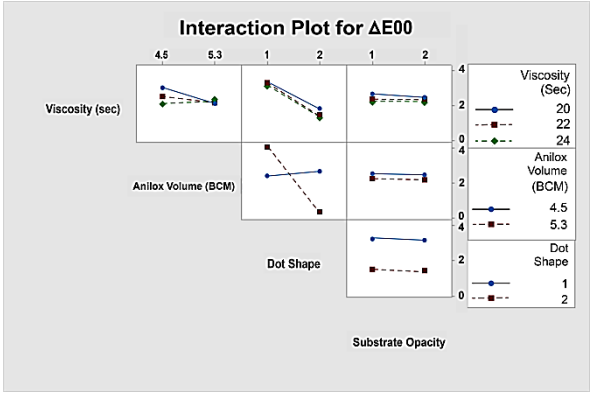

Figure 10. Interaction plot for ΔE*00

Table 7. ANOVA for ΔE00

Source	df	Adj SS	Adj MS	F	P
Regression	5	90.435	18.087	297.47	0.000
Viscosity (sec)	1	2.7209	2.7209	43.85	0.000
Anilox Volume (BCM)	1	0.0113	0.0113	0.18	0.671
Dot Shape	1	41.1262	41.1262	662.74	0.000
Viscosity* Anilox Volume	1	2.4753	2.4753	39.89	0.000
Anilox Volume *Dot Shape	1	48.1001	48.1001	775.12	0.000
Error	42	2.6063	0.0621		
Lack of Fit	18	1.5767	0.0876	2.04	0.051
Pure Error	24	1.0296	0.0429		
Total	47	93.0411			

S=0.249108 R-sq =97.20%

R-sq(adj)= 96.87% R-sq(pred)= 96.42%

Regression Equation for ΔE*00

$$\Delta E2000 = 9.57 - 1.792 Viscosity(\text{sec}) - 0.53 AniloxVolume(BCM) + 22.753 DotShape + 0.3477 Viscosity*AniloxVolume - 5.005 AniloxVolume(BCM) + 22.753 DotShape \quad (14)$$

The constants of the regression equation were derived from the coefficients of each factor and their interactions with each other. The ANOVA Table (Table 7) shows that all the main effects and interaction of viscosity with anilox volume, dot shape and anilox volume with dot shape as significant factors affecting Delta E. Dot shape was had a influential role in minimizing Delta E. The model summary indicates 97.20% of variability explained by the model while 96.8% adjusted R-Sq implies significant improvement of the model by using four factors. The lack of fit with p value of 0.051 represents the accuracy of the model.

4.6. Print mottle

Print Mottle is defined as the undulations present on the surface of substrate. Verity IA Print Target v3 software with Stochastic Frequency Distribution Analysis (SFDA) algorithm was used to measure Mottle on the solid patch. The output result of this algorithm is an index, quantifying mottle. SFDA firstly determines the properties of the texture of the image and then calculates the spatial distribution of the texture. When the scanned image area in digital format is fed to SFDA for analysis, the entire image area is sampled into a regular pattern of continuous and adjoining larger target areas which are further sub-divided into smaller pixel targets (Figure 11). The larger targets are measured for two parameters stored in separate databases simultaneously; one database stores the two-dimensional standard deviation (s) within the smaller target area while the second database stores the mean luminance value (M_{TL}) of the pixels present in the smaller target area that describes the overall visual impact of the analyzed larger target area. When an area of interest is selected within the scanned image, the s and M_{TL} values are extracted from their databases and the mottle index for the respective area of interest is displayed as a result.

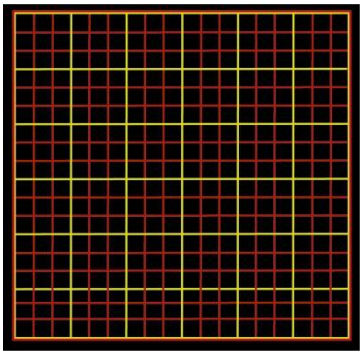

Figure 11. Area of interested divided into target areas

The standard deviation "s" is calculated as:

$$s = \sqrt{\frac{\sum(P_L - M_{TL})^2}{n}} \quad (15)$$

Where,

P_L -Individual pixel luminance

M_{TL} -Mean luminance of the pixels in the target area

n -Number of pixels in the target.

The level of uniformity among the targets is indicated by the degree of variation in the value of "s" while the uniformity in luminance is indicated by the variance of "M_{TL}".

The mottle of the larger target is then calculated using the following formula.

$$Mottle = K^* (\sigma_s * M_s * \sigma_m) \quad (16)$$

Where,

K -Scaling Factor,

σ_s -Standard deviation of s values

σ_m -Standard deviation of M_{TL} values

M_s -Mean of "s" values

The variation in the texture of image also needs to be calculated for more accurate mottle measurement. For calculating the mottle index of the entire area of interest, spatial distribution of texture mottle is calculated between the larger targets, by the following formula:

$$SpatialMottle = K^* (\sigma_o * M_o) \quad (17)$$

σ_O = Standard deviation of large target mottle number

M_O = Mean of large target mottle number

The Print Mottle was measured on solid patch of the printed sample. The solid print mottle was minimized at higher level of viscosity (24 sec), anilox volume (5.3 BCM), substrate opacity and lower level of dot shape (Figure 12). The higher ink spreading at lower viscosity (20 sec) due to higher spreading coefficient of ink results in uneven ink deposition on the substrate, thereby leading to higher print mottle.

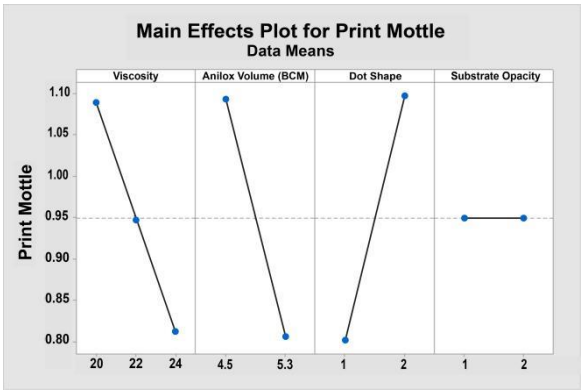

Figure 12. Main effect plot for print mottle

The even lay down of ink on the substrate at higher viscosity (24 sec) reproduces good dot circularity, thereby resulting in lower print mottle. Too higher viscosity will result in higher print mottle due anilox cell clogging. The outcome of this result will be uneven deposition of ink on the substrate. The print mottle was

reduced at higher anilox volume and circular dot (dot shape 1) due to higher and uniform ink film deposition. Though the print mottle was minimized with higher opacity substrate but the difference between both the substrate was negligible. This is because of lower surface energy of substrate 2 that led to less ink spread as compared to substrate 1.

The interaction plot (Figure 13) shows lower solid mottle at 24 sec viscosity, 5.3 BCM anilox volume with a circular dot on 82% mean substrate opacity. The interaction of lower anilox volume and lower viscosity yields a high mottle index. The higher solvent content at lower viscosity (20 sec) with lower anilox volume (4.5 BCM) results in uneven ink deposition on to the substrate, thereby higher print mottle. The lower dot circularity at lower viscosity with square dot leads to uneven distribution of ink on the substrate, thereby resulting in higher solid mottle. There was no significant interaction of substrate opacity with other factors and hence was not responsible for any change in solid mottle.

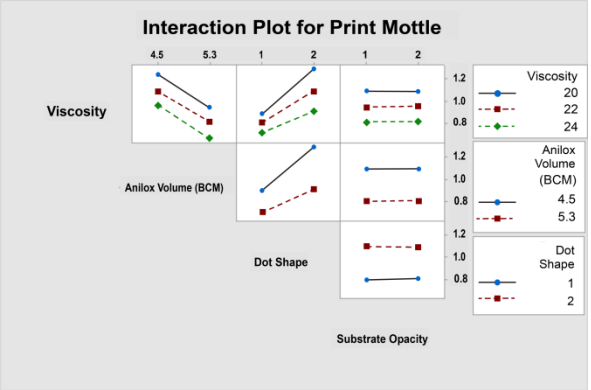

Figure 13. Interaction plot for print mottle

Table 8. ANOVA for print mottle

Source	df	Adj SS	Adj MS	F	P
Regression	5	2.827	0.56531	4829.11	0.000
Viscosity (sec)	1	0.611	0.6105	5215.23	0.000
Anilox Volume (BCM)	1	0.989	0.989	8448.42	0.000
Dot Shape	1	1.0355	1.0355	8845.42	0.000
Viscosity*Dot Shape	1	0.0861	0.0861	735.61	0.000
Anilox Volume *Dot Shape	1	0.1055	0.1055	900.95	0.000
Error	42	0.0052	0.0001		
Lack of Fit	18	0.0025	0.0001	1.34	0.247
Pure Error	24	0.0024	0.0001		
Total	47	2.3148			
S=0.0108196			R-sq =99.83%		
R-sq(adj)= 99.81%			R-sq(pred)= 99.78%		

Regression Equation for Print Mottle

Print *Mottle* = 0.3250 + 0.00875*Viscosity*(sec)
- 0.0073*AniloxVolume(BCM)* + 2.5384*DotShape*
- 0.05188*Viscosity* DotShape*
- 0.23438*AniloxVolume* DotShape* (18)

The regression constants were derived from the coefficients of factors Viscosity, Anilox Volume, Dot Shape and the interactions of Dot Shape with Viscosity and Anilox Volume. Table 8 indicates that viscosity, anilox volume and dot shape along with their interactions have significant effect on minimizing print mottle. The lack of fit with p value of 0.247 represents model adequacy.

The regression equations for Ink GSM, Delta E and Print Mottle were validated by conducting additional runs. The data between Actual and Predicted runs showed R^2 value of 0.9242, 0.9372 and 0.9226 for Ink GSM, Delta E and Print Mottle respectively; hence justifying the predictive ability of the models.

4.7. Response optimization

The paramount settings for all the print attributes were optimized from the trials conducted as per the experimental design through response optimizer to identify the set of variables for multiple responses. The optimal settings for a single response are evaluated by individual desirability while composite desirability for multiple responses in the range of zero to one. The individual desirability will be 1 if the predicted response is closer to the target. The combination of individual desirability is calculated into an overall value as composite desirability for multiple responses. The higher the composite desirability value, the better the product quality. The response optimizer provides the "best" combination of variable settings as the global solution. The goal was set to minimize the response such as print mottle, ink GSM, and delta E. The composite desirability was estimated at different levels of anilox cell volume (BCM), viscosity, dot shape, and substrate opacity to identify the sweet spot between parameters fulfilling the goal.

The desirability to minimize a response is calculated as below.

$$d_i = 0 \ (\bar{y}_i > U_i) \quad (19)$$

$$d_i = ((U_i - \bar{y}_i)/(U_i - T_i))^{ri} \ (yT_i \leq \bar{y}_i \leq U_i) \quad (20)$$

$$d_i = 1 \ (\bar{y}_i < T_i) \quad (21)$$

Where,

$\bar{y}_i$ = predicted value of i^{th} response

T_i = target value for i^{th} response

U_i = highest acceptable value for i^{th} response

d_i = desirability for i^{th} response

Individual Desirability = (Upper value – Predicted response)/(Upper value – Target)

Composite Desirability,

$$D = (d_1 * d_2 * \ldots * d_n)^{1/n} \quad (22)$$

Where

n = number of responses

D = Composite Desirability

The optimization plot (Figure 14) revealed global solution as 22 viscosity, 5.3 BCM anilox volume, dot shape 2 (square) having 82% substrate opacity (2) with 0.9726 composite desirability for minimization of Ink GSM, Delta E and Print Mottle on 40µ PE film.

The optimized settings with 22 sec viscosity, 5.3 BCM anilox cell volume, dot shape 2 (square dot) and 82% substrate opacity was run and average data of 20 printed sheets was considered.

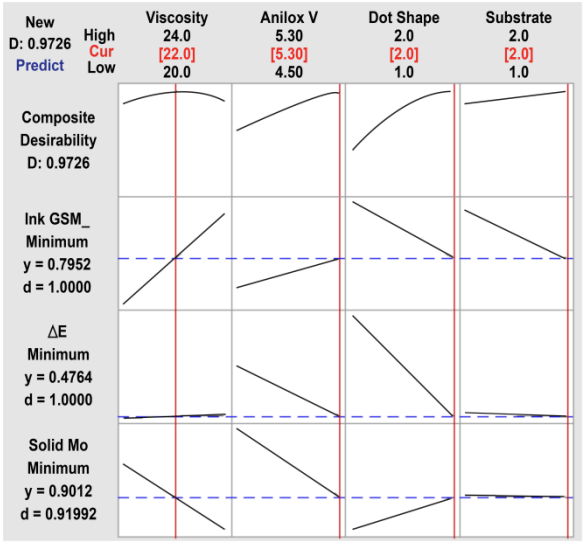

Figure 14. Optimization plot for the responses

Table 9. Comparison of the mean-field predictions

Response	Base-line	Optimized Run	% Improve-ment
Ink GSM	0.98	0.8	18
ΔE00	1.07	0.48	52
Print Mottle	0.91	0.9	1

The results revealed reduction of Ink GSM, ΔE00 and Print Mottle by 18%, 52% and 1% respectively (Table 9).

Table 10. Ink consumption

Runs	Ink Consu mption per Area	Ink Consu mption per KG	Ink Consu mption per Tonne	% Improve -ment (Ink Consum p-tion)
Production	0.23	25.99	25990	18.26%
Optimized	0.19	21.24	21240	

The area of one repeat of the job was 0.23 m^2 and accommodates 113 repeats/prints in a Kg. An Ink GSM of 0.98 was achieved during the production run while 0.80 for optimized run. The ink consumption per 0.23 m^2 for production run was 0.23 gm while 0.19 gm for optimized run. Table 10 shows minimization in ink consumption by 18.26% at optimized run of 22s viscosity and 5.3 BCM anilox volume with square dot plate (dot shape 2) on 40µ PE film a substrate having mean opacity 82% (substrate opacity 2).

5. Conclusion

A general full factorial DOE was designed to optimize flexo process parameters. The process parameters considered for experimentation were anilox volume (BCM) and dot shape at two levels while ink viscosity at three levels for both the substrates having mean opacity of 79% and 82%. The analysis of the data was assessed by main effects, interaction plot and ANOVA to determine the best combination of flexo process parameters enhancing printability. Furthermore, regression models were generated for the output response Ink GSM, Delta E, Print Mottle and validated. The validation runs for Ink GSM, Delta E and Print Mottle revealed good predictive ability of the models with R^2 value of 0.9242, 0.9372 and 0.9226 respectively. The results revealed that ink viscosity, anilox volume, dot shape and substrate opacity were significant factors affecting the response. The other factors such as a press speed, plate type, plate thickness, backing tape, doctor blade angle will also have a significant impact on ink transfer, thereby affecting the responses. The Response Optimizer revealed the optimized settings as 22 sec viscosity, 5.3 BCM anilox cell volume, dot shape 2 (square dot) and 82% mean substrate opacity on 40µ polyethylene film. However, the same methodology can be applied for other inks to validate the results for optimization and ink consumption. The optimal settings minimized the ink consumption by 18.26% while maintaining the desired ΔE*00 and reduction in overall manufacturing cost of a package.

Acknowledgments

The author would like to thank Parakh Flexipacks and Windmöller & Hölscher India Private Limited for their infrastructure and financial support.

References

[1] Mordor Intelligence Report (2020). Flexible Plastic Packaging Market by Type (Pouches, Rollstocks, Bags, Wraps), Material (Plastic & Aluminum Foil), Application (Food, Beverage, Pharma & Healthcare, Personal care & Cosmetics), Technology, and Region - Global Forecast to 2025 [online]. Available from: https://www.marketsandmarkets.com/Market-Reports/flexible-packaging-market-1271.html. [Accessed 20 May 2021].

[2] Indian Diaper Market (2016). India Diaper Market Overview, 2016 - Research and Markets [online]. Available from: http://www.businesswire.com/news/home/20161128005918/en/India-Diaper-Market-Overview-2016---Research. [Accessed 20 May 2021].

[3] Kipphan, H. (2001). Handbook of Print Media.

Springer-Verlag, Heidelberg, Berlin.

[4] Rogers A. (2011). Choosing the right anilox-roll engraving for the application [online]. Available from: http://www.harperimage.com/media/downloads/Choosing%20the%20right%20engraving_Converting%20Q%204thQrtr2011.pdf. [Accessed 20 May 2021].

[5] Ardent D. (2006). Ink Mileage: Measure & Manage [online]. Available from: http://www.pffc-online.com/process-management/5017-paper-ink-mileage-measure. [Accessed 20 May 2021].

[6] Rastetter J., & Bingham J. (2016). Lower Your Anilox Line Screen and Cell Volume for Better Performance FlexoGlobal [online]. Available from: http://www.flexoglobal.com/blog/2016/08/01/pamarco-lower-anilox-line-screen-cell-volume/. [Accessed 20 May 2021].

[7] Teufler S. (2010). Weighing Your Coating Options [online]. Available from: http://www.harperimage.com/media/downloads/Weighing%20Your%20Coating%20Options%20FLEXO%20Feb%202010.pdf. [Accessed 22 May 2021].

[8] Teufler S. (2015). Anilox Rollers - Choosing the Right Lineature [online]. Available from: http://www.harperimage.com/media/downloads/Anilox%20Rollers_Choosing%20The%20Right%20Lineature_Flexible%20Packaging%20Issue%201.pdf. [Accessed 22 May 2021].

[9] Hogan P. (2018). Aniloxes - Yesterday, Today and Tomorrow [online]. Available from: http://www.harperimage.com/media/downloads/Aniloxes_Yesterday%20Today%20and%20Tomorrow_%20L&NW%20NovDec%202018.pdf. [Accessed 22 May 2021].

[10] Harper C. (2005). Do you know what ink film thickness is transferred [online]. Available from: http://www.harperimage.com/media/downloads/Harper_FGA_1_2005.pdf. [Accessed 22 May 2021].

[11] Green C. (2013). Understanding Common Flexo Print Defects - Part 2 FlexoGlobal [online]. Available from: http://www.flexoglobal.com/blog/tag/anilox/page/4/. [Accessed 22 May 2021].

[12] Poulson B. & Hudson K. (2010). Correlating Ink Labs Drawdown to Press [online]. Available from: http://www.harperimage.com/media/downloads/Radtech%20Report%20Sep-Oct%202010.pdf. [Accessed 24 May 2021].

[13] Harnandez R. (2019). Releasing the Anilox's Power [online]. Available from: http://www.harperimage.com/media/downloads/Releasing%20Anilox%20Power_FLEXO%20Jan%202019.pdf. [Accessed 24 May 2021].

[14] Olson, R., Yang, L. Stam J. V., & Lesrelius, M. (2006). Effects of ink setting flexographic printing: Coating polarity and dot gain. *Nordic Pulp and Paper Research Journal*, 21(5), 569–574.

[15] Gencoglu, E. N. (2012). Influence of Ink Viscosity on Dot Gain and Print Density in Flexography. *Asian Journal of Chemistry*, 24(5), 1999–2002.

[16] Theopold, A., Neumann, J., Massfelder, D., & Dörsam, E. (2012). Effects of Solvents on Flexographic Plates. *Advances in Printing and Media Technology*, 39, 159–168.

[17] Simseker, O. (2011). Investigation of Different Solvents in Flexographic Printing Ink's Effects to Print Quality on Coated and Uncoated Paper. *Asian Journal of Chemistry*, 23(7), 2903–2906.

[18] Hizir, F.E., & Hardt, D.E. (2014). Effect of Substrate Contact Angle on Ink Transfer in Flexographic Printing [online]. Available from: http://www.comsol.co.in/paper/download/194575/hizir_paper.pdf. [Accessed 26 May 2021].

[19] Izdebska, J., Podsiadlo, H., & Hari, L. (2012). Influence of Surface Free Energy of Biodegradable Films on Optical Density of Ink Coated Fields of Prints. *Advances in Printing and Media Technology*, 39, 245–252.

[20] Rong, X., & Keif, M. (2007). A Study of PLA Printability with Flexography. *The Technical Association of the Graphic Arts*, 3, 605–613.

[21] Mesic, B., Lestelius, M., & Engstrom, G. (2006). Influence of Corona Treatment Decay on Print Quality in Water-borne Flexographic Printing of Low-density Polyethylene-coated Paperboard. *Packaging Technology and Science*, 19(2), 61–70.

[22] Valdec, D., Zjakić, I., & Milković, M. (2013). The Influence of Variable Parameters of Flexographic Printing on Dot Geometry of Pre-printed Printing Substrate. *Tehnički vjesnik*, 20(4), 659–667.

[23] Claypole, T.C., Jewell, E.H., & Bould, D.C. (2012). Effects of Flexographic Press Parameters on the Reproduction of Colour Images. *Advances in Printing and Media Technology*, 39, 187–194.

[24] Gilbert, D.E., & Lee, F. (2008). Flexographic Plate Technology: Conventional Solvent Plates Versus Digital Solvent Plates. *Journal of Industrial Technology*, 24(3), 1–7.

[25] Bould, D.C., Claypole, T.C., & Bohan, M.F.J. (2004). An Investigation into Plate Deformation in Flexographic Printing. *Journal of Engineering Manufacture*, 218(11), 1499–1511.

[26] Ebnesajjad, S., & Landrock, A. (2015). Surface Tension and Its Measurement. In: S. Ebnesajjad, 3rd ed. Adhesives Technology Handbook. William Andrew, Elsevier Inc, 19–29.

Akshay V. Joshi *received Bachelor's and Masters Degree in Printing Engineering from University of Pune, India. He was awarded Ph.D. (Engineering) from Jadavpur University, Kolkata in 2015. Dr. Akshay Joshi is working as Assistant Professor, Printing Engineering Department at P. V. G's College of Engineering & Technology and G. K. Pate (Wani) Institute of Management, Pune, India since*

1996. He is Coordinator, Board of Studies and Member, Research and Recognition Committee for Printing Technology at Savitribai Phule Pune University. His area of research is Gravure, Flexo and Flexible Packaging. Dr. Akshay Joshi has published several papers in Journals and guided candidates for Master Program in Printing Engineering and evaluated Ph.D. candidates. He is been internationally qualified as G7 Expert by Idealliance USA and implemented first G7 calibration for Gravure and Flexography printing processes in India. He is a Life Member of Indian Society for Technical Education.

http://orcid.org/0000-0002-8733-1747

An International Journal of Optimization and Control: Theories & Applications (http://ijocta.balikesir.edu.tr)

INSTRUCTIONS FOR AUTHORS

Aims and Scope

An International Journal of Optimization and Control: Theories & Applications (IJOCTA) is a scientific, peer-reviewed, open-access journal that publishes original research papers and review articles of high scientific value in all areas of applied mathematics, optimization and control. It aims to focus on multi/inter-disciplinary research into the development and analysis of new methods for the numerical solution of real-world applications in engineering and applied sciences. The basic fields of this journal cover mathematical modeling, computational methodologies and (meta)heuristic algorithms in optimization, control theory and their applications. Note that new methodologies for solving recent optimization problems in operations research must conduct a comprehensive computational study and/or case study to show their applicability and practical relevance.

Journal Topics

The topics covered in the journal are (not limited to):

Applied Mathematics, Financial Mathematics, Control Theory, Optimal Control, Fractional Calculus and Applications, Modeling of Bio-systems for Optimization and Control, Linear Programming, Nonlinear Programming, Stochastic Programming, Parametric Programming, Conic Programming, Discrete Programming, Dynamic Programming, Nonlinear Dynamics, Stochastic Differential Equations, Optimization with Artificial Intelligence, Operational Research in Life and Human Sciences, Heuristic and Metaheuristic Algorithms in Optimization, Applications Related to Optimization in Engineering.

Submission of Manuscripts

New Submissions

Solicited and contributed manuscripts should be submitted to IJOCTA via the journal's online submission system. You need to make registration prior to submitting a new manuscript (please click here to register and do not forget to define yourself as an "Author" in doing so). You may then click on the "New Submission" link on your User Home.

IMPORTANT: If you already have an account, please click here to login. It is likely that you will have created an account if you have reviewed or authored for the journal in the past.

On the submission page, enter data and answer questions as prompted. Click on the “Next” button on each screen to save your work and advance to the next screen. The names and contact details of at least four internationally recognized experts who can review your manuscript should be entered in the "Comments for the Editor" box.

You will be prompted to upload your files: Click on the “Browse” button and locate the file on your computer. Select the description of the file in the drop down next to the Browse button. When you have selected all files you wish to upload, click the “Upload” button. Review your submission before sending to the Editors. Click the “Submit” button when you are done reviewing. Authors are responsible for verifying all files have uploaded correctly.

You may stop a submission at any phase and save it to submit later. Acknowledgment of receipt of the manuscript by IJOCTA Online Submission System will be sent to the corresponding author, including an assigned manuscript number that should be included in all subsequent correspondence. You can also log-on to submission web page of IJOCTA any time to check the status of your manuscript. You will receive an e-mail once a decision has been made on your manuscript.

Each manuscript must be accompanied by a statement that it has not been published elsewhere and that it has not been submitted simultaneously for publication elsewhere.

Manuscripts can be prepared using LaTeX (.tex) or MSWord (.docx). However, manuscripts with heavy mathematical content will only be accepted as LaTeX files.

Preferred first submission format (for reviewing purpose only) is Portable Document File (.pdf). Please find below the templates for first submission.

Click here to download Word template for first submission (.docx)

Click here to download LaTeX template for first submission (.tex)

Revised Manuscripts

Revised manuscripts should be submitted via IJOCTA online system to ensure that they are linked to the original submission. It is also necessary to attach a separate file in which a point-by-point explanation is given to the specific points/questions raised by the referees and the corresponding changes made in the revised version.

To upload your revised manuscript, please go to your author page and click on the related manuscript title. Navigate to the "Review" link on the top left and scroll down the page. Click on the "Choose File" button under the "Editor Decision" title, choose the revised article (in pdf format) that you want to submit, and click on the "Upload" button to upload the author version. Repeat the same steps to upload the "Responses to Reviewers/Editor" file and make sure that you click the "Upload" button again.

To avoid any delay in making the article available freely online, the authors also need to upload the source files (Word or LaTex) when submitting revised manuscripts. Files can be compressed if necessary. The two-column final submission templates are as follows:

Click here to download Word template for final submission (.docx)

Click here to download LaTeX template for final submission (.tex)

Authors are responsible for obtaining permission to reproduce copyrighted material from other sources and are required to sign an agreement for the transfer of copyright to IJOCTA.

Article Processing Charges

There are **no charges** for submission and/or publication.

English Editing

Papers must be in English. Both British and American spelling is acceptable, provided usage is consistent within the manuscript. Manuscripts that are written in English that is ambiguous or incomprehensible, in the opinion of the Editor, will be returned to the authors with a request to resubmit once the language issues have been improved. This policy does not imply that all papers must be written in "perfect" English, whatever that may mean. Rather, the criteria require that the intended meaning of the authors must be clearly understandable, i.e., not obscured by language problems, by referees who have agreed to review the paper.

Presentation of Papers

Manuscript style

Use a standard font of the **11-point type: Times New Roman** is preferred. It is necessary to single line space your manuscript. Normally manuscripts are expected not to exceed 25 single-spaced pages including text, tables, figures and bibliography. All illustrations, figures, and tables are placed within the text at the appropriate points, rather than at the end.

During the submission process you must enter: (1) the full title, (2) names and affiliations of all authors and (3) the full address, including email, telephone and fax of the author who is to check the proofs. Supply a brief **biography** of each author at the end of the manuscript after references.

- Include the name(s) of any **sponsor(s)** of the research contained in the paper, along with **grant number(s).**
- Enter an **abstract** of no more than 250 words for all articles.

Keywords

Authors should prepare no more than 5 keywords for their manuscript.

Maximum five **AMS Classification number** (http://www.ams.org/mathscinet/msc/msc2010.html) of the study should be specified after keywords.

Writing Abstract

An abstract is a concise summary of the whole paper, not just the conclusions. The abstract should be no more than 250 words and convey the following:

1. An introduction to the work. This should be accessible by scientists in any field and express the necessity of the experiments executed.
2. Some scientific detail regarding the background to the problem.
3. A summary of the main result.
4. The implications of the result.
5. A broader perspective of the results, once again understandable across scientific disciplines.

It is crucial that the abstract conveys the importance of the work and be understandable without reference to the rest of the manuscript to a multidisciplinary audience. Abstracts should not contain any citation to other published works.

Reference Style

Reference citations in the text should be identified by numbers in square brackets "[ ]". All references must be complete and accurate. Please ensure that every reference cited in the text is also present in the reference list (and vice versa). Online citations should include date of access. References should be listed in the following style:

Journal article

Author, A.A., & Author, B. (Year). Title of article. Title of Journal, Vol(Issue), pages.

Castles, F.G., Curtin, J.C., & Vowles, J. (2006). Public policy in Australia and New Zealand: The new global context. Australian Journal of Political Science, 41(2), 131–143.

Book

Author, A. (Year). Title of book. Publisher, Place of Publication.

Mercer, P.A., & Smith, G. (1993). Private Viewdata in the UK. 2nd ed. Longman, London.

Chapter

Author, A. (Year). Title of chapter. In: A. Editor and B. Editor, eds. Title of book. Publisher, Place of publication, pages.

Bantz, C.R. (1995). Social dimensions of software development. In: J.A. Anderson, ed. Annual review of software management and development. CA: Sage, Newbury Park, 502–510.

Internet document

Author, A. (Year). Title of document [online]. Source. Available from: URL [Accessed (date)].

Holland, M. (2004). Guide to citing Internet sources [online]. Poole, Bournemouth University. Available from: http://www.bournemouth.ac.uk/library/using/guide_to_citing_internet_sourc.html [Accessed 4 November 2004].

Newspaper article

Author, A. (or Title of Newspaper) (Year). Title of article. Title of Newspaper, day Month, page, column.

Independent (1992). Picking up the bills. Independent, 4 June, p. 28a.

Thesis

Author, A. (Year). Title of thesis. Type of thesis (degree). Name of University.

Agutter, A.J. (1995). The linguistic significance of current British slang. PhD Thesis. Edinburgh University.

Illustrations

Illustrations submitted (line drawings, halftones, photos, photomicrographs, etc.) should be clean originals or digital files. Digital files are recommended for highest quality reproduction and should follow these guidelines:

- 300 dpi or higher
- Sized to fit on journal page
- TIFF or JPEG format only
- Embedded in text files and submitted as separate files (if required)

Tables and Figures

Tables and figures (illustrations) should be embedded in the text at the appropriate points, rather than at the end. A short descriptive title should appear above each table with a clear legend and any footnotes suitably identified below.

Proofs

Page proofs are sent to the designated author using IJOCTA EProof system. They must be carefully checked and returned within 48 hours of receipt.

Offprints/Reprints

Each corresponding author of an article will receive a PDF file of the article via email. This file is for personal use only and may not be copied and disseminated in any form without prior written permission from IJOCTA.

Submission Preparation Checklist

As part of the submission process, authors are required to check off their submission's compliance with all of the following items, and submissions may be returned to authors that do not adhere to these guidelines.

1. The submission has not been previously published, nor is it before another journal for consideration (or an explanation has been provided in Comments for the Editor).
2. The paper is in PDF format and prepared using the IJOCTA's two-column template.
3. All references cited in the manuscript have been listed in the References list (and vice-versa) following the referencing style of the journal.
4. There is no copyright material used in the manuscript (or all necessary permissions have been granted).
5. Details of all authors have been provided correctly.
6. ORCID profile numbers of "all" authors are mandatory, and they are provided at the end of the manuscript as in the template (visit https://orcid.org for more details on ORCID).
7. The text adheres to the stylistic and bibliographic requirements outlined in the Author Guidelines.
8. Maximum five AMS Classification number (http://www.ams.org/mathscinet/msc/msc2010.html) of the study have been provided after keywords.
9. The names and email addresses of at least FOUR (4) possible reviewers have been indicated in "Comments for the Editor" box in "Paper Submission Step 1-Start". Please note that at least two of the recommendations should be from different countries. Avoid suggesting reviewers you have a conflict of interest.

Peer Review Process

All contributions, prepared according to the author guidelines and submitted via IJOCTA online submission system are evaluated according to the criteria of originality and quality of their scientific content. The corresponding author will receive a confirmation e-mail with a reference number assigned to the paper, which he/she is asked to quote in all subsequent correspondence.

All manuscripts are first checked by the Technical Editor using plagiarism detection software (iThenticate) to verify originality and ensure the quality of the written work. If the result is not satisfactory (i.e. exceeding the limit of 30% of overlapping), the submission is rejected and the author is notified.

After the plagiarism check, the manuscripts are evaluated by the Editor-in-Chief and can be rejected without reviewing if considered not of sufficient interest or novelty, too preliminary or out of the scope of the journal. If the manuscript is considered suitable for further evaluation, it is first sent to the Area Editor. Based on his/her opinion the paper is then sent to at least two independent reviewers. Each reviewer is allowed up to four weeks to return his/her feedback but this duration may be extended based on his/her availability. IJOCTA has instituted a blind peer review process where the reviewers' identities are not known to authors. When the reviews are received, the Area Editor gives a decision and lets the author know it together with the reviewer comments and any supplementary files.

Should the reviews be positive, the authors are expected to submit the revised version usually within two months the editor decision is sent (this period can be extended when the authors contact to the editor and let him/her know that they need extra time for resubmission). If a revised paper is not resubmitted within the deadline, it is considered as a new submission after all the changes requested by reviewers have been made. Authors are required to submit a new cover letter, a response to reviewers letter and the revised manuscript (which ideally shows the revisions made in a different color or highlighted). If a change in authorship (addition or removal of author) has occurred during the revision, authors are requested to clarify the reason for change, and all authors (including the removed/added ones) need to submit a written consent for the change. The revised version is evaluated by the Area editor and/or reviewers and the Editor-in-Chief brings a decision about final acceptance based on their suggestions. If necessary, further revision can be asked for to fulfil all the requirements of the reviewers.

When a manuscript is accepted for publication, an acceptance letter is sent to the corresponding author and the authors are asked to submit the source file of the manuscript conforming to the IJOCTA two-column final submission template. After that stage, changes of authors of the manuscript are not possible. The manuscript is sent to the Copyeditor and a linguistic, metrological and technical revision is made, at which stage the authors are asked to make the final corrections in no more than a week. The layout editor prepares the galleys and the authors receive the galley proof for final check before printing. The authors are expected to correct only typographical errors on the proofs and return the proofs within 48 hours. After the final check by the layout editor and the proofreader, the manuscript is assigned a DOI number, made publicly available and listed in the forthcoming journal issue. After printing the issue, the corresponding metadata and files published in this issue are sent to the databases for indexing.

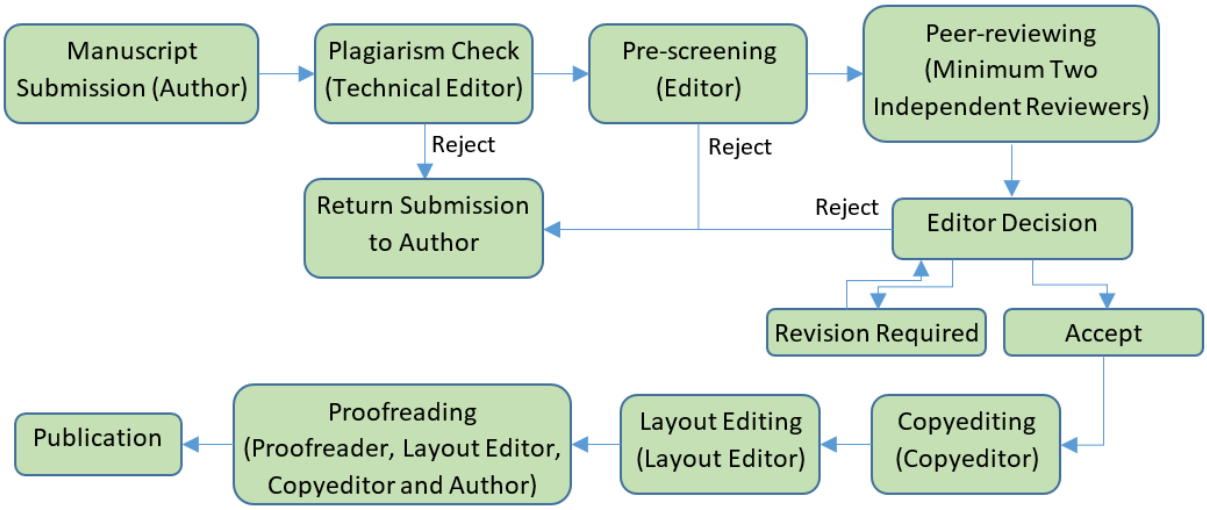

Publication Ethics and Malpractice Statement

IJOCTA is committed to ensuring ethics in publication and quality of articles. Conforming to standards of expected ethical behavior is therefore necessary for all parties (the author, the editor(s), the peer reviewer) involved in the act of publishing.

International Standards for Editors

The editors of the IJOCTA are responsible for deciding which of the articles submitted to the journal should be published considering their intellectual content without regard to race, gender, sexual orientation, religious belief, ethnic origin, citizenship, or political philosophy of the authors. The editors may be guided by the policies of the journal's editorial board and constrained by such legal requirements

as shall then be in force regarding libel, copyright infringement and plagiarism. The editors may confer with other editors or reviewers in making this decision. As guardians and stewards of the research record, editors should encourage authors to strive for, and adhere themselves to, the highest standards of publication ethics. Furthermore, editors are in a unique position to indirectly foster responsible conduct of research through their policies and processes.

To achieve the maximum effect within the research community, ideally all editors should adhere to universal standards and good practices.

- Editors are accountable and should take responsibility for everything they publish.
- Editors should make fair and unbiased decisions independent from commercial consideration and ensure a fair and appropriate peer review process.
- Editors should adopt editorial policies that encourage maximum transparency and complete, honest reporting.
- Editors should guard the integrity of the published record by issuing corrections and retractions when needed and pursuing suspected or alleged research and publication misconduct.
- Editors should pursue reviewer and editorial misconduct.
- Editors should critically assess the ethical conduct of studies in humans and animals.
- Peer reviewers and authors should be told what is expected of them.
- Editors should have appropriate policies in place for handling editorial conflicts of interest.

Reference:

Kleinert S & Wager E (2011). Responsible research publication: international standards for editors. A position statement developed at the 2nd World Conference on Research Integrity, Singapore, July 22-24, 2010. Chapter 51 in: Mayer T & Steneck N (eds) Promoting Research Integrity in a Global Environment. Imperial College Press / World Scientific Publishing, Singapore (pp 317-28). (ISBN 978-981-4340-97-7) [Link].

International Standards for Authors

Publication is the final stage of research and therefore a responsibility for all researchers. Scholarly publications are expected to provide a detailed and permanent record of research. Because publications form the basis for both new research and the application of findings, they can affect not only the research community but also, indirectly, society at large. Researchers therefore have a responsibility to ensure that their publications are honest, clear, accurate, complete and balanced, and should avoid misleading, selective or ambiguous reporting. Journal editors also have responsibilities for ensuring the integrity of the research literature and these are set out in companion guidelines.

- The research being reported should have been conducted in an ethical and responsible manner and should comply with all relevant legislation.
- Researchers should present their results clearly, honestly, and without fabrication, falsification or inappropriate data manipulation.
- Researchers should strive to describe their methods clearly and unambiguously so that their findings can be confirmed by others.
- Researchers should adhere to publication requirements that submitted work is original, is not plagiarised, and has not been published elsewhere.
- Authors should take collective responsibility for submitted and published work.
- The authorship of research publications should accurately reflect individuals' contributions to the work and its reporting.
- Funding sources and relevant conflicts of interest should be disclosed.
- When an author discovers a significant error or inaccuracy in his/her own published work, it is the author's obligation to promptly notify the journal's Editor-in-Chief and cooperate with them to either retract the paper or to publish an appropriate erratum.

Reference:

Wager E & Kleinert S (2011) Responsible research publication: international standards for authors. A position statement developed at the 2nd World Conference on Research Integrity, Singapore, July 22-24, 2010. Chapter 50 in: Mayer T & Steneck N (eds) Promoting Research Integrity in a Global Environment.

Imperial College Press / World Scientific Publishing, Singapore (pp 309-16). (ISBN 978-981-4340-97-7) [Link].

Basic principles to which peer reviewers should adhere

Peer review in all its forms plays an important role in ensuring the integrity of the scholarly record. The process depends to a large extent on trust and requires that everyone involved behaves responsibly and ethically. Peer reviewers play a central and critical part in the peer-review process as the peer review assists the Editors in making editorial decisions and, through the editorial communication with the author, may also assist the author in improving the manuscript.

Peer reviewers should:

- respect the confidentiality of peer review and not reveal any details of a manuscript or its review, during or after the peer-review process, beyond those that are released by the journal;
- not use information obtained during the peer-review process for their own or any other person's or organization's advantage, or to disadvantage or discredit others;
- only agree to review manuscripts for which they have the subject expertise required to carry out a proper assessment and which they can assess within a reasonable time-frame;
- declare all potential conflicting interests, seeking advice from the journal if they are unsure whether something constitutes a relevant conflict;
- not allow their reviews to be influenced by the origins of a manuscript, by the nationality, religion, political beliefs, gender or other characteristics of the authors, or by commercial considerations;
- be objective and constructive in their reviews, refraining from being hostile or inflammatory and from making libellous or derogatory personal comments;
- acknowledge that peer review is largely a reciprocal endeavour and undertake to carry out their fair share of reviewing, in a timely manner;
- provide personal and professional information that is accurate and a true representation of their expertise when creating or updating journal accounts.

Reference:

Homes I (2013). COPE Ethical Guidelines for Peer Reviewers, March 2013, v1 [Link].

Copyright Notice

An International Journal of Optimization and Control: Theories & Applications

Volume: 12 Number: 1
January 2022

CONTENTS

www.ijocta.org
editor@ijocta.org

ISSN 2146-0957